Removal of Textile Dyes from Aqueous Solutions Using Graphene Based Adsorbents

A Thesis Submitted to the Department of Applied Chemistry and Chemical Engineering, University of Dhaka, in Partial Fulfillment of the Requirements for the Degree

of

DOCTOR OF PHILOSOPHY

Submitted by

DEWAN MD. MAHMUDUNNABI

(Registration No: 156/ 2014-2015)

Department of Applied Chemistry and Chemical Engineering

University of Dhaka

DECLARATION

It is hereby declared that this thesis or any part of it has not been submitted elsewhere for the award of any degree or diploma.

Signature of the Candidate

Dewan Md. Mahmudunnabi
Registration Number: 156
Session: 2014-2015

CERTIFICATE

This is to certify that the thesis entitled "Removal of Textile Dyes from Aqueous Solutions Using Graphene Based Adsorbents" being submitted by Dewan Md. Mahmudunnabi, Registration No. 156, Session: 2014-2015, Department of Applied Chemistry and Chemical Engineering, University of Dhaka, in partial fulfillment of the requirement for the degree of Doctor of Philosophy, is an original study of the author carried out under our joint supervisions. No part of this thesis has been submitted before to any other University or institute for the award of any degree or diploma.

Supervisor

(Dr. Md. Nurnabi)
Professor
Department of Applied Chemistry
and Chemical Engineering
University of Dhaka

Co-Supervisor

(Dr. Md. Zahangir Alam)
Professor
Department of Applied Chemistry
and Chemical Engineering
University of Dhaka

Dedicated

To

My Family Members

Acknowledgement

First of all, I wish to express my gratitude to the most merciful and almighty Allah, since without his blessings I will not be able to finish my PhD work.

My greatest gratitude goes to my supervisors, Professor Dr. Md. Nurnabi and Professor Dr. Md. Zahangir Alam, Department of Applied Chemistry and Chemical Engineering, University of Dhaka, for giving me the opportunity, trust and above all the freedom that allowed me to explore. It is indeed a great pleasure for me to express my sincere and profound gratefulness to them for their scholastic guidance, constructive suggestion and encouragement which I received from them in order to complete this research work and to write the dissertation.

I am indebted to Professor Dr. Md. Nurul Amin and Professor Dipti Saha, Chairman, Department of Applied Chemistry and Chemical Engineering, University of Dhaka, providing of all necessary laboratory facilities for the smooth completion of this dissertation.

I am also very grateful to Professor Dr. Md. A.N.M. Hamidul Kabir, Department of Applied Chemistry and Chemical Engineering, University of Dhaka for providing some necessary laboratory facilities for this research.

Many thanks to Dr. Mohammad Ismail and Dr. Md. Ashraful Islam Mollah, Associate Professor, Department of Applied Chemistry and Chemical Engineering, University of Dhaka, Dr. Md. Al-Mamun, Senior Scientific Officer, AEC, Dhaka, who have given a tremendous support during the completion of this research work.

I also thankful to Dr. Md. Nurul Huda, Md. Aminul Islam, Mohammad Shah Jamal, S.M. Asaduzzaman, Mohammad Mominul Islam, Md. Abu sayid Mia and Jarief Farabi who helped me throughout the work with necessary suggestions.

I am very much grateful to University grants Commission of Bangladesh for financial support throughout the research. I must remain thankful to the Center for Advance Research in Sciences, University of Dhaka, for analytical support.

Special Thanks to my wife Nasrin Akter and daughter Tasfia Nabi Moumita for their unconditional support and inspiration which helped me to complete this research work successfully. Thanks to my brother, sister and all my well-wishers for their moral support and inspiration trough out this research work.

Dewan Md. Mahmudunnabi

ABSTRACT

This thesis is composed of five parts: Introduction (Chapter 1), Literature Review (Chapter 2), Materials and Methods (Chapter 3), Results and Discussion (Chapter 4) and Conclusions (Chapter 5).

Background and objectives of the study has been discussed in Chapter 1 and the literature reviews related to the research are elaborated in Chapter 2.

Chapter 3 represents information about the materials used in this research. Here the methods and different equations and models used for the research are also stated.

Chapter 4 deals with main research work and it is divided into three parts.

Part 1 describes the synthesis, characterization of graphene oxide (GO) and its application for the removal of industrially used two synthetic anionic dyes such as FD-R H/C, TURQUOISE GN and one cationic dye, Maxilon Blue (GRL) from aqueous solutions. Here, GO was prepared from graphite powder by modified Hummer's method. Characterization of prepared GO was carried out by FTIR spectroscope, Raman spectroscope, ESEM, AFM, XRD and elemental analysis.

The Langmuir and Freundlich isotherm models have been applied to explain the distribution of Dyes on GO surface. The results showed that the adsorption preferably followed the Langmuir model. From Langmuir isotherm the adsorption capacity was found 151.29 mg/g for FD-R H/C at pH of 2. For TURQUOISE GN the adsorption capacities were 565.61 mg/g and 294.12 mg/g at pH of 2 and 7, respectively. For Maxilon Blue (GRL) the adsorption capacity was 1253.13 mg/g at pH of 7.The experimental data were analyzed using pseudo-first-order and pseudo-second-order models. Analyzing the kinetic parameters it was found that the pseudo-second order kinetic model showed better correlation compared to the pseudo-first-order model.

The thermodynamic analyses are also carried out. From thermodynamic analyses Gibb's free energy ΔG^o values were found -1.69, -1.17 and -0.86 KJ mol^{-1} for dye FD-R H/C at 303K, 313K and 323K, respectively. While for TURQUOISE GN, ΔG^o values were -3.66, -2.92, -2.39 KJ mol^{-1} and for Maxilon Blue (GRL) ΔG^o values were -4.11, -3.80, -2.77 KJ mol^{-1} at 303K, 313K and 323K, respectively. These results confirm that the adsorption of the dyes on GO are more spontaneous at lower temperature and were physical adsorption.

The used GO was regenerated using 2 % HCl and used for adsorption study. For dye TGN, fresh GO showed the adsorption capacity of 102.39 mg/g for 200 ppm dye solution while the regenerated GO of 1st, 2nd, 3rd and 4th recycle showed the adsorption capacities of 75.91 mg/g, 65.73 mg/g, 44.32 mg/g and 41.25 mg/g. For dye MBG, fresh GO showed the adsorption capacity of 1421.10 mg/g for 1000 ppm dye solution while the regenerated GO of 1st, 2nd and 3rd recycle showed the adsorption capacities of 1066.06 mg/g, 792.50 mg/g and 713.18 mg/g.

Part 2 describes the synthesis, characterization of reduced graphene oxide (RGO) and its application for the removal of dye TURQUOISE GN from aqueous solutions. RGO was prepared by reduction of GO using hydrazine hydrate. Characterization of prepared RGO was carried out by ESEM, Raman spectroscope, XRD and elemental analysis.

The Langmuir and Freundlich isotherm models have been applied to explain the distribution of Dye on RGO surface. The results showed that the adsorption preferably followed the Langmuir model. From Langmuir model the adsorption capacity was found 588.24 mg/g for TURQUOISE GN at pH of 7. The experimental data were analyzed using pseudo-first-order and pseudo-second-order models. Analyzing the kinetic parameters it was found that the pseudo-second order kinetic model showed better correlation compared to the pseudo-first-order model.

The used RGO was regenerated using 2 % HCl and used for adsorption study. For TGN, fresh RGO showed the adsorption capacity of 414.80 mg/g for 700 ppm dye solution while the regenerated RGO of 1st, 2nd, 3rd and 4th recycle showed the adsorption capacities of 143.03 mg/g, 135.23 mg/g, 111.28 mg/g and 82.53 mg/g.

Part 3 describes the preparation of sodium-alginate (SA) and GO composite (SA-GO), characterization and its application for the removal of dye Maxilon Blue (GRL) from aqueous solutions. Porous composite SA-GO was prepared by adding the mixture of sodium-alginate, $CaCO_3$ and GO dropwise into 2% HCl. Sodium alginate and GO ratio was maintained as 10:1. Characterization of prepared composite was carried out by FTIR spectroscope, SEM and XRD.

The Langmuir and Freundlich isotherm models have been applied to explain the distribution of Dye on SA-GO composite surface. The results showed that the adsorption preferably followed the Langmuir model. From Langmuir isotherm the adsorption capacity was found 1111.11 mg/g for Maxilon Blue (GRL) at pH of 7. The experimental data were analyzed using pseudo-first-order and pseudo-second-order models. Analyzing the kinetic parameters

it was seen that the pseudo-second order kinetic model showed better correlation compared to the pseudo-first-order model.

The thermodynamic analyses are also carried out. From thermodynamic analyses Gibb's free energy ΔG^o values were found -5.27, -3.75 and -2.55 KJ mol^{-1} for dye Maxilon Blue (GRL) at 303K, 313K and 323K, respectively. These results confirm that the adsorption of the dye Maxilon blue on the composite is more spontaneous at lower temperature and was physical adsorption.

The used SA-GO composite was regenerated using 2 % HCl and used for adsorption study. For MBG, fresh SA-GO composite showed the adsorption capacity of 874.26 mg/g for 900 ppm dye solution while the regenerated SA-GO of 1^{st}, 2^{nd} , 3^{rd} , $4^{th}$and 5^{th} recycle showed the adsorption capacities of 683.27 mg/g, 667.84 mg/g, 664.31 mg/g, 653.43 mg/g and 657.38 mg/g.

Finally, the conclusions and scope of further works are outlined in chapter 5.

Contents

Chapter 5: Conclusions and Scope of Further Study

List of Tables

List of Figures

List of Abbreviations

AC	Activated Carbon
AOP	Advanced Oxidation Process
BOD	Biochemical Oxygen Demand
CARS	Center for Advance Research in Sciences
COD	Chemical Oxygen Demand
GO	Graphene Oxide
LCA	Low Cost Adsorbent
MBG	Maxilon Blue (GRL)
RGO	Reduced Graphene Oxide
SA	Sodium Alginate
SA-GO	Sodium Alginate-GO
TDS	Total Dissolved Solids
TGN	Turquoise GN
TSS	Total Suspended Solids
% Removal	Percentage of Removal

Chapter 1

Introduction

Chapter 2

Literature Review

Chapter 3

Materials and Methods

Chapter 4

Results and Discussion: PART-1

Chapter 4

Results and Discussion: PART-2

Chapter 4

Results and Discussion: PART-3

Chapter 5

Conclusions and Scope of Further Study

Chapter 1

Introduction

1.1.Background of the study

For last few decades textile industries have been playing a vital role for the advancement of Bangladesh's economy. According to Bangladesh Textile Mills Association (BTMA), there are about 1461 textile related industries in Bangladesh that provide the employments for more than 5 million of skilled and unskilled people of which about 80% are women. These employment accounts 45% of all industrial employment and contributes more than 12% of the total GDP of Bangladesh. So, this sector is extremely important for the national economy as well as for socioeconomic development of Bangladesh. In spite of the importance of textile sector it creates a huge problem to our environment by directly discharging effluents containing more or less 2% of dye [1, 2]. Dyes are highly colored, stable to light, non-biodegradable, toxic and causes harm to human and other living beings by entering into food chain [3, 4]. Saving water is to save the planet and to make the future of mankind safe which is a pressing need today. For the treatment of textile effluents some physical as well chemical or biological methods are generally used [5]. Oxidation, precipitation, filtration, electrochemical processes, etc. are also common techniques reported for the removal of dyes from wastewaters.

Among these methods adsorption gives the best result to remove coloring materials from effluents [6-7]. Activated carbon shows very high adsorption capacity and commonly used adsorbent [8], but owing to high cost it is not well accepted by the industrialists. Regeneration of saturated activated carbon is very difficult and also non-selective, non-effective to vat or disperse dyes [9]. For dye adsorption some non-conventional adsorbents such as peat [10, 11], bagasse [12, 13], rice straw [14], rice husk [15, 16], sawdust [17, 18], fly ash [19, 20], clay materials [21, 22] were also used. These adsorbents are very cheap and abundant but demonstrated comparatively low adsorption capacity, required high retention time and their regeneration is difficult.

Different biological treatment methods are claimed to be more economical compared to other physical and chemical methods in this purpose [23, 24]. But drawbacks of these methods are enormous, such as requirement of large land area, high retention time, low adsorption capacity, pH and temperature dependency. Some chemicals used in this process are toxic, complex in structure and obtained from synthetic organic origin [25], some dyes are recalcitrant to this

treatment and due to xenobiotic nature total degradation of azo dyes are not possible. Another traditional method used for dye removal from effluent is coagulation-flocculation method [26]. But there are also some drawbacks of this process such as lack of versatility, requiring varying coagulant dose, low dye removal capacity etc. It also needs large land area, forms too much sludge and very much pH dependent [27].

Recently, graphene oxide and its derivatives have emerged as very effective adsorbents and some research groups reported that they showed very good results for the removal of dyes [28-32] or both dyes and heavy metals [33, 34] due to their high surface area. But the prepared GO and its derivatives are very costly and applied for the removal of model dyes, mainly for cationic dyes. So, still there are rooms to develop new technique for the synthesis of GO and its derivatives which will be attractive as well as economically viable adsorbents.

1.2. Problem statement

Now-a-days, about 9000 types of dyes have been incorporated in the color index. Due to low biodegradability of dyes, the discharge of colored wastewater from these industries had caused many troubles in the environment. In Bangladesh, industrial units are mostly located along the banks of the rivers. Unfortunately, industrial units drain effluents directly into the rivers without proper treatment and consideration of the environmental impact which causes severe water pollution.

1.3. Objective of study

The study protocol will include the following objectives:

- Development of suitable technique for the synthesis of graphene oxide (GO).
- Synthesis of reduced graphene oxide (RGO) from graphene oxide (by reduction).
- Preparation of composite of GO and Na-alginate.
- Characterization of prepared GO, RGO and composite material.
- Study of adsorption capacity of prepared GO, RGO and composite, using industrially used dye solution.

Chapter 2

Literature Review

2.1. A brief description of various types of dyes [35]**:**

On the basis of properties dyes can be classified as-

a) Acid dyes: The principal chemical classes of these dyes are azo, anthraquinone, triphenylmethane, azine, xanthene, nitro and nitroso. These dyes are generally water soluble and used for nylon, wool, silk, modified acrylics and to some extent for paper, leather, ink-jet printing, food and cosmetics.

b) Basic (cationic) dyes: The principal chemical classes of these dyes are diazahemicyanine, triarylmethane, cyanine, hemicyanine, thiazine, oxazine and acridine. These dyes are also water soluble and yield coloured cations in solution. These are mainly used for paper, polyacrylonitrile, modified nylons, modified polyesters, cation dyeable polyethylene terephthalate and to some extent in medicine.

c) Disperse dyes: These type of dye generally contain azo, anthraquinone, styryl, nitro and benzodifuranone groups. These are substantially water-insoluble nonionic dyes and used mainly on polyester and to some extent on nylon, cellulose, cellulose acetate, and acrylic fibers.

d) Direct dyes: These type of dyes are polyazo compounds, along with some stilbenes, phthalocyanines and oxazines. These dyes are water-soluble anionic dyes and have high affinity for cellulosic fibers in the presence of electrolytes in aqueous solution. These dyes are used in the dyeing of cotton and rayon, paper, leather and to some extent to nylon.

e) Reactive dyes: These types of dyes contain chromophoric groups such as azo, anthraquinone, triarylmethane, phthalocyanine, formazan, oxazine etc. and form a covalent bond with the fiber. Dyeing of reactive dyes are brighter which makes them advantageous over direct dyes and generally used for cotton and other cellulosics, but are also used to a small extent on wool and nylon.

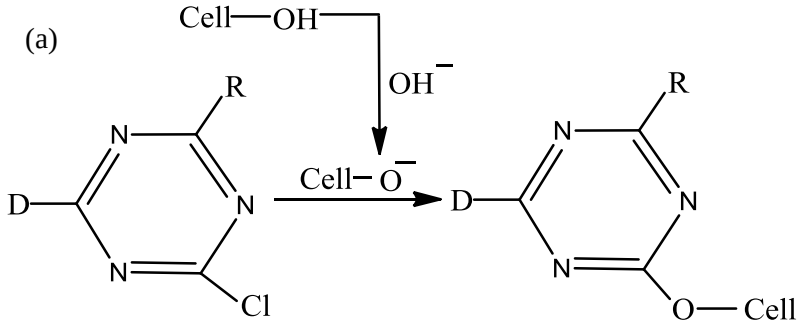

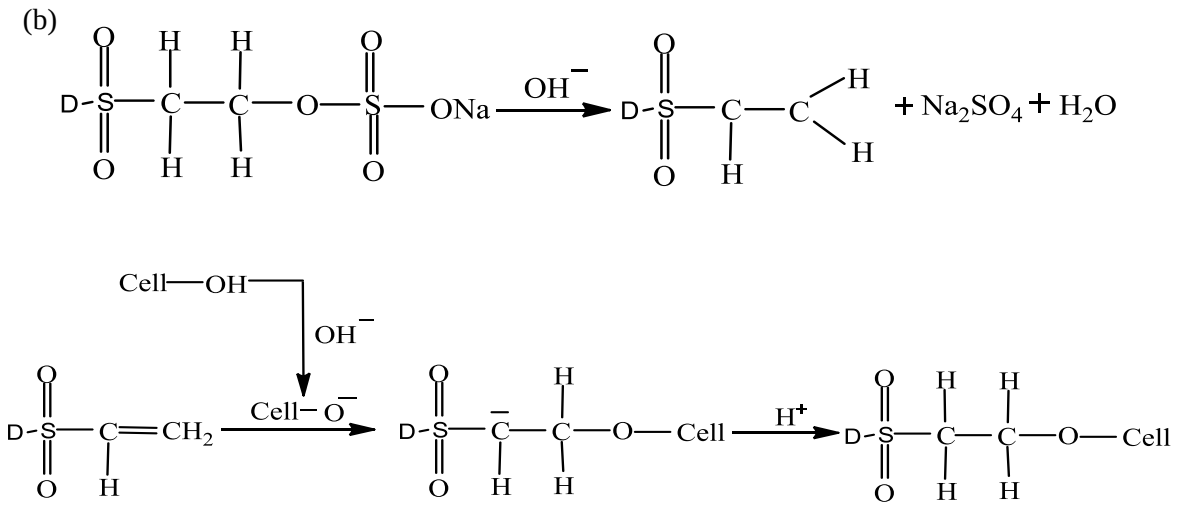

Here, D = Dye and Cell = Cellulose

Fig. 1: Mechanism of interaction of monochloro trizine (a) and vinyl sulfone (b) type dye with cotton

f) Solvent dyes: Due to lacking of polar solubilizing groups these dyes are nonpolar or little polar. As a result they are generally insoluble in water and solvent soluble. The principal chemical classes are azo, anthraquinone, phthalocyanine and triarylmethane and used for plastics, gasoline, lubricants, oils, and waxes.

g) Sulfur dyes: These types of dye have intermediate structures and form a relatively small group. Moreover, their cost is low and possess good washing property. So, this class of dye is very important from an economic point of view. This type of dye is used for cotton and rayon and have limited use with polyamide fibers, silk, leather, paper and wood.

h) Vat dyes: These types of dyes are water-insoluble containing anthraquinone and indigoids. Besides these, there are some other classes like azo groups and used for cotton and other cellulosic materials. They also contain fluorescent brighteners and used for soaps, detergents, fibers, oils, paints and plastics.

Besides these, at present there are more than 100,000 commercial dyes with a rough estimated production of 7×10^5–1×10^6 tons per year. The big consumers of these dyes are textile, dyeing, paper-pulp, tannery and paint industries. Hence the effluents of these industries contain dyes in sufficient quantities. As such it is important to treat colored effluents for the removal of dyes.

2.2. Methodologies of dye removal

At earlier stages of the use of dye, attention was not given regarding to the use and discharge limit of dye in wastewaters. But with the growing concern on health, people started paying much attention regarding to this. At the beginning there was no discharge limit of dye in wastewater and treatment started just with some physical treatment processes such as

sedimentation, equalization to maintain the pH, reduction of total dissolved solids (TDS) and total suspended solids (TSS) of the discharged water.

After few years secondary treatment methods (filter beds for biodegradation) and recently activated sludge process (aerobic biodegradation) were incorporated. In pretreatment process industrial-wastewaters are pretreated by equalization, neutralization and suspended solids are removed by either physical or chemical separation. Then the wastewaters are given a secondary treatment usually involving microorganisms (primarily bacteria) which stabilize the waste components. The third step is physical–chemical treatment which include adsorption, ion exchange, stripping, chemical oxidation, and membrane separations.

The common methodologies used for waste water treatment are discussed briefly-

2.2.1. Sedimentation

Sedimentation is used to separate suspended particles and it is the basic form of primary treatment used at most municipal and industrial wastewater treatment facilities [36]. To enhance gravity settling of suspended particles chemical flocculants, sedimentation basins and clarifiers are used.

2.2.2. Filtration

The common filtration methods includes microfiltration, ultrafiltration, nanofiltration, and reverse osmosis and are used for the treatment of drinking water as well as wastewater treatment. Among the filtration technique ultrafiltration and nanofiltration are more effective over microfiltration because of its pore size [36]. Though ultrafiltration and nanofiltration techniques are effective for the removal of all classes of dyestuffs but dye molecules cause frequent clogging of the membrane pores. As a result high working pressures are needed which cause significant energy consumption. High cost of membrane and a relatively short membrane life also make their use limited for treating of textile effluent.

Reverse osmosis is more effective filtration technique which forces water under pressure through a membrane that is impermeable to most contaminants. This membrane is somewhat better at rejecting salts than non-ionized weak acids and bases and smaller organic molecules whose molecular weight are below 200. So, this process has been used as effective decoloring and desalting process against the most diverse range of dyes and successfully employed for recycling of textile effluents [37]. The water produced by reverse osmosis is close to pure H_2O.

2.2.3. Coagulation-flocculation

Generally, the process is economically feasible (but sometimes becomes expensive due to the cost of chemicals) with satisfactory removal of disperse, sulfur, and vat dyes. The process involves adding aluminum (Al^{3+}), calcium (Ca^{2+}) or ferric (Fe^{3+}) ions and some other agents

to the dye effluent which induces flocculation. The main drawback of the process is the final concentrated sludge that is produced in large quantities [27]. Moreover, the process is very much pH dependent [38] and control of coagulant dosage is very important. Besides this, the process is not good for highly soluble dyes and not so effective to azo, reactive, acid and especially to the basic dyes [39].

2.2.4. Oxidation

Oxidation is a method in which wastewater from primary treatment (sedimentation) is treated by using chlorine, hydrogen peroxide, fenton's reagent, ozone or potassium permanganate. Oxidation is the most commonly used method for decolourisation processes since it needs low quantities of oxidants and reaction time is also short. A complete oxidation of dye can reduce the complex molecules of dye to carbon dioxide and water. Oxidation is also used to partially or completely degrade the dyes. pH and catalysts play an important role in oxidation process.

Chlorine is applied as calcium hypochlorite and sodium hypochlorite for oxidation of dyes. Water soluble dyes such as reactive, acid, direct and metal complex dyes are decolorized readily by hypochlorite. But water insoluble disperse and vat dyes are resistant to decolorization in this process. The decolorization of reactive dyes generally require long reaction times and metal complex dye solution remains partially colored even after an extended period of treatment. Dyes having amino or substituted amino groups on a naphthalene ring, are most susceptible to chlorine and decolorize more easily than other dyes [40]. In the decomposition of metal complex dyes metals, like iron, copper, nickel and chromium are liberated and these metals have a catalytic effect that increases decolorization. Though the use of chlorine gas is a low-cost methodology for decolourizing dye waste water, it causes some unavoidable side reactions and produces organochlorine compounds including toxic trihalomethane, thereby increasing the absorbable organic halogens in treated water. It also liberate metals in metal complex dyes and cause corrosion in metallic vessels.

Hydrogen peroxide (H_2O_2) has strong oxidizing and bleaching properties. Hydrogen peroxide is also used for making peroxidase enzymes, which are used for decolourization of dyes. This process is pH dependent and produces sludge.

Fenton's reagent is a solution of hydrogen peroxide and an iron catalyst [41]. It is stronger than hydrogen peroxide and also used to oxidize dye waste waters. Generally, it is effective in decolorization of both soluble and insoluble dyes (acid, reactive, direct, metal complex dyes) but vat and disperse dyes were found to be resistant to it. It not only remove the colour, but also reduce chemical oxygen demand (except with reactive dyes), total organic carbon and toxicity of treated water. The process is also applicable even with high-suspended solid

concentration. From a biological point of view, this process is also preferable because in this process the quality of the sludge is improved and the phosphates can also be eliminated. The process is very much pH dependent and is usually effective within pH range of <3.5 [42]. It also produces huge sludge and takes longer reaction time.

Ozonation carried out by ozone and has been found to be a very effective way of decolorizing textile effluents. Color removal of the effluent containing reactive dyes can be achieved in 5 min of contact time for yellow and blue shades at an ozone consumption of 37.5 and 36 mg L^{-1}, respectively. Ozonation also effectively removed chemical oxygen demand (COD) of the waste water [43].

2.2.5. Electrochemical methodology

Electrochemical methodology is used as a tertiary treatment method [44]. In this process decolorization can be achieved either by electro oxidation with non-soluble anodes or by electro-coagulation using consumable materials. Several anode materials like iron, conducting polymer, boron doped diamond electrode with different experimental conditions have been used successfully in the electro-degradation of dyes [45, 46]. A color removal of 83–100% was observed for Direct Red 80 using iron, polypyrrole doped with chromium and boron doped diamond electrodes. This technique is effective in decolourisation of both soluble and insoluble dyes with reduction of COD. The rate of color and organic load removal depends on the anode's material and the working potential. The main drawbacks of the process are high electricity cost, sludge production as well as pollution from chlorinated organics and heavy metals due to indirect oxidation [47].

2.2.6. Advanced oxidation processes (AOPs)

Advanced Oxidation Processes (AOPs) are the processes involving simultaneous use of more than one oxidation processes. As sometimes single oxidation system is not sufficient for the total decomposition of dyes, Advanced Oxidation Processes are used. These processes involve the accelerated production of the hydroxyl free radical and the organic contaminants are commonly oxidized to CO_2. A wide variety of advanced oxidation processes are available like chemical oxidation processes using ozone, combined ozone and peroxide, ultra violet enhanced oxidation such as UV/hydrogen peroxide, UV/ozone, UV/air wet air oxidation and catalytic wet air oxidation (where air is used as the oxidant) [48, 49].

The drawbacks in general AOPs are production of some undesirable by-products, complete mineralization is not possible and the process is pH dependent. Though the advanced oxidation processes have proven potential and technically sound for color removal but they are quite expensive especially for small-scale sector of developing countries.

2.2.7. Biological treatment

Biological treatment is the most common and widespread technique used in dye wastewater treatment [23, 24, 50, 51]. A large number of species have been used for decolouration and mineralization of various dyes. The advantages of this technology are relatively inexpensive, having low running costs and the end products of complete mineralization not being toxic. The process can be aerobic (in presence of oxygen), anaerobic (without oxygen) or combined aerobic–anaerobic.

In biological treatment, two microorganisms e.g. bacteria and fungi have been most widely used to treat wastewaters. In aerobic conditions, enzymes secreted by bacteria present in the wastewater break down the organic compounds. The factors that affect the decolourisation process are concentration of pollutants, dyestuff concentration, initial pH and temperature of the effluent. It has been suggested that after the fungal treatment, an improvement in the treatability of the effluent by other microorganisms can be observed.

An anaerobic pretreatment step could be a cheap alternative compared with aerobic systems as expensive aeration is omitted and problems with bulking sludge are avoided. In addition, advantages of anaerobic treatment to be that dyes can be reductively decolorized, no foaming problems with surfactants, high effluent temperatures can be favorable, high pH effluent can be acidified and degradation of refractory organics (surfactants, chlorinated aromatics) can be initiated. Nevertheless, the drawbacks were suggested to be that BOD removal can be insufficient [3], dyes and other refractory organics are not mineralized, nutrients (N, P) are not removed and sulfates give rise to sulfide.

In order to get better remediation of colored compounds from the textile effluents, a combination of aerobic and anaerobic treatment are also used. An advantage of such system is the complete mineralization which is achieved due to the synergistic action of different organisms [52]. The reduction of the azo bond can be achieved under the reducing conditions in anaerobic bioreactors and the resulting colorless aromatic amines may be mineralized under aerobic conditions. Thus though this methodology is cost-competitive an anaerobic decolorization followed by aerobic post-treatment is generally recommended for treating dye wastewaters. Generally the factors like concentration of dyes, initial pH and temperature of the effluent, affect the decolorization of this process. The main drawbacks of the biological treatment is low biodegradability of the dyes, less flexibility in design and operation, larger land area requirement and longer times required for decolorization and makes incapable of removing dyes from effluent [53].

2.2.8. Ion exchange

Ion exchange is a reversible chemical process wherein an ion from solution is exchanged for a similarly charged ion attached to an immobile solid particle. By far the largest application of ion exchange to drinking water that is, the removal of calcium, magnesium and other polyvalent cations in exchange for sodium. Ion exchange shares various common features along with adsorption, in regard to application in batch and fixed-bed processes to have high water quality. Various studies have been carried out using ion exchange for the removal of dyes and has been fruitfully used for the removal of colors [54].

A starch-based polymers was prepared [55] by a crosslinking reaction of starch-enriched flour using epichlorohydrin as a crosslinking agent in the presence of NH_4OH. These crosslinked starch-based materials, containing tertiary amine groups were used for the recovery of various dyes from aqueous solutions and the sorption mechanism was correlated to the structure of the polymer.

2.2.9. Adsorption

Adsorption is one of the processes used for dye removal as well as in wastewater treatment [6-7]. Adsorption method gives the best result to remove coloring materials. The term adsorption refers to a process wherein a material is concentrated at a solid surface from its liquid or gaseous surroundings. Adsorption can be classified in two catagories:

a) Physisorption: When the attraction between the solid surface and the adsorbed molecules is physical in nature, the adsorption is referred to as physical adsorption or physisorption. Generally, in physical adsorption the attractive forces between adsorbed molecules and the solid surface are van der Waals forces and as they being weak in nature results in reversible adsorption.

b) Chemisorption: When the attraction forces are due to chemical bonding, the adsorption process is called chemisorption. In view of the higher strength of the bonding in chemisorption, it is difficult to remove chemisorbed species from the solid surface.

Adsorption is comparatively more effective and cheap technique and gives the best result to remove coloring materials from effluents. A brief description on different types of adsorbents is given below-

2.2.9.1. Activated carbon

Activated carbon is the oldest adsorbent and is usually prepared from coal, coconut shells, lignite, wood etc. [56], having a very porous structure with a large surface area ranging from 500 to 2000 m^2g^{-1} [57]. Activated carbon can be used in both physical and chemical adsorption. It has been found that adsorption on activated carbon is not usually selective as it occurs through van der Waals forces. Activated carbon is available in two main forms:

powdered activated carbon (PAC) and granular activated carbon (GAC). Besides PAC and GAC two other forms of ACs are Activated Carbon Pellet and Activated Carbon Fiber (ACF). The comparison of adsorption capacity of commercial activated carbon (CAC) and indigenously prepared activated carbon for methylene blue (MB) are given in Table-1.

Table 1: Comparison of adsorption capacities of various activated carbon with commercial activated carbon

Name of Dye	Name of Adsorbent	Adsorption capacity (mg/g)	Reference
Methylene Blue (MB)	Commercial activated carbon	980.3 mg g^{-1}	[58]
	Bamboo dust carbon (BDC)	143.2 mg g^{-1}	
	Coconut shell carbon (CSC)	277.9 mg g^{-1}	
	Groundnut shell carbon (GNSC)	164.9 mg g^{-1}	
	Rice husk carbon (RHC)	343.5 mg g^{-1}	
	Straw carbon (SC)	472.1 mg g^{-1}	

Though activated carbon is an effective and commercially used adsorbent for removing color and other pollutants from textile and dye wastes use is sometimes restricted due to higher cost. Once AC has been exhausted, it has to be regenerated for further use in purifying water and a number of methods like thermal, chemical, oxidation, electrochemical are used for this purpose. It is worth noting that regeneration of activated carbon add cost, furthermore, regeneration process results in a loss of carbon. This has resulted in attempts by various workers to prepare low-cost alternative adsorbents [59] which may replace activated carbons in pollution control through adsorption process.

2.2.9.2. Low-cost alternative adsorbents

The natural materials or the wastes/by-products of industries or synthetically prepared materials, which are of less cost and can be used as such or after some minor treatment as adsorbents are generally called low-cost adsorbents (LCAs). Numerous studies for the development, utilization and application of low-cost adsorbents generally adopted by researcher and reported in literature as substitutes for activated carbons.

On the basis of availability these low-cost alternative adsorbents may be classified as-

1. Natural materials
2. Industrial/Agricultural/Domestic wastes or by-products

2.2.9.2.1. Natural materials

Natural materials generally used as LCAs exist in nature and used in treatment processes to remove organic pollutants, dyes, and heavy metals. Some of the materials used in this purpose are demonstrated in Table-2.

Table 2: Comparison of adsorption capacity of some low cost natural materials

Name of adsorbent	Adsorption capacity (mg/g)	Reference
Pine Wood	Acid blue 264: 1176 mg g^{-1} Basic blue 69 : 1119 mg g^{-1}	[60]
Bark	Basic red 2: 1119 mg g^{-1} Basic blue 9: 519 mg g^{-1}	[61]
Peat	Basic blue 69 : 195 mg g^{-1} Acid blue 25: 12.7 mg g^{-1}	[62]
Treated peat	Basic violet 14: 400 mg g^{-1} Basic green 4: 350 mg g^{-1}	[63]
Chitosan	Acid orange 12: 973.3 mg g^{-1} Acid orange 10: 922.9 mg g^{-1}	[64]
Coal	Basic blue 9: 250 mg g^{-1} Basic red 2: 120 mg g^{-1}	[61]
Cotton	Acid blue 25: 589 mg g^{-1} Acid yellow 99: 448 mg g^{-1} Reactive yellow 23: 302 mg g^{-1}	[65]
Cotton waste	Basic red 2: 875 mg g^{-1} Basic blue 9: 277 mg g^{-1}	[61]
Clay	Basic blue 9: 300 mg g^{-1} Basic red 18: 157 mg g^{-1}	[66, 67]
Dolomite	Reactive red: 950 mg g^{-1}	[68]
Activated Bentonite	Acid blue 93: 740.5 mg g^{-1}	[69]
Diatomite	Basic blue 9: 198 mg g^{-1}	[70]
Biomass	Reactive black 5: 588.2 mg g^{-1} Reactive red 5: 555.6 mg g^{-1}	[71, 72]
Yeasts	Remazol blue: 173.1 mg g^{-1} Reactive black 5: 88.5 mg g^{-1}	[73]

2.2.9.2.2. Industrial/agricultural/domestic wastes or by-products

In addition to the above discussed natural materials, a number of agricultural wastes or by-products has also been investigated as adsorbents for the removal of pollutants by a number of researchers. The adsorption capacity of some of these materials are demonstrated in Table-3.

Table 3: Comparison of adsorption capacity of some low cost waste materials or by-products

Name of adsorbent	Adsorption capacity (mg/g)	Reference
Sawdust	Direct brown: 526.3 mg g^{-1} Direct brown 2: 416.7 mg g^{-1} Basic blue 86: 136.9 mg g^{-1}	[74]
Bagasse	Basic red 22: 942 mg g^{-1} Acid blue 25: 674 mg g^{-1} Acid blue 80: 391 mg g^{-1}	[75, 76]
Rice husk	Acid blue: 50 mg g^{-1} Acid yellow 36: 86.9 mg g^{-1} Basic blue 9: 312 mg g^{-1} Basic red 2: 838 mg g^{-1}	[15, 17, 61]
Fly ash	Basic blue 9: 75.52 mg g^{-1} Alizarin sulfonic: 11.21 mg g^{-1}	[77, 78]
Orange peel	Acid violet: 19.88 mg g^{-1} Basic violet 10: 14.3 mg g^{-1}	[79, 80]
Banana peel	Methyl orange: 21 mg g^{-1} Basic blue 9: 20.8 mg g^{-1} Basic violet 10: 20.6 mg g^{-1}	[80]
Coir pith	Basic blue 9: 120.43 mg g^{-1}	[81]
Activated sludge	Basic red 18: 285.71 mg g^{-1} Basic blue 9: 256.41 mg g^{-1} Reactive blue 2: 250 mg g^{-1}	[82, 83]

2.2.9.2.3. Other wastes or by-products

Some researchers also study adsorption capacities of other waste materials such as waste newspaper, sewage sludge, sugar industry mud, tree fern, rice hull ash etc. Waste newspaper shows adsorption capacity of 390 mg g^{-1} for Basic blue 9 [84], sewage sludge shows adsorption capacity of 188 mg g^{-1} for Basic red 46 [85], sugar industry mud shows adsorption capacity of 519 mg g^{-1} for Basic red 22 [86], tree fern shows adsorption capacity of

408 mg g^{-1} for Basic red 13 [87], rice hull ash shows adsorption capacity of 171 mg g^{-1} for Direct red 28 [88].

Besides these some cheap and readily available solid agricultural wastes such as date pits, pith, barley husk, wheat straw and various other materials such as waste tyre rubber [89], polymeric materials [90], de-oiled soya [91], bottom ash [92], rosa canina seeds [93] etc. have also been explored as adsorbents for the removal of dyes from aqueous solutions.

2.2.9.3. Graphene based adsorbents

In the past few years, graphene and graphene based materials have attracted tremendous interest in the world. Graphene is a two-dimensional carbon nanomaterial with single layer of sp^2-hybridized carbon atoms arranged in six-membered rings. Graphene has strong mechanical, thermal, and electrical properties, with a theoretical value of specific surface area of 2630 m^2/g. Recently, graphene based materials have been emerged as adsorbent for the removal of dyes and heavy metals because of their large surface area. Some of graphene based adsorbents with their adsorption capacity are described in Table-4.

Table 4: Adsorption capacities of some graphene based materials

Name of the adsorbent	Adsorption capacity (mg/g)	Reference
Superparamagnetic graphene oxide-Fe_3O_4 hybrid composite (GO- Fe_3O_4)	Methylene Blue: 167.2 mg g^{-1} Neutral Red: 171.3 mg g^{-1}	[29]
Thermally reduced graphene (TRG), produced by thermal exfoliation of graphene oxide	Methyl Orange: 89.3 mg g^{-1}	[32]
Single-walled carbon nanotubes (SWCNTs), carboxylate group functionalized single-walled carbon nanotubes (SWCNT-COOH), Graphene (G) and Graphene oxide (GO).	Adsorption capacity of SWCNTs, SWCNT-COOH, graphene and GO were 38.35 mg g^{-1}, 49.45 mg g^{-1}, 30.32 mg g^{-1} and 55.57 mg g^{-1} for Basic Red 46 (BR 46).	[94]
Chitosan and graphite oxide modified polyurethane foam (PUF)	Crystal Violet: 64.935 mg g^{-1}	[95]
Magnetic graphene oxide (MGO)	Methylene Blue: 64.23 mg g^{-1} Orange G (OG): 20.85 mg g^{-1}	[33]

But these researches are for model dyes and still in pre-mature stage. So, there have rooms to develop attractive and cheap technique for the preparation of graphene and its derivative and their application for the removal of industrially used synthetic dyes.

Chapter 3

Materials and Methods

3.1. Materials

Commercial dye FD-R H/C, TURQUOISE GN (TGN) and Maxilon Blue (MBG) were collected as commercial grade from a local dyeing industry of Bangladesh. Graphite powder (≤50 μm 99.5%), hydrogen peroxide (30%) and hydrazine hydrate (88%) were bought from Merck (India), sulfuric acid (98%), nitric acid (65%) were obtained from Active Fine Chemicals (Bangladesh), potassium permanganate was purchased from Merck (Germany), sodium nitrate was purchased from Uni-chem (China), hydrochloric acid (37%) was purchased from RCI Labscan (Thailand) and sodium alginate was purchased from Research-Lab Fine Chem. Industries (India).

The name of TURQUOISE GN is (Copper,[29H,31H-phthalocyaninato(2)-N29,N30,N31,N32]-,sulfo[[4-[[(sulfooxyl)ethyl]sulfonyl]phenyl]amino]sulfonyl derivative. TURQUOISE GN is an anionic reactive dye and also known as reactive blue 21 (M.F-$C_{40}H_{25}CuN_9O_{14}S_5$ and M.W-1079.535 g/mol) [96]. It is commercially available and widely used in textile dyeing processes.

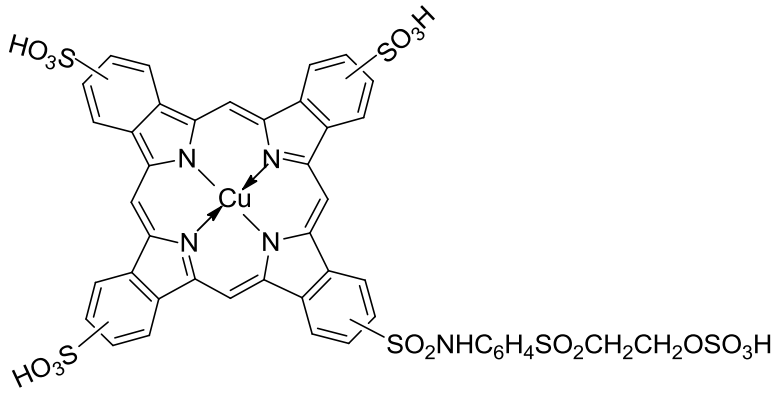

Fig. 2: Molecular structure of dyeTurquoise GN

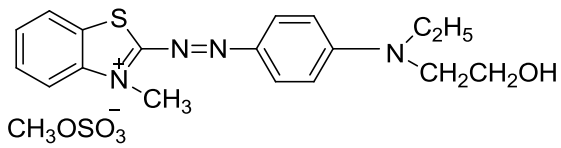

Fig. 3: Molecular structure of dye Maxilon Blue (GRL)

The structure or chemical formula of FD-R H/C was not known to us because of the policy of the supplier. So, the functional group present in the dye was determined by IR-spectroscopy.

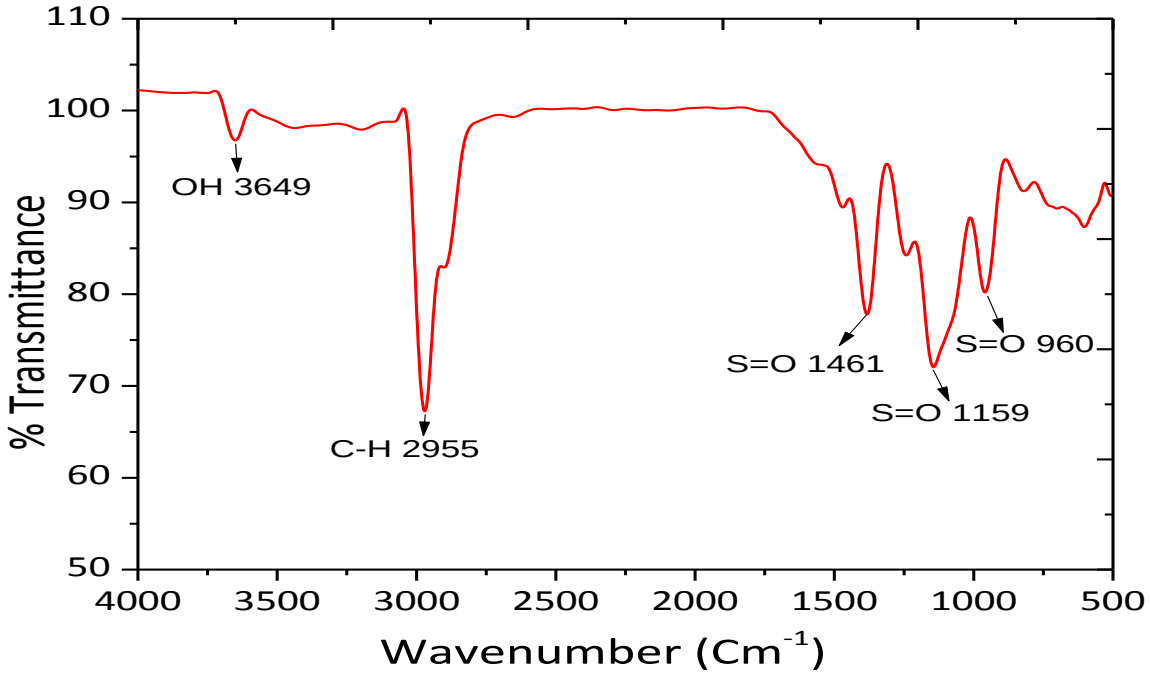

Fig. 4: IR spectrum of dye FD-R H/C

Presence of sulphur in dye is also detected by Lassagine's test. Lassagine extract forms black precipitate with lead acetate.

$$Pb(CH_3COO)_2 + Na_2S \longrightarrow PbS + CH_3COONa$$

3.2. Methods of synthesis of adsorbents

3.2.1. Synthesis of graphene oxide (GO)

Graphene oxide was prepared by modified Hummers' method [97]. Briefly, in a round bottom flask graphite powder (3.0 g) was dispersed in the 3:1 mixture of concentrated H_2SO_4 and concentrated HNO_3 (75ml) with vigorous stirring. Then $KMnO_4$ (9.0 g) and $NaNO_3$ (1.5 g) were added slowly to the flask and stirred for 2 hours and the mixture was stirred overnight to afford a thick paste. Then deionized (DI) water (90 ml) was added and stirred for 3 hours to produce deep brown reaction mixture followed by addition of DI water (300 ml) and 30% H_2O_2 (20 ml) with continuous stirring until the color changed to bright yellow. Finally, 5% HCl (200ml) was added to remove the manganese ions from graphene oxide. The synthesized GO was washed with DI water (10× 500 ml) to adjust pH to 7.

.

3.2.2. Synthesis of reduced graphene oxide (RGO)

Graphene oxide (500 mg) was dispersed in DI water (500 ml) through sonication. Then hydrazine hydrate (0.82 ml or 13.5 mmol) was added and the mixture was heated at 90°C for 4 hrs in an oil bath. After that the unreacted hydrazine was removed through washing with DI water.

3.2.3. Preparation of sodium-alginate (SA) and GO (SA-GO) composite

Graphene oxide (300 mg) was dispersed in DI water (150 ml) through sonication. Then Na-alginate (3 g) and $CaCO_3$ (0.75 g) were mixed with it. After that the mixture was added dropwise to 2 % HCl. As a result porous composite of SA-GO was produced. Finally, the product was washed with distilled water upto pH reached to 7.

3.3. Characterization method of GO, RGO and SA-GO composite

Composition of GO and RGO were determined by elemental analysis with Vario Micro CHNS. The chemical structures of graphite and GO were studied with Fourier transformed infrared (FT-IR) spectrophotometer (IR Prestige-21, SHIMADZU, Japan). The morphology and microstructure of GO and RGO were studied with Environmental Scanning Electron Microscopy (ESEM) (TESCAN VEGA3). The structure of SA and SA-GO composite was studied with Scanning Electron Microscopy (SEM) (JSM-6010 PLUS/LA). The height of the prepared GO layer was measured by atomic forced microscopy, AFM (Nanosurf Acoustic Enclosure 100). X-ray diffraction of graphite, GO, RGO, SA and SA-GO composite were performed on Multipurpose X-ray diffraction system (Ultima IV) with Cu Kα radiation (λ=0.154 nm, 40 kV, 1.64 mA) in the range 05-100º. The presence of D-band and G-band in GO and RGO were determined by the Raman spectroscopy (MonoVista CRS+). Zeta potential as a function of pH for GO, RGO and SA-GO composite were measured by Malvern Zetasizer Nano-ZS analyser.

3.4. Adsorption study

The batch adsorption experiments were carried out with the variation of pH, dosage, time and initial concentration of dye. To determine the dye adsorption capacity of the adsorbents, calibration curve of the dyes were prepared by spectrophotometric method (UV-1700 Pharma Spec UV-VIS Spectrophotometer, SHIMADZU, Japan). The concentration of the dye solutions before and after adsorption were determined with respect to these calibration curves and adsorption capacity q (mg/g), equilibrium adsorption capacity

q_e (mg/g) and %of removal were calculated. The adsorption capacity were calculated by the following equation-

$$q = \frac{(C_0 - C_t) \times V}{W} \quad (1)$$

where,

C_o = initial concentration of dye (ppm)

C_t = concentration of dye (ppm) at time t

V= volume (L) of the dye solution and

W= mass (g) of the adsorbent.

The equilibrium adsorption capacity q_e (mg/g) was calculated by the following equation-

$$q_e = \frac{(C_0 - C_e) \times V}{W} \quad (2)$$

where C_e = concentration of dye (ppm) at equilibrium condition.

and the % of dye removal was calculated by the following formula-

$$\% \text{ removal} = \frac{(C_0 - C_t) \times 100}{Co} \quad (3)$$

3.4.1. Study the effect of pH on adsorption

3.4.1.1. Effect of pH on adsorption of dye FD-R H/C by GO

To study the effects of pH on adsorption of dye FD-R H/C by GO, a set of 9 experiments were carried out. 10 ml of 200 ppm dye solutions were taken in 9 volumetric flasks and pH were adjusted from 2-10 using dilute HCl and NaOH solutions. Then 10 mg of disperse GO was added in each solution and the mixtures were shaken at 200 rpm for 60 minutes. After shaking the mixtures were filtered and absorbance of the filtrates were measured by UV-Vis spectroscopy at 409 nm. Then concentrations of the solutions were determined with respect to the standard calibration curve. The adsorption capacities at different pH were calculated using eq. (1).

3.4.1.2. Effect of pH on adsorption of dye TGN by GO

The adsorption experiments of dye TGN by GO at different pH were carried out following the same procedure as 3.4.1.1. For this, 10 mg of disperse GO were added to the solutions and the mixtures were shaken for 10 minutes and the absorbance of the filtrates were measured at 660 nm.

3.4.1.3. Effect of pH on adsorption of dye MBG by GO

For the adsorption of dye MBG by GO, pH effects were carried out following the same procedure as 3.4.1.1. Here, 4 mg of disperse GO were added to 10 ml 1000 ppm dye solutions and the mixtures were shaken for 30 minutes. Then the absorbance of the filtrates were measured at 554 nm.

3.4.1.4. Effect of pH on adsorption of dye TGN by RGO

The adsorption of dye TGN by RGO at different pH were carried out following the same procedure as 3.4.1.1. For this, a set of 6 experiments were carried out and 10 mg of disperse RGO were added to 10 ml 700 ppm dye solutions. Then the mixtures were shaken for 30 minutes and the absorbance of the filtrates were measured at 660 nm.

3.4.1.5. Effect of pH on adsorption of dye MBG by SA-GO composite

For the adsorption of dye MBG by SA-GO composite, pH effects were carried out following the same procedure as 3.4.1.1. In this case, a set of 5 experiments were carried out and 9 mg of SA-GO composite were added to 10 ml 700 ppm dye solutions. Then the absorbance of the filtrates were measured at 554 nm.

3.4.2. Study the effect of adsorbent dosage on adsorption

3.4.2.1. Effect of adsorbent dosage on adsorption of dye FD-R H/C by GO

To determine the optimum dosage of GO for the adsorption of dye FD-R H/C, a set of 6 experiments were carried out. For this, 10 ml of 200 ppm of dye solutions were taken in 6 volumetric flasks and pH were adjusted at 2 by using dilute HCl solution. Then 5, 10, 15, 20, 25, 30 mg of disperse GO were added to the flasks and the mixtures were shaken for 60 minutes at 200 rpm. After shaking the mixtures were filtered and absorbance of the filtrates were measured by UV-Vis spectroscopy at 409 nm. Concentrations of the solutions were determined with respect to the standard calibration curve. The adsorption capacities and % of removals were calculated using eq. (1) and eq. (3), respectively. Then the values of adsorption capacities and % of removals were plotted against adsorbent dosage. The point of intersection of the values of adsorption capacities and % of removals was considered as optimum dosage.

3.4.2.2. Effect of adsorbent dosage on adsorption of dye TGN by GO

For the adsorption of dye TGN by GO, the optimum dosage were determined following the same procedure as 3.4.2.1. Here, a set of 4 experiments were carried out using 10 ml 300

ppm dye solutions. Then 5, 10, 15, 20 mg of disperse GO were added to the flasks and the mixtures were shaken for 10 minutes. The absorbance of the filtrates were measured by UV-Vis spectroscopy at 660 nm.

3.4.2.3. Effect of adsorbent dosage on adsorption of dye MBG by GO

The optimum dosage of adsorbent for the adsorption of dye MBG on GO, the experiments were carried out following the same procedure as 3.4.2.1. Here, a set of 4 experiments were carried out using 10 ml 1000 ppm dye solutions at pH of 7. Then 2, 5, 8, 10 mg of disperse GO were added to the flasks and the mixtures were shaken for 30 minutes. The absorbance of the filtrates were measured by UV-Vis spectroscopy at 554 nm.

3.4.2.4. Effect of adsorbent dosage on adsorption of dye TGN by RGO

For the adsorption of dye TGN by RGO, the optimum dosage were determined following the same procedure as 3.4.2.1. For this, a set of 4 experiments were carried out using 10 ml 700 ppm dye solutions at pH of 7. Then 5, 10, 15, 20 mg of disperse RGO were added to the flasks and the mixtures were shaken for 30 minutes. The absorbance of the filtrates were measured by UV-Vis spectroscopy at 660 nm.

3.4.2.5. Effect of adsorbent dosage on adsorption of dye MBG by SA-GO composite

The optimum dosage of adsorbent for the adsorption of dye MBG on SA-GO composite**,** the experiments were carried out following the same procedure as 3.4.2.1. Here, a set of 4 experiments were carried out using 10 ml 1000 ppm dye solutions at pH of 7. Then 5, 10, 15, 20 mg of SA-GO composite were added to the flasks and the mixtures were shaken for 60 minutes. The absorbance of the filtrates were measured by UV-Vis spectroscopy at 554 nm.

3.4.3. Study the effect of dye concentration and contact time on adsorption

3.4.3.1. Effect of dye concentration and contact time on adsorption of dye FD-R H/C on GO

To study the effect of dye concentration and contact time on the adsorption of dye FD-R H/C on GO, 10 ml of 100 ppm dye solutions were taken in 8 different volumetric flasks. Then pH of the solutions were adjusted to 2 by using dilute HCl solution and 10 mg of disperse GO were added to each solution. The mixtures were shaken at 303 K in various intervals of time ranging from 5-60 minutes at 200 rpm. After shaking the mixtures were filtered and absorbance of the filtrates were measured by UV-Vis spectroscopy at 409 nm. Then concentrations of the solutions were determined with respect to standard curve. The adsorption capacities at different pH were calculated using eq. (1). To observe the effect of

dye concentration on adsorption, similar experiments were carried out using 200 and 300 ppm dye solutions in the same intervals of time.

3.4.3.2. Effect of dye concentration and contact time on adsorption of dye TGN on GO

The adsorption experiments of dye TGN by GO at different concentrations and time were carried out following the same procedure as 3.4.3.1. In this case 10 mg of disperse GO were added to 10 ml 200 ppm dye solutions at pH of 2 and the mixtures were shaken at 303 K in various intervals of time ranging from 2-60 minutes. The absorbance of the filtrates were measured by UV-Vis spectroscopy at 660 nm. To observe the effect of dye concentration on adsorption, similar experiments were carried out using 300, 400 and 500 ppm dye solutions in the same intervals of time.

For the adsorption of dye TGN on GO, a set of 7 another experiments were carried out at pH of 7 following the same procedure as 3.4.3.1. For this the experiments were carried out using 200, 300, 400 and 600 ppm dye solutions in the intervals of time ranging from 10-60 minutes.

3.4.3.3. Effect of dye concentration and contact time on adsorption of dye MBG on GO

The adsorption experiments of dye MBG by GO at different concentrations and time were carried out following the same procedure as 3.4.3.1. In this case, a set of 6 experiments were carried out at pH of 7 and 4 mg of disperse GO were added to 10 ml 500 ppm dye solutions. Then the mixtures were shaken at 303 K in various intervals of time ranging from 5-45 minutes. The absorbance of the filtrates were measured by UV-Vis spectroscopy at 554 nm. To observe the effect of dye concentration on adsorption, similar experiments were carried out using 600, 800 and 1000 ppm dye solutions in the same intervals of time.

3.4.3.4. Effect of dye concentration and contact time on adsorption of dye TGN on RGO

The adsorption experiments of dye TGN by RGO at different concentrations and time were carried out following the same procedure as 3.4.3.1. In this case, a set of 7 experiments were carried out at pH of 7 and 10 mg of disperse RGO were added to 10 ml 400 ppm dye solutions. Then the mixtures were shaken at 303 K in various intervals of time ranging from 10-60 minutes. The absorbance of the filtrates were measured by UV-Vis spectroscopy at 660 nm. To observe the effect of dye concentration on adsorption, similar experiments were carried out using 500, 600 and 700 ppm dye solutions in the same intervals of time.

3.4.3.5. Effect of dye concentration and contact time on adsorption of dye MBG on SA-GO composite

The adsorption experiments of dye MBG by SA-GO composite at different concentrations and time were carried out following the same procedure as 3.4.3.1. In this case, a set of 7 experiments were carried out at pH of 7 and 9 mg of SA-GO composite were added to 10 ml 500 ppm dye solutions. Then the mixtures were shaken at 303 K in various intervals of time ranging from 10-90 minutes. The absorbance of the filtrates were measured by UV-Vis spectroscopy at 554 nm. To observe the effect of dye concentration on adsorption, similar experiments were carried out using 600, 800 and 900 ppm dye solutions in the same intervals of time.

The adsorption capacities at different concentrations were plotted against different period of time. For a certain concentration the adsorption capacity increased with increasing time and after certain time the adsorption capacity became almost constant. This is considered as equilibrium adsorption capacity (q_e). The concentration at which the adsorption capacity became constant was considered as equilibrium concentration (C_e).

3.4.4. Adsorption isotherms

The distribution of adsorbate molecules on the adsorbent surfaces were determined by analyzing the experimental results with Langmuir and Freundlich isotherms [98, 99]. The theoretical maximum adsorption capacities q_m were calculated by plotting C_e/q_e versus C_e according to Langmuir model. The linear form of the Langmuir isotherm is-

$$\frac{C_e}{q_e} = \frac{1}{q_m b} + \frac{1}{q_m} c_e \qquad (4)$$

where,

C_e = equilibrium concentration

q_e = equilibrium adsorption capacity

q_m = the maximum theoretical adsorption capacity and

b =Langmuir constant.

The separation factor R_L is related to Langmuir constant b, which gives a qualitative measure of the favorability of the adsorption process; R_L greater than 1 indicates unfavorable monolayer adsorption while R_L between 0 and 1 indicates a favorable monolayer adsorption process [32].

The separation factor R_L is related to b through the equation-

$$R_L = \frac{1}{1+C_m b} \quad (5)$$

where C_m is the maximum initial dye concentration used in the adsorption experiments.

Freundlich isotherm assumes multilayer adsorption with non-uniform distribution of the adsorbents. The following Freundlich isotherm Eq. (6) were used for the present study-

$$\ln q_e = \ln k_F + \frac{1}{n} \ln c_e \quad (6)$$

The multilayer adsorption mechanisms were tested using eq. (6) by plotting $\ln C_e$ versus $\ln q_e$. The value of n gives an assumption about favorability of adsorption. As n decreases, the adsorption becomes more difficult (good adsorption at n = 2-10, difficult adsorption at n = 1-2 and poor adsorption at n < 1) [32].

3.4.5. Adsorption kinetics

Adsorption kinetics are of great significance to evaluate the performance of an adsorbent and gain insight into the underlying mechanisms. In this study, two kinetic models were employed to describe the adsorption processes. In 1998, Lagergren presented pseudo-first-order rate equation and In 1995 Ho and Mckay presented pseudo-second order rate equation to describe the kinetic process. The linear form of pseudo-first-order rate equation is

$$\log(q_e - q_t) = \log q_e - \frac{k_1}{2.303} t \quad (7)$$

where,

q_e= equilibrium adsorption capacity

q_t = adsorption capacity at time t

k_1= rate constant of pseudo-first order adsorption (L/min).

Pseudo-first-order model was obtained by plotting $\log(q_e - q_t)$ versus t, where a linear relationship between $\log(q_e - q_t)$ and t was observed.

The linear form of pseudo-second-order rate equation is-

$$\frac{t}{q_t} = \frac{1}{k_2 q_e^2} + \frac{1}{q_e} t \quad (8)$$

where,

k_2 = the rate constant of pseudo-second order adsorption (g/mg min).

The pseudo-second-order model was obtained by plotting t/q_t versus t.

3.4.6. Thermodynamic study of dye adsorption

To observe the effect of temperature on dye adsorption, the experiments were carried out at three different temperatures (303K, 313 and 323 K). The Gibb's free energy (ΔG^o), the average standard enthalpy change (ΔH^o) and entropy change (ΔS^o) were also calculated. The changes in Gibb's free energy (ΔG^o) gives an assumption about the adsorption process. An increase in ΔG^o values with an increase in temperature indicate physical adsorption and the process is favorable at low temperature. In this study, the changes in Gibb's free energy for dye adsorption on adsorbents at different temperature were calculated by Equation-

$$\Delta G^o = -RT \ln k_d \quad (9)$$

where,

k_d is the distribution constant for the equilibrium sorption

R is the universal gas constant (8.314 J mol^{-1} K^{-1}) and T is the absolute temperature (K). K_d was calculated by using Eqation-

$$k_d = \frac{q_e}{c_e} \quad (10)$$

The average standard enthalpy change ΔH^o and entropy change ΔS^o for the adsorption were calculated using the van't Hoff equation as follow-

$$\ln k_d = \frac{-\Delta H^0}{RT} + \frac{\Delta S^0}{R} \quad (11)$$

A straight line was obtained by plotting $\ln k_d$ versus 1/T. The value of standard enthalpy change ΔH^o and entropy change ΔS^o were obtained from the slope and intercept, respectively.

3.4.7. Regeneration method of the adsorbents

Regeneration ability of an adsorbent provide useful information about the effectiveness and commercial application of an adsorbent. In our study, all the adsorbents were regenerated by 2% HCl and used for adsorbent study.

Chapter 4

Result and Discussion

4.1. Part 1. Synthesis and characterization of graphene oxide (GO) and its application for the removal of dyes FD-R H/C, TURQUOISE GN and Maxilon Blue (GRL) from aqueous solutions

4.1.1 Synthesis of graphene oxide (GO)

Graphene oxide was prepared by modified Hummers' method. Here Graphite powder was oxidized to graphene oxide by the mixture of concentrated H_2SO_4 and HNO_3. To complete the oxidation $KMnO_4$, $NaNO_3$ and H_2O_2 were also added. As a result oxidation as well as layer separation of graphite powder took place. Moreover, oxygenated functional group (-COOH group) was introduced into the graphene oxide structure [100].

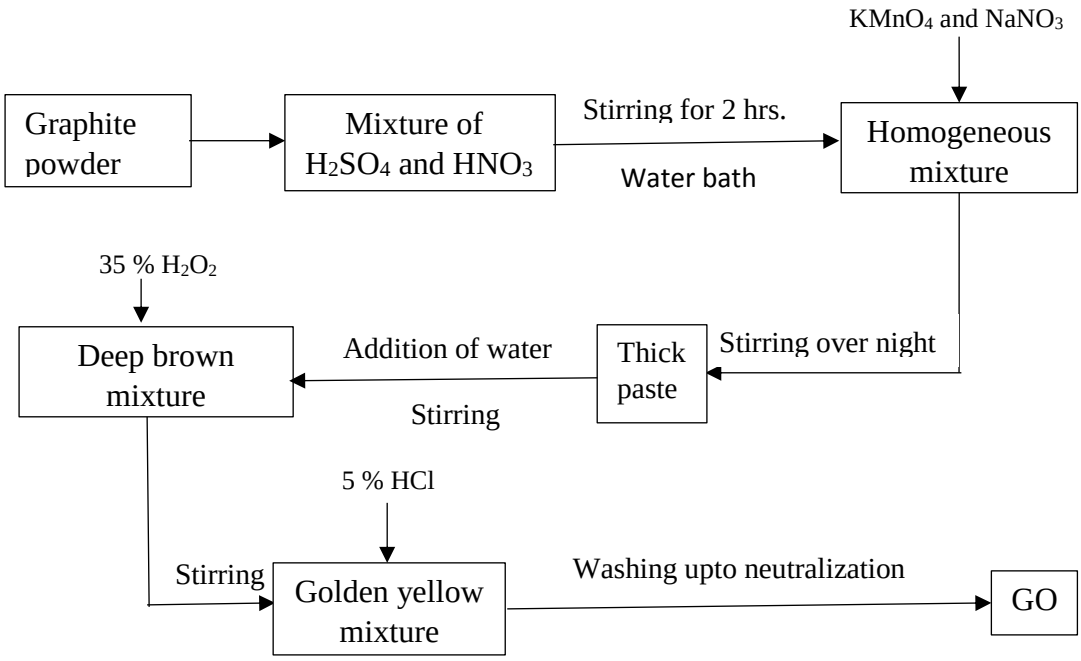

Fig. 5: Flow diagram of graphene oxide (GO) synthesis

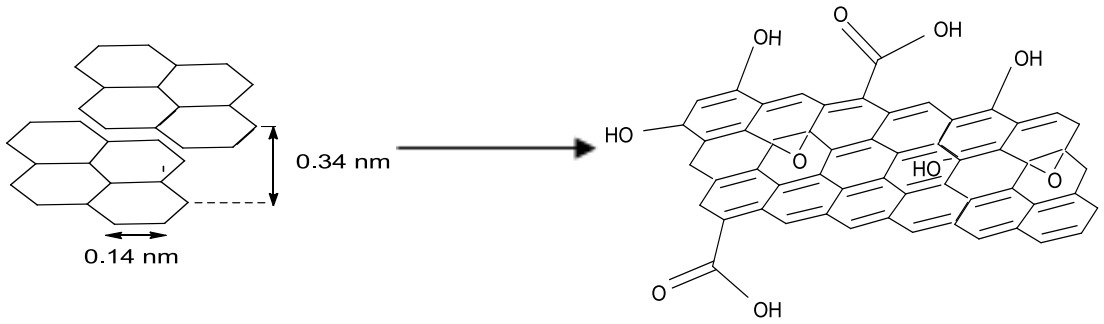

Fig. 6: Oxidation of graphite powder to graphene oxide

4.1.2. Characterization of GO

4.1.2.1. Elemental analysis

Composition of GO was determined by elemental analysis and found to contain 40.99 % C, 3.09 % H, 4.08 % N and 0.40 % S. It was also found to contain a considerable amount of oxygen (51.44 %) that was determined indirectly. The elemental analysis was in good agreement with the literature [101].

4.1.2.2. Fourier transform infrared (FTIR) spectroscopy

The functional groups present in graphite and GO were studied with FTIR spectroscopic analysis.

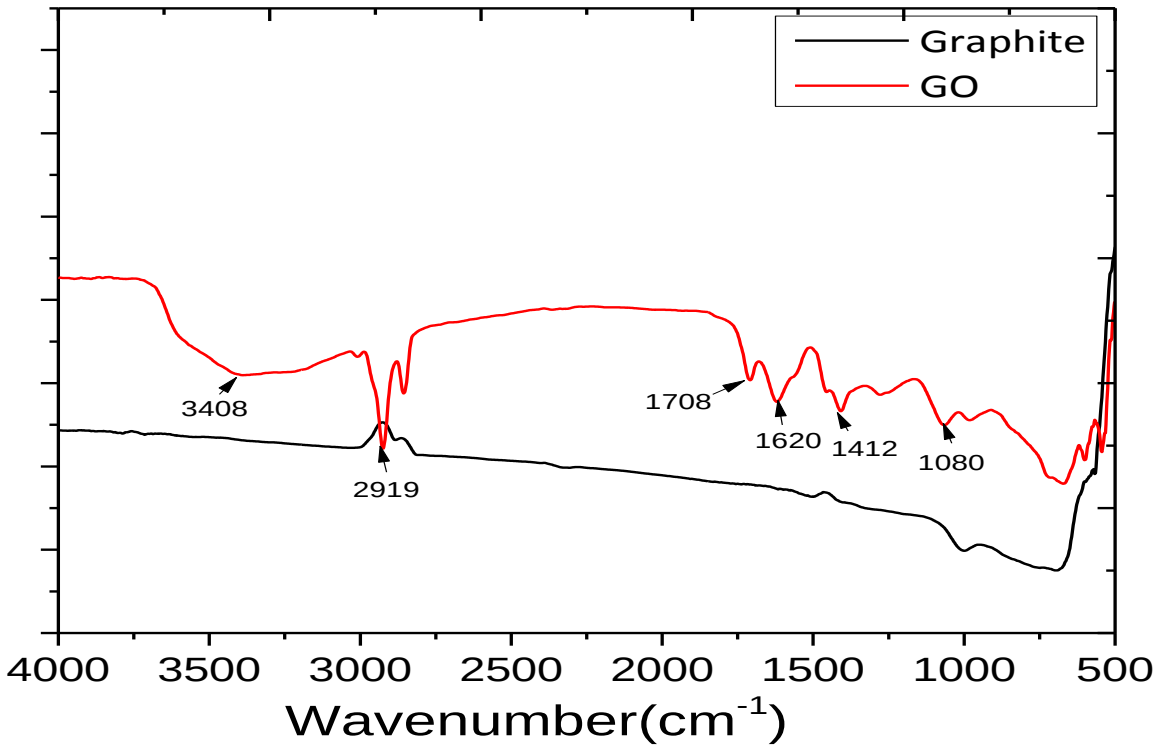

Fig. 7: FT-IR spectra of graphene oxide and graphite powder

From Fig. 7, it was evident that for GO vibrational peaks were observed at 1080 cm^{-1}, 1412 cm^{-1}, 1620 cm^{-1}, 1708 cm^{-1}, 2919 cm^{-1} and 3408 cm^{-1} which were attributable to carboxy C-O, C-OH bending, aromatic C=C, carbonyl stretching C=O, C-H stretching and –OH groups, respectively. These data indicate the presence of –COOH group in GO, while the peaks represent –COOH group were absent in case of graphite powder. Thus it was evident that graphite powder was oxidized to graphene oxide under the reaction protocol [102, 103].

4.1.2.3. Environmental scanning electron microscopy (ESEM)

The morphology and microstructure of GO were studied with Environmental scanning electron microscopy ESEM (Fig. 8). The figure showed fluffy and layered structure with many wrinkled sheets. It is assumed that the fluffiness and wrinkles in the GO are due to oxidation and layer separation.

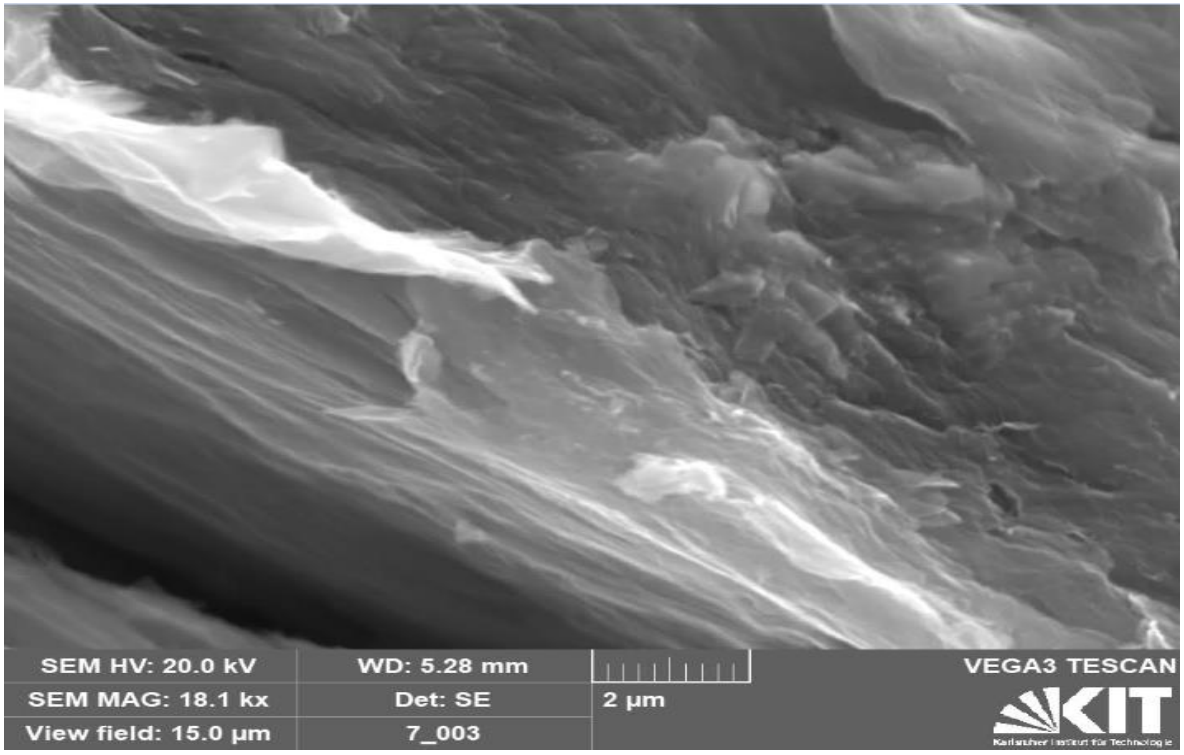

Fig. 8: ESEM image of graphene oxide

4.1.2.4. Atomic forced microscopy (AFM)

To determine the layer thickness of the prepared GO layer the sample was prepared by drop-casting onto a glass substrate for AFM study. From the AFM image (Fig. 9) and the section line analysis the thickness was found to be 7.37 nm. From the result it can be assumed that the prepared film is formed by multilayer GO deposition [104].

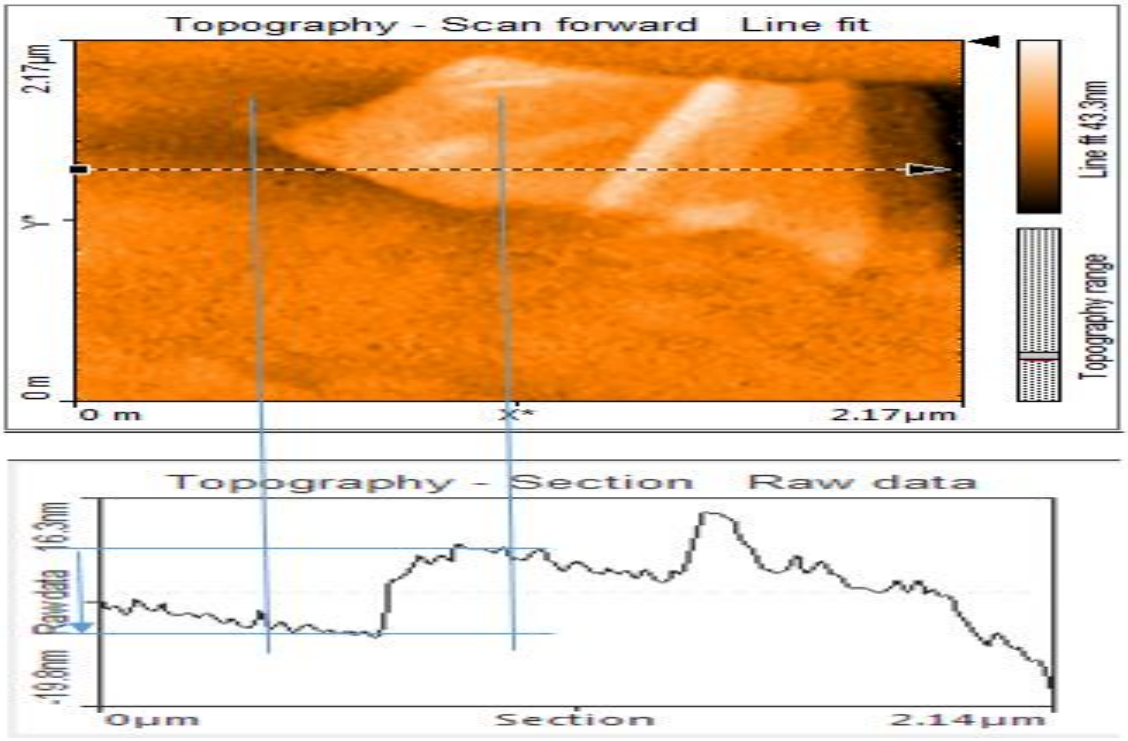

Fig. 9: AFM height image and the section line analysis of graphene oxide

4.1.2.5. X-Ray diffraction (XRD) analysis of graphite powder and GO

The XRD patterns of graphite and GO was represented in Fig. 10. A sharp and strong peak was observed at 2θ=26.73º for graphite powder corresponding to an interlayer spacing of 3.33 Å. This was due to the crystalline structure of graphite.

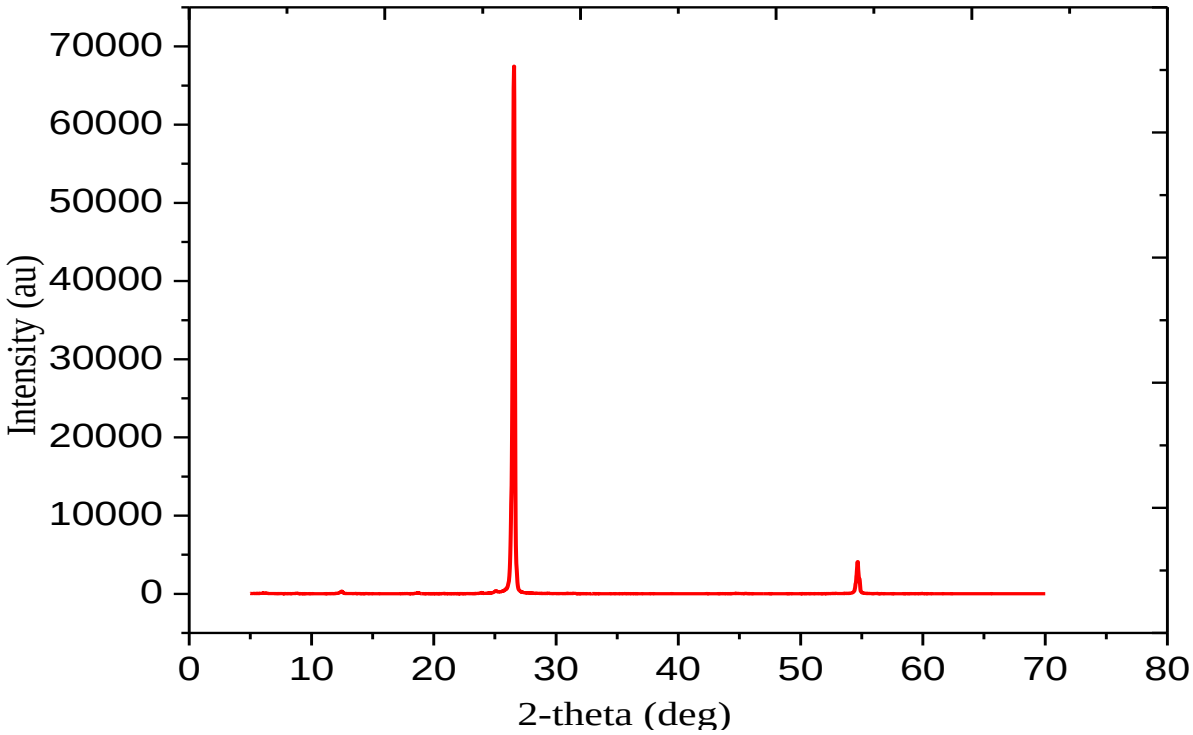

Fig. 10: XRD patterns of graphite powder

For GO a broad peak was observed at 2θ=9.97° (Fig. 11) corresponding to an interlayer spacing of 8.87 Å. The shift of the peak of GO compared to graphite powder was assumed due to the damage of the crystalline structure of graphite resulting the formation of amorphous structure and introduction of oxygen [105, 106].

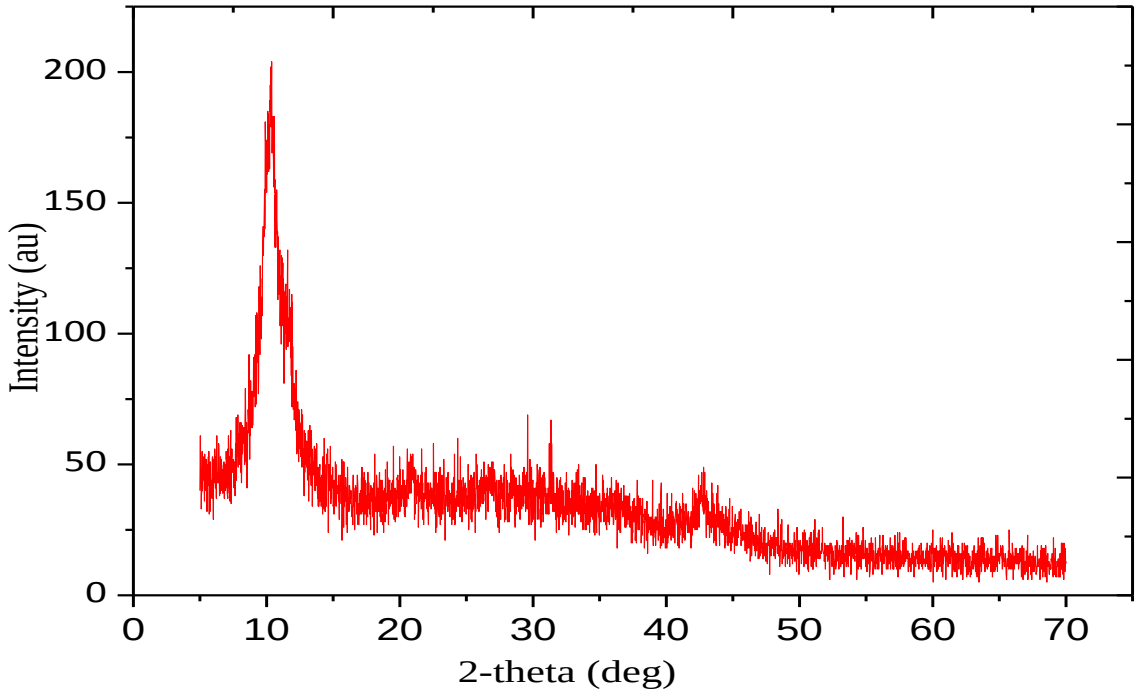

Fig. 11: XRD patterns of graphene oxide

4.1.2.6. Raman spectrum analysis of GO

Raman spectrum of GO (Fig. 12) confirmed the existence of both the D-band and G-band.

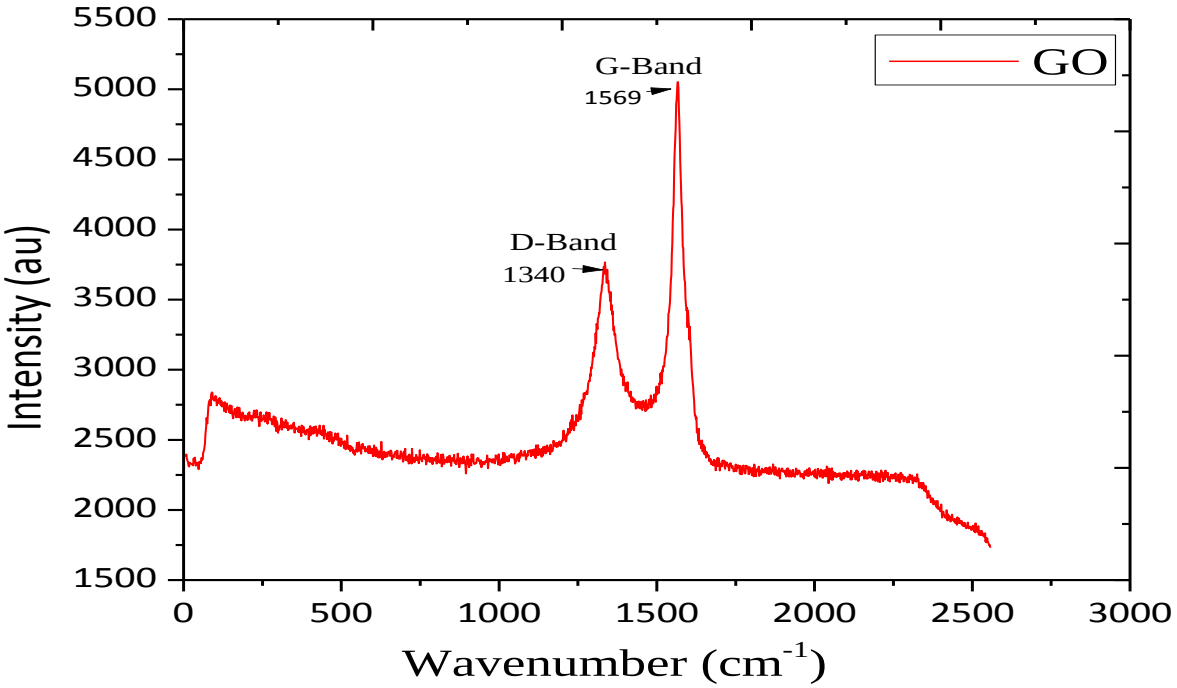

Fig. 12: Raman spectrum of graphene oxide

The G-band was located at 1569 cm^{-1} and the D-band was located at 1340 cm^{-1}. These values were in good agreement with the literature published elsewhere. The existence of D-band revealed the presence of defect sites in the GO sheets and the size of the in-plane sp^2 domain [107, 108]. The intensity ratio of D-band and G-band, (I_D/I_G) was 0.74 for GO.

4.1.2.7. Zeta potential value of graphene oxide

Zeta potential is the potential difference existing between the surface of a solid particle immersed in a conducting liquid and the bulk of the liquid. Zeta potential determination is a significant characterization technique of nanocrystals to estimate the surface charge, which can be employed for understanding the physical stability of nanosuspensions. A large positive or negative value of zeta potential of nanocrystals indicate good physical stability of nanosuspensions due to electrostatic repulsion of individual particles. A zeta potential value other than −30 mV to +30 mV is generally considered to have sufficient repulsive force to attain better physical colloidal stability. On the other hand, a small zeta potential value can result in particle aggregation and flocculation due to the van der Waals attractive forces act upon them. These may result in physical instability.

Table 5: pH vs Zeta potential data of GO

pH	2	4	6	8	10
Zeta potential (mV)	-18.1	-20.0	-29.1	-34.6	-36.0

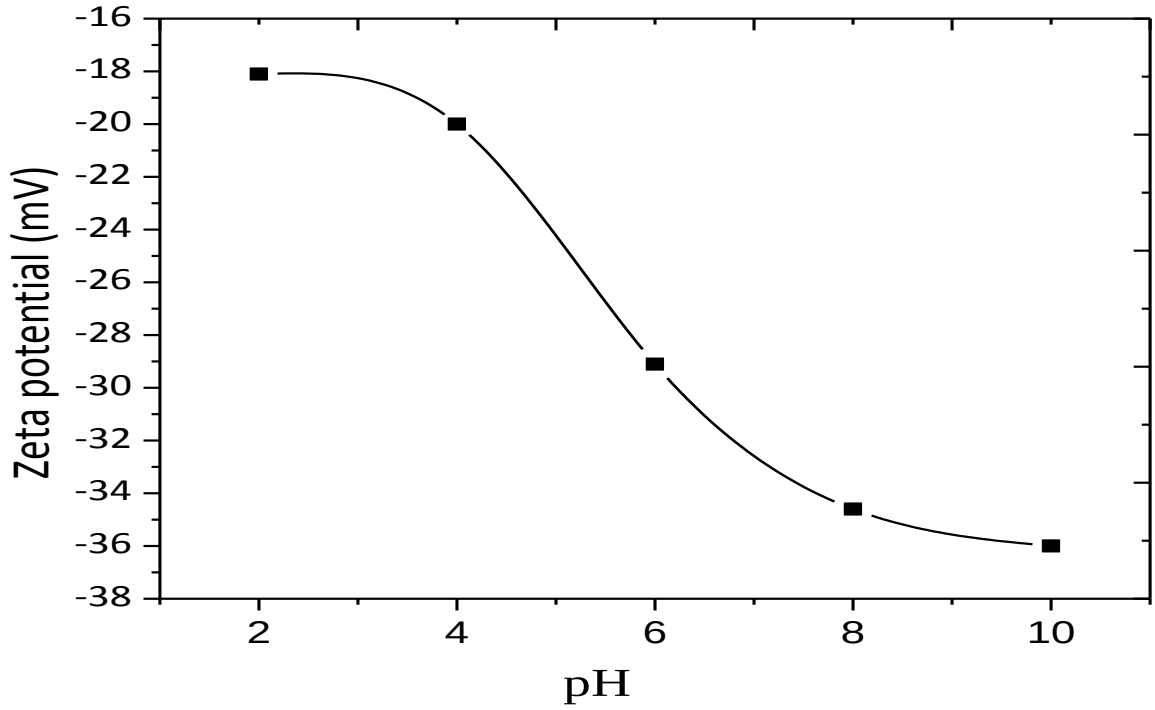

Fig. 13: Zeta potential value of GO at different pH

Zeta potential of GO as a function of pH was also studied. For this study GO sample was prepared by dispersing GO in DI water. The analysis was carried out in the pH range of 2-10. The results showed that (Table-5, Fig. 13) the zeta potential values of GO were negative over the whole pH range and the values varied from -18.1 to -36 mV with an increase of pH from 2 to 10. The zeta potential values were also in good agreement with the literature values [109].

4.1.3. Adsorption of dyes on GO

4.1.3.1. Adsorption of dye FD-R H/C on GO

4.1.3.1.1. Calibration curve of dye FD-R H/C

A calibration curve was prepared using 10-200 ppm dye solution for FD-R H/C by spectrophotometric method at 409 nm. Then adsorption capacity and % removal were calculated by measuring of the dye concentration before and after adsorption with respect to this calibration curve and employing the Eq. (1) and Eq. (3), respectively.

Table 6: Concentration Vs absorbance data of dye FD-R H/C

Concentration (ppm)	10	20	30	50	75	100	125	150	175	200
Absorbance	0.244	0.358	0.494	0.764	1.065	1.495	1.817	2.142	2.358	2.799

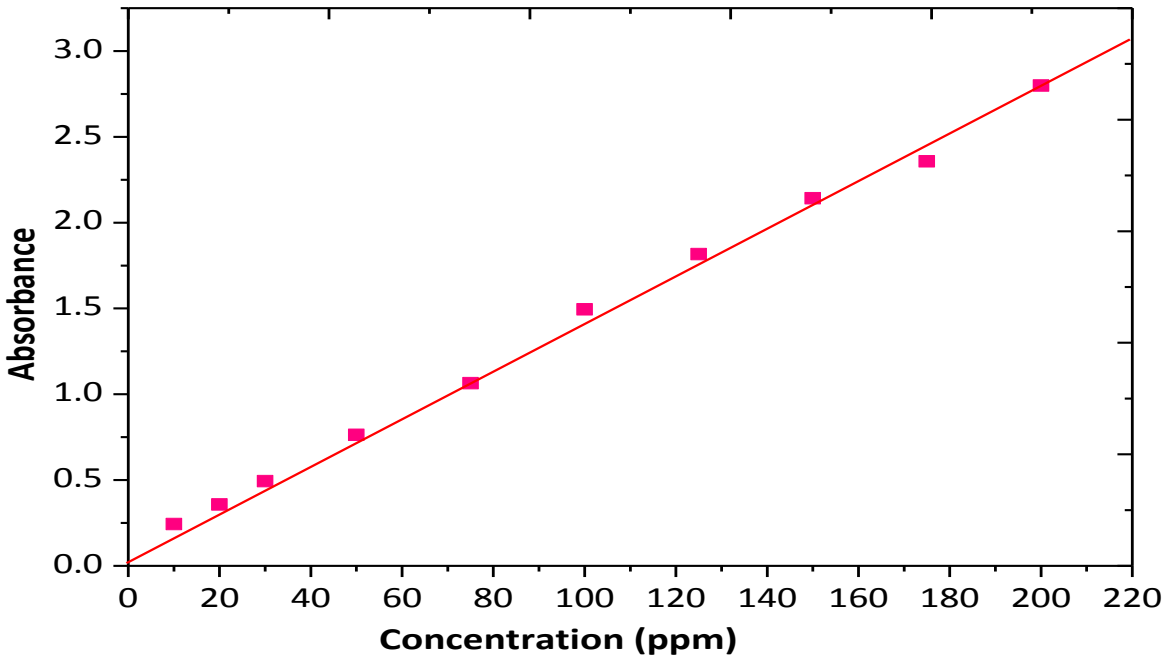

Fig. 14: Calibration curve of dye FD-R H/C

4.1.3.1.2. Effect of pH on adsorption of dye FD-R H/C by GO

pH of a solution is a very important parameter in adsorption study because it can change the surface charge of adsorbent and adsorbate. To study the effects of pH on adsorption of dye FD-R H/C by GO, a set of 9 experiments were studied. Here 10 ml of 200 ppm dye solutions were taken in 10 ml volumetric flasks and pH were adjusted from 2-10 using dilute HCl and NaOH solutions. Then 10 mg of disperse GO was added in each solution and the mixtures were shaken at 200 rpm for 60 minutes. After shaking the mixtures were filtered and absorbance of the filtrates were measured by UV-Vis spectroscopy at 409 nm. Then concentrations of the solutions were determined with respect to the standard calibration curve (Fig. 14). The adsorption capacities at different pH were calculated using Eq. (1). The results showed that maximum adsorption capacity was 133.99 mg/g (Table-7, Fig. 15) at pH of 2 and decreased with increasing pH.

Table 7: pH vs adsorption capacity data of GO for dye FD-R H/C

pH	2	3	4	5	6	7	8	9	10
Adsorption capacity (mg/g)	133.99	66.38	63.39	56.19	51.39	47.56	42.23	38.57	31.25

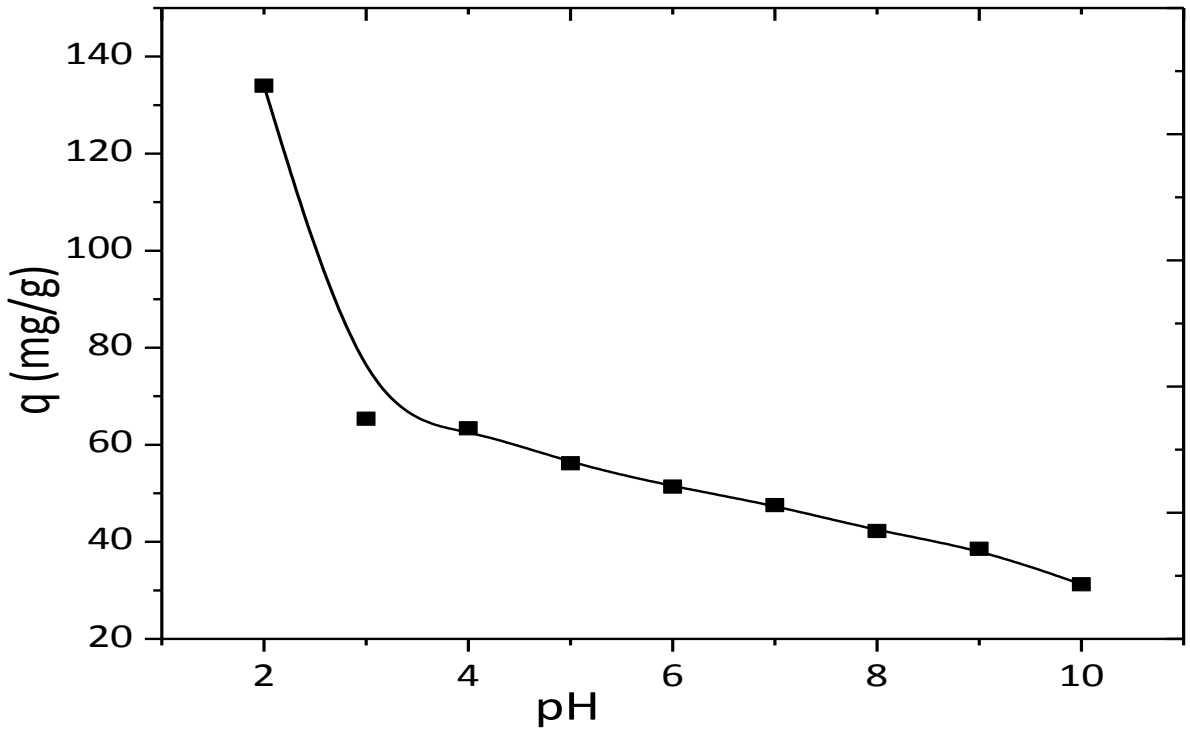

Fig. 15: Effect of pH on adsorption of dye FD-R H/C by GO

It is assumed that at higher pH carboxyl groups of GO dissociated extensively and surface of GO became highly negatively charged [110], while at higher pH the entire dye molecules existed as anion (Dye^-) which is more water soluble and underwent electrostatic repulsion with the negatively charged surface of GO and thus resulted lower adsorption. On the other hand at low pH some of the carboxyl groups of GO was protonated and formed positive ions [111] and demonstrated electrostatic attraction between anionic dye and adsorbent, which led to the higher adsorption.

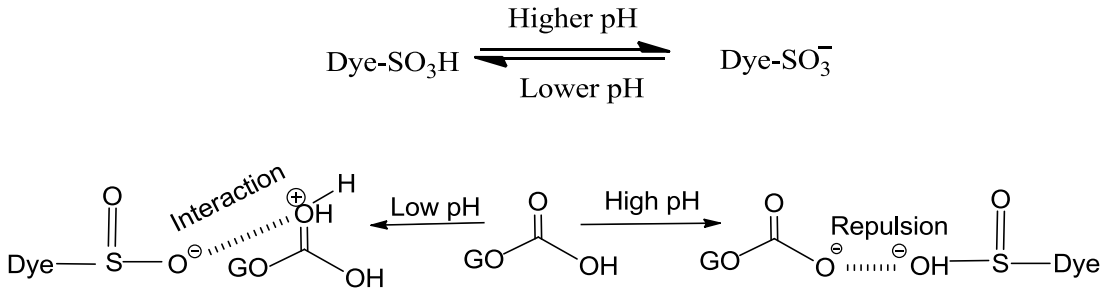

Fig. 16: Mechanism of dye FD-R H/C adsorption on GO at low and high pH

4.1.3.1.3. Effect of adsorbent dosage on adsorption of dye FD-R H/C by GO

The effects of adsorbent dosage on adsorption of dye were also studied. To determine the optimum dosage of GO for the adsorption of dye FD-R H/C, a set of 6 experiments were carried out. For this, 10 ml of 200 ppm of dye solutions were taken in 6 volumetric flasks and pH were adjusted at 2 by using dilute HCl solution. Then 5, 10, 15, 20, 25, 30 mg of disperse GO were added to the flasks and the mixtures were shaken for 60 minutes at 200 rpm. After shaking the mixtures were filtered and absorbance of the filtrates were measured by UV-Vis spectroscopy at 409 nm. Then concentrations of the solutions were determined with respect to the standard calibration curve (Fig. 14). The adsorption capacities and % of removals were calculated using Eq. (1) and Eq. (3), respectively. Then the values of adsorption capacities and % of removals were plotted against adsorbent dosage. It was apparent that (Table-8, Fig. 17) with the increase of adsorbent dosage adsorption capacity decreased but percentage removal of dye increased.

Table 8: Dosage Vs adsorption capacity and % removal data of GO for dye FD-R H/C

Dosage (mg)	5	10	15	20	25	30
Adsorption capacity (mg/g)	161.52	133.99	101.07	93.16	76.10	64.29
% of removal	40.38	67.00	75.80	93.16	95.12	96.43

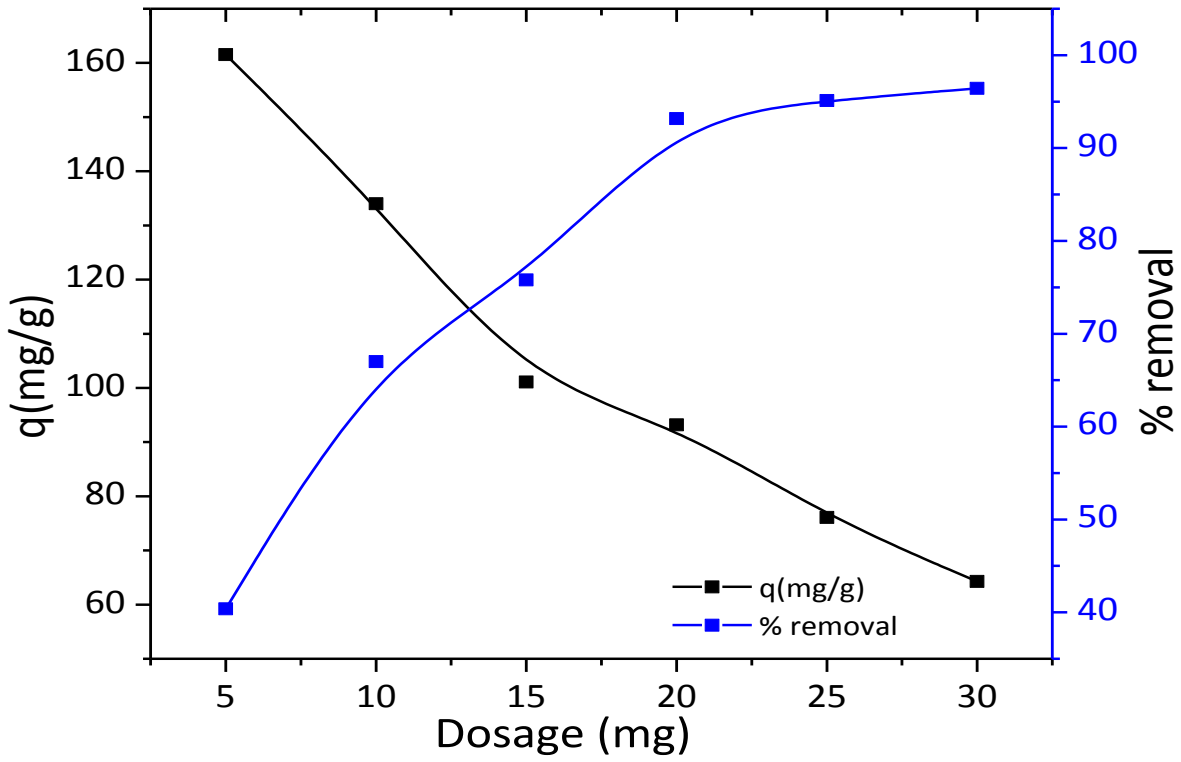

Fig. 17: Effect of adsorbent dosage on adsorption of dye FD-R H/C by GO

It is readily understood that with the increase of adsorbent dose, the amount of adsorbate per unit mass of adsorbent decreased [112] and demonstrate lower adsorption capacity. The point of intersection of the values of adsorption capacities and % of removals was considered as optimum dosage. It was observed that at dosage of 13mg/10 ml solution demonstrate the best percentage removal as well as the best adsorption capacity. However for simplicity 10 mg/10 ml solution dosage were maintained throughout the study.

4.1.3.1.4. Effect of dye concentrations and contact times on adsorption of dye FD-R H/C by GO

To study the effect of dye concentration and contact time on the adsorption of dye FD-R H/C on GO, a set of 8 experiments were carried out. Here, 10 ml of 100 ppm dye solutions were prepared in 8 different volumetric flasks. pH of the samples were adjusted at 2 by using HCl solution and 10 mg of disperse GO were added to each solution. Then the mixtures were shaken at 303 K in various intervals of time ranging from 5-60 minutes at 200 rpm. After shaking the mixtures were filtered and absorbance of the filtrates were measured by UV-Vis spectroscopy at 409 nm. Then concentrations of the solutions after adsorption were determined with respect to standard curve (Fig. 14). The adsorption capacities at different pH were calculated using Eq. (1). To observe the effect of dye concentration on adsorption, similar experiments were carried out using 200 and 300 ppm dye solutions in the same

intervals of time. The results showed that (Table-9, Fig. 18) adsorption capacity increased with an increase of time until it reached at equilibrium and became constant.

Table 9: Time vs adsorption capacity data of GO at different times and concentrations for dye FD-R H/C

Time (min)	100 ppm	200 ppm	300 ppm
0	0	0	0
2	43.52	78.56	125.28
5	50.36	90.78	131.62
10	59.13	107.60	133.57
15	67.47	118.23	135.13
20	74.35	128.63	136.32
30	83.39	132.38	139.57
45	83.62	132.78	140.23
60	83.63	133.29	140.92

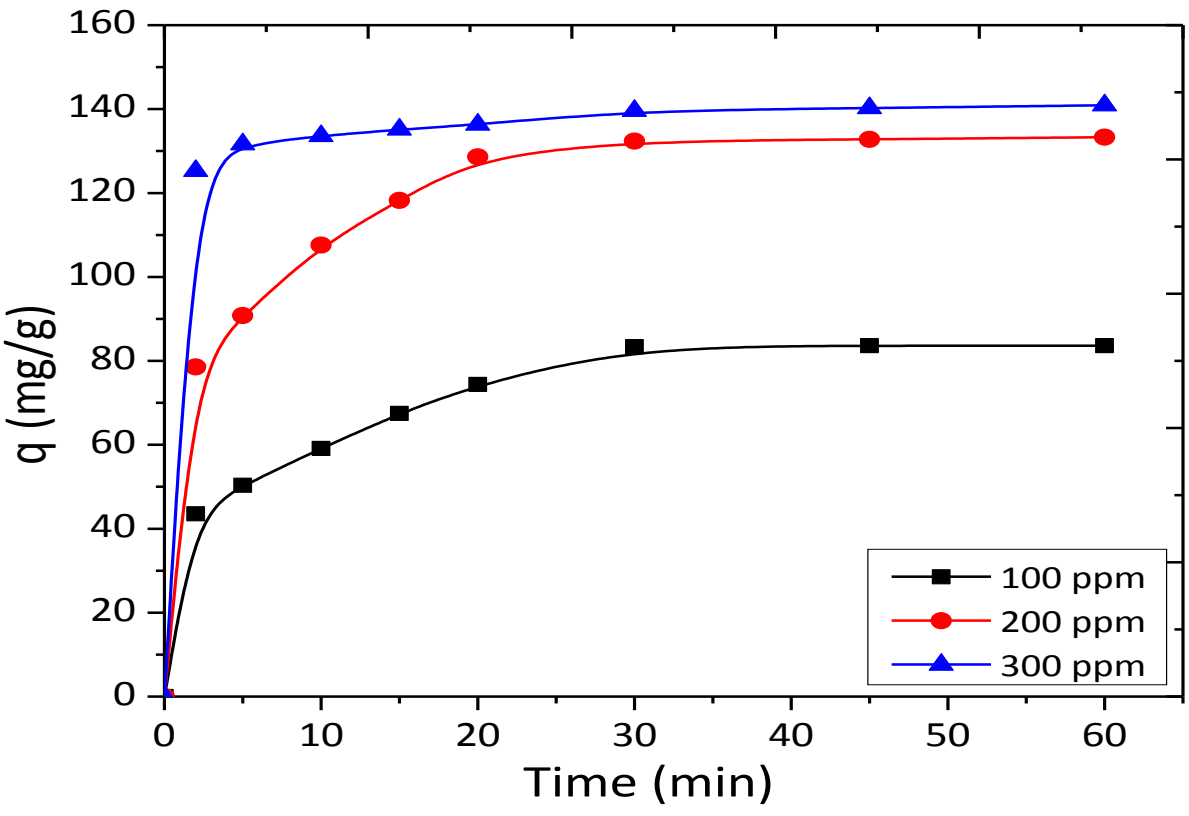

Fig. 18: Effect of dye concentration and contact time on adsorption of dye FD-R H/C by GO

The reason was, at the beginning more active sites were available and with the increase of time these sites became saturated [113]. As a result, the adsorption capacity became almost constant after a certain time. On the other hand, the adsorption capacity increased with an increase in initial dye concentrations. It was due to the increase of concentration gradient between the dye molecule in the bulk solution and adsorbent surface, resulted in higher mass transfer between the aqueous and solid phases.

4.1.3.1.5. Adsorption isotherms for adsorption of dye FD-R H/C on GO

The distribution of adsorbate molecules on the adsorbent surface was investigated by analyzing the experimental results with Langmuir and Freundlich isotherms. Langmuir isotherm assume monolayer adsorption of adsorbate on well-defined, energetically equal sites with no interaction between the adsorbate molecules [98]. On the other hand, Freundlich isotherm assume multilayer adsorption with non-uniform distribution of adsorbents [99].

4.1.3.1.5.1. Langmuir adsorption isotherm

Langmuir model was tested by Eq. (4) plotting C_e/q_e versus C_e (Table-10, Fig. 19). A linear relationship between C_e/q_e and C_e was observed with acceptable regression factor (R^2= 0.999).

Table 10: C_e and C_e/q_e data of GO at different concentrations for dye FD-R H/C

Initial concentration (ppm)	100 ppm	200 ppm	300 ppm
Equilibrium concentration (C_e)	16.61	67.62	160.43
C_e/q_e	0.20	0.51	1.15

From Langmuir isotherm ($\frac{C_e}{q_e} = \frac{1}{q_m b} + \frac{1}{q_m} c_e$) the value of slope was found 0.006641. So,

$$1/q_m = 0.006641$$

$$\therefore q_m = 151.29 \text{ mg/g}$$

The theoretical maximum sorption capacity, q_m was calculated from the slope was 151.29 mg/g.

The separation factor R_L is related to Langmuir constant, which gives a qualitative measure of the favorability of the adsorption process; R_L greater than 1 indicates unfavorable adsorption while R_L between 0 and 1 indicates a favorable process. R_L value was calculated

by Eq. (5). The value of R_L was 0.038, which indicate a very favorable monolayer adsorption process [32].

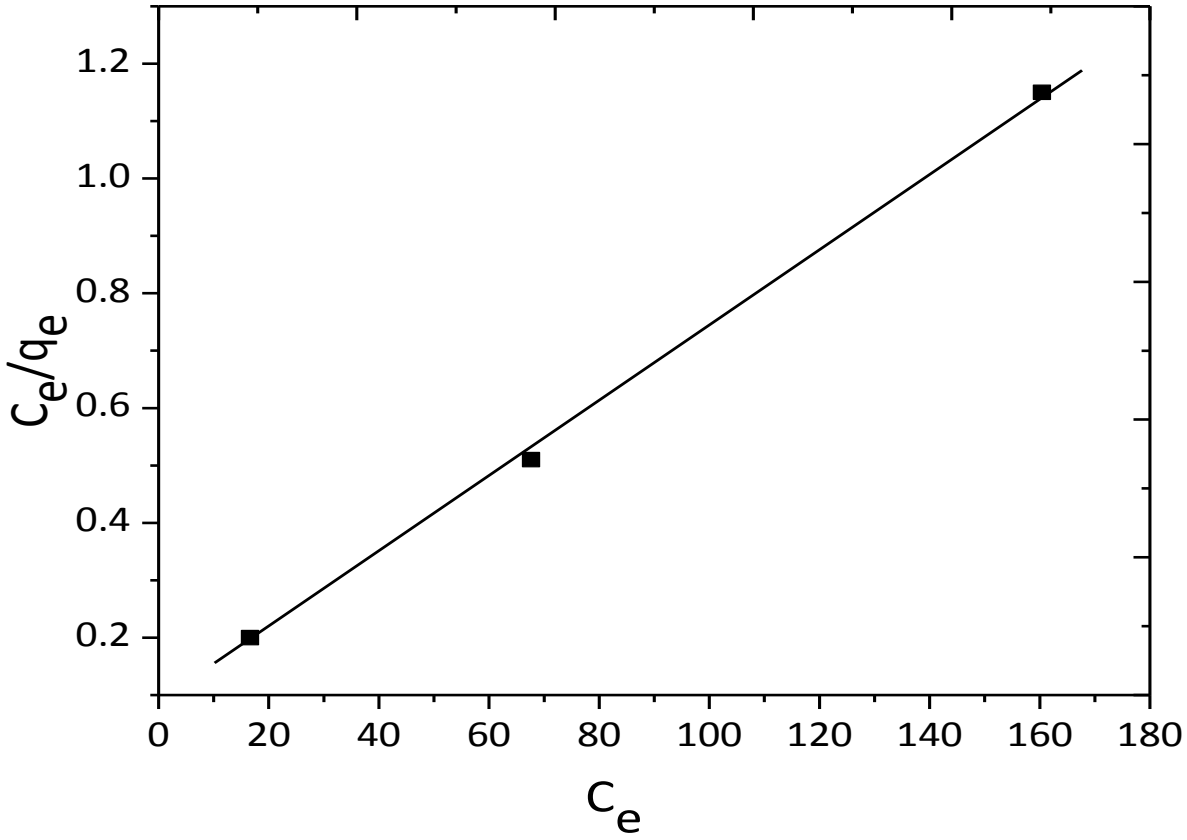

Fig. 19: Langmuir adsorption isotherm at 303 K temperature for dye FD-R H/C on GO

4.1.3.1.5.2. Freundlich adsorption isotherm

The experimental data were also tested for the multilayer adsorption mechanism employing the Freundlich isotherm using Eq. (6) by plotting $\ln C_e$ versus $\ln q_e$ (Table-11, Fig. 20) and linear relationship were observed with good regression coefficient (R^2= 0.911). The value of n was calculated using Eq. (6) and found to be 4.184 which showed that the adsorption were moderate to good. As n decreases, the adsorption became more difficult (good adsorption at n = 2-10, difficult adsorption at n = 1-2 and poor adsorption at n < 1) [32].

Table 11: $\ln C_e$ and $\ln q_e$ data of GO at different concentrations for dye FD-R H/C

Initial concentration (ppm)	100 ppm	200 ppm	300 ppm
$\ln C_e$	2.81	4.21	5.08
$\ln q_e$	4.42	4.89	4.94

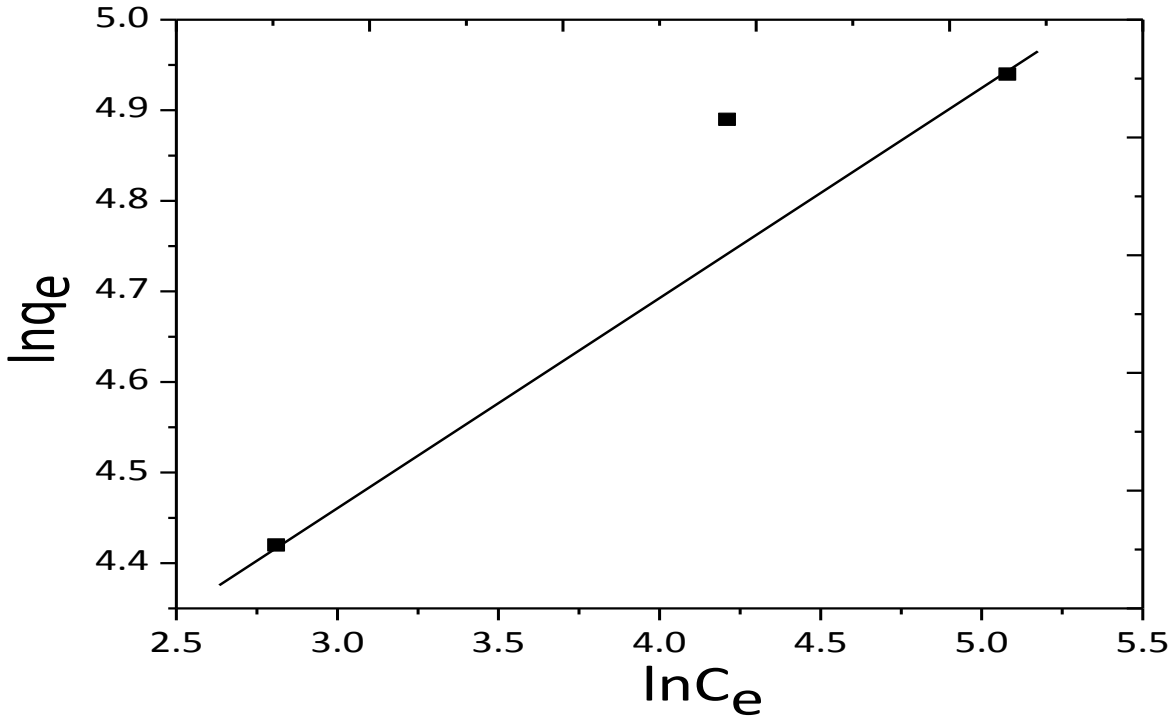

Fig. 20: Freundlich adsorption isotherm at 303 K temperature for dye FD-R H/C on GO

The values of different parameters of Langmuir isotherm and Freundlich isotherm were provided in Table. 12 and it was evident that the adsorption of FD-R H/C on GO followed preferably the Langmuir model.

Table 12: Theoritical values of q_m,b,R_L, n, K_F and R^2 of GO for dye FD-R H/C

Name of isotherm	q_m(mg/g)	R^2	b, Lmg^{-1}	R_L	, n	K_F
Langmuir Isotherm	151.29	0.999	0.0847	0.038	-	-
Freundlich isotherm	-	0.911	-	-	4.184	44.03

4.1.3.1.6. Adsorption kinetics for adsorption of dye FD-R H/C on GO

Adsorption kinetics is of great significance to evaluate the performance of an adsorbent and gain insight into the underlying mechanisms. In this study, two kinetic models were employed to describe the adsorption processes.

4.1.3.1.6.1. The pseudo-first-order reaction kinetics

In 1998, Lagergren presented first-order rate equation (Eq. 7) to describe the kinetic process. Pseudo-first-order model was obtained by plotting $\log(q_e-q_t)$ versus t (Table-13, Fig. 21) where a linear relationship between $\log(q_e-q_t)$ and t was observed.

Table 13: t and log(q_e-q_t) data at different time and concentrations for adsorption dye FD-R H/C on GO

Time (min)	(logq_e-q_t) at 100 ppm	(logq_e-q_t) at 200 ppm	(logq_e-q_t) at 300 ppm
2	1.60	1.73	1.16
5	1.52	1.62	0.90
10	1.38	1.39	0.78
15	1.20	1.15	0.65
20	0.96	0.57	0.51

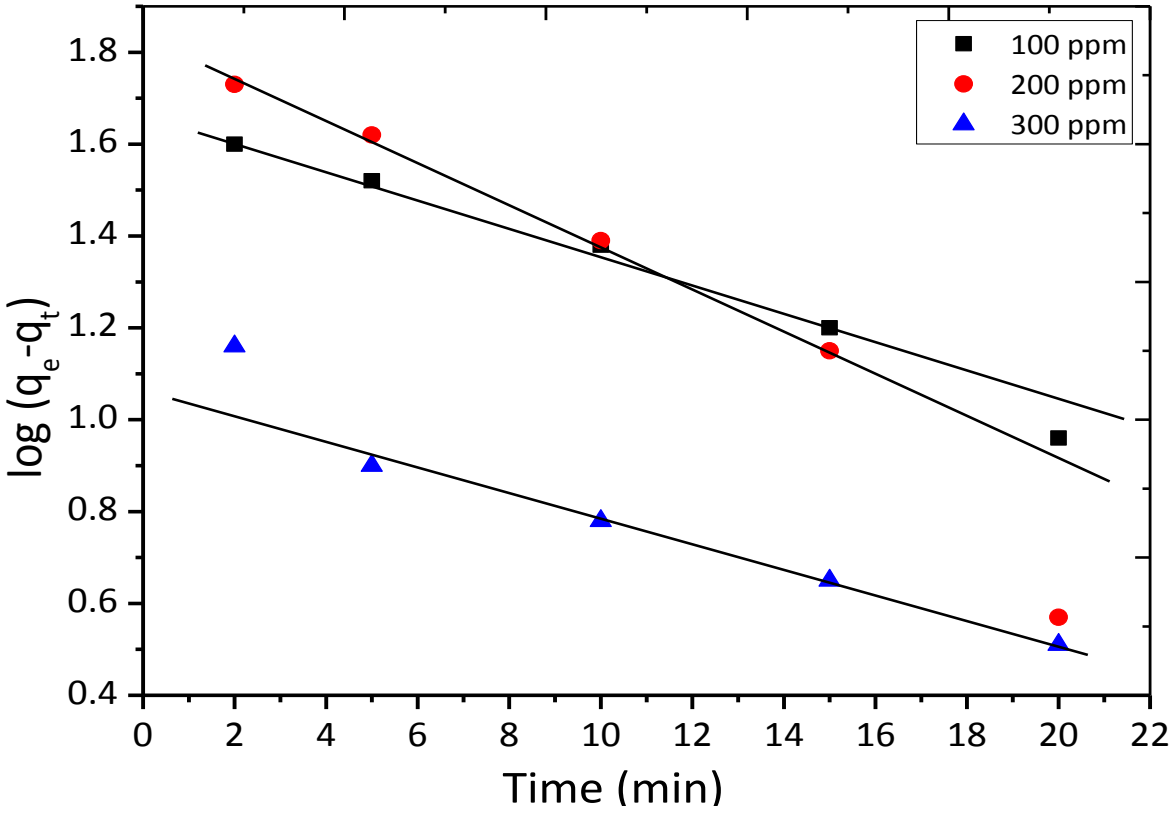

Fig. 21: Pseudo-first order adsorption kinetics for dye FD-R H/C on GO

4.1.3.1.6.2. The pseudo-second-order reaction kinetics

In 1995 Ho and Mckay presented a pseudo-second order rate equation (Eq. 8). Pseudo-second-order model was obtained by plotting t/q_t versus t.

Table 14: t and t/q_t data at different time and concentrations for adsorption dye FD-R H/C on GO.

Time (min)	t/q_t at 100 ppm	t/q_t at 200 ppm	t/q_t at 300 ppm
2	0.046	0.025	0.016
5	0.099	0.055	0.038
10	0.169	0.093	0.075
15	0.222	0.127	0.111
20	0.269	0.155	0.147
30	0.360	0.227	0.215
45	0.538	0.339	0.320
60	0.717	0.448	0.426

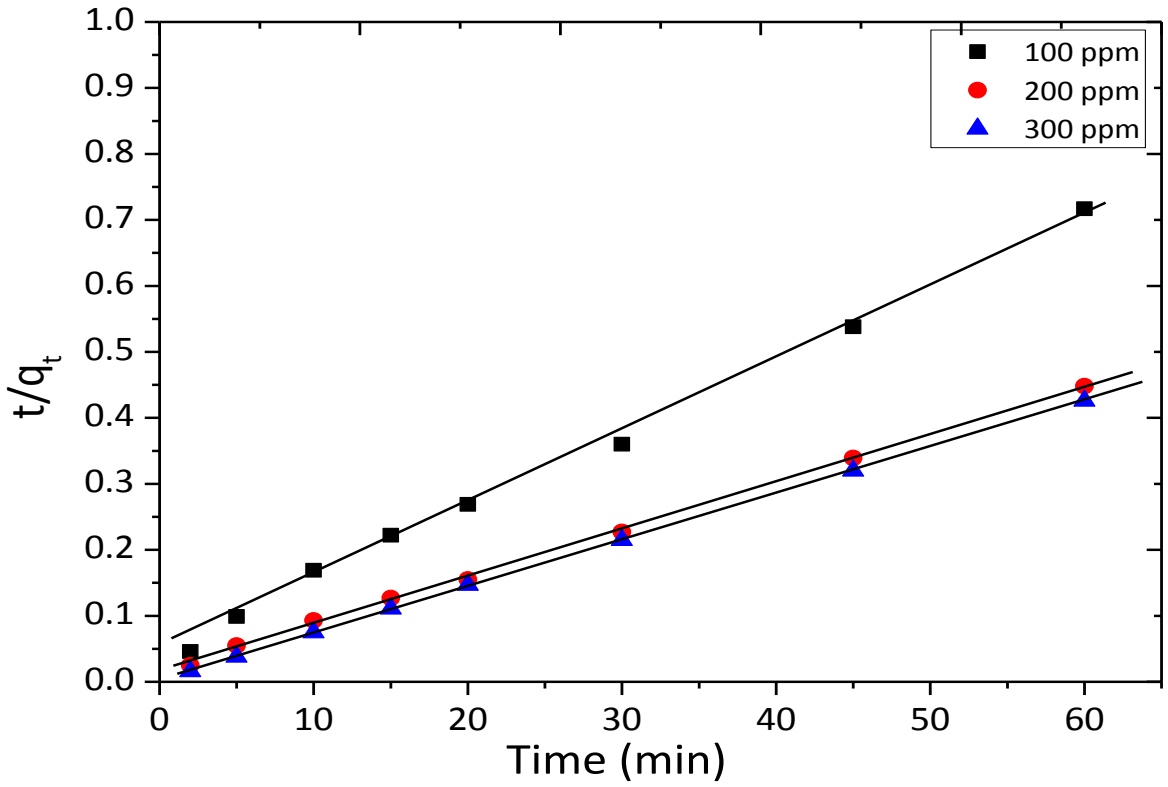

Fig. 22: Pseudo-second-order adsorption kinetics for dye FD-R H/C on GO

Considering the kinetic parameters stated in Table 15 the orders of the adsorption processes were also studied and it was observed that the values of correlation coefficient for second-order kinetics were much better than that of first-order kinetics.

Table 15: Pseudo-first-order and pseudo-second-order kinetics parameters for the adsorption of dye FD-R H/C on GO

Types of kinetics model	Parameters	Initial concentration of dye		
		100 ppm	200 ppm	300 ppm
	$q_{e,exp}$ (mg/g)	83.39	132.38	139.57
Pseudo-first order	$q_{e,cal}$ (First-order)	49.66	84.92	13.87
	K_1	0.08	0.14	0.08
	R^2	0.985	0.942	0.940
Pseudo-second order	$q_{e,cal}$ (Second-order)	89.61	139.35	142.00
	K_2	0.00304	0.00343	0.00163
	R^2	0.997	0.999	0.999

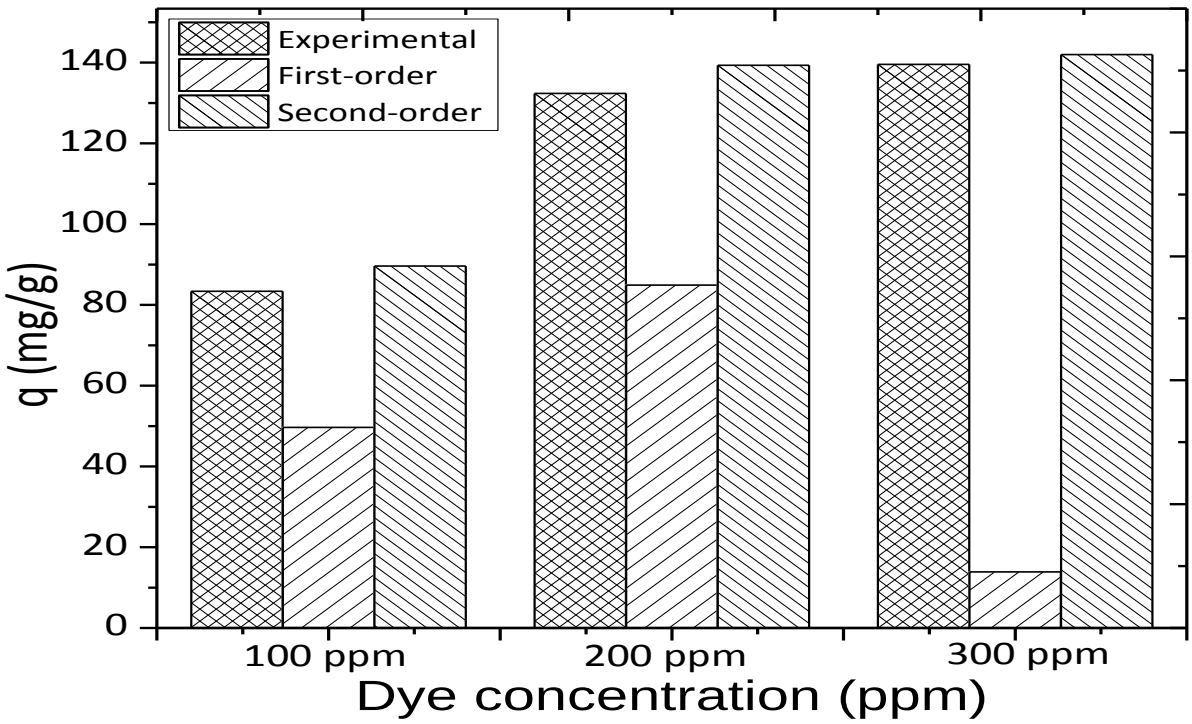

Fig. 23: Comparison of adsorption capacities of pseudo-first-order and pseudo-second-order kinetics for dye FD-R H/C on GO

From Fig. 23, it is also observed that the calculated adsorption capacities of second-order kinetics matched well with the experimental values. So, it revealed that pseudo-second order kinetic model showed better correlation for the adsorption of dye FD-R H/C onto GO compared to the pseudo-first-order model.

4.1.3.1.7. Thermodynamic analysis for adsorption of dye FD-R H/C on GO

The changes in Gibb's free energy for FD-R H/C adsorption on GO at different temperatures were also studied using Eq. (9, 10). In this case, a set of 7 experiments were studied at pH of 2. For this 10 ml of 200 ppm dye solutions were taken in 7 volumetric flasks, pH were adjusted and 10 mg of GO were added to each flask. The mixtures were shaken at 303K for different time periods ranging from 5-60 minutes. After shaking the mixtures were filtered and absorbance of the filtrates were measured by UV-Vis spectroscopy at 409 nm. Then concentrations of the solutions after adsorption were determined with respect to standard curve (Fig. 14). Then the adsorption capacities were calculated using Eq. (1). Similarly two sets of experiments were studied at 313K and 323K. The effects of contact time and temperature on adsorption capacity of GO for FD-R H/C were also studied and plotted in Table-16 and Fig. 24.

Table 16: Adsorption capacity data of dye FD-R H/C on GO at different time and temperatures

Time (min)	q at 303 K	q at 313 K	q at 323 K
0	0	0	0
5	90.78	90.33	87.46
10	107.60	105.91	99.21
15	118.23	114.55	105.33
20	128.63	122.14	113.32
30	132.38	121.87	115.85
45	132.78	124.59	116.86
60	133.29	120.22	113.37

The adsorption capacities decreased when temperatures were increased. This might be explained as the kinetic energy increased with temperature and resulted in releases of the adsorbate from GO. The equilibrium adsorption capacity was 132.38 mg/g at 303 K that decreased to 122.14 mg/g and 115.85 mg/g at 313 K and 323 K. The Gibb's free energies were calculated with Eq. (9, 10) and found to be -1.69, -1.17, -0.86 KJ mol^{-1} at 303K, 313K and 323K, respectively.

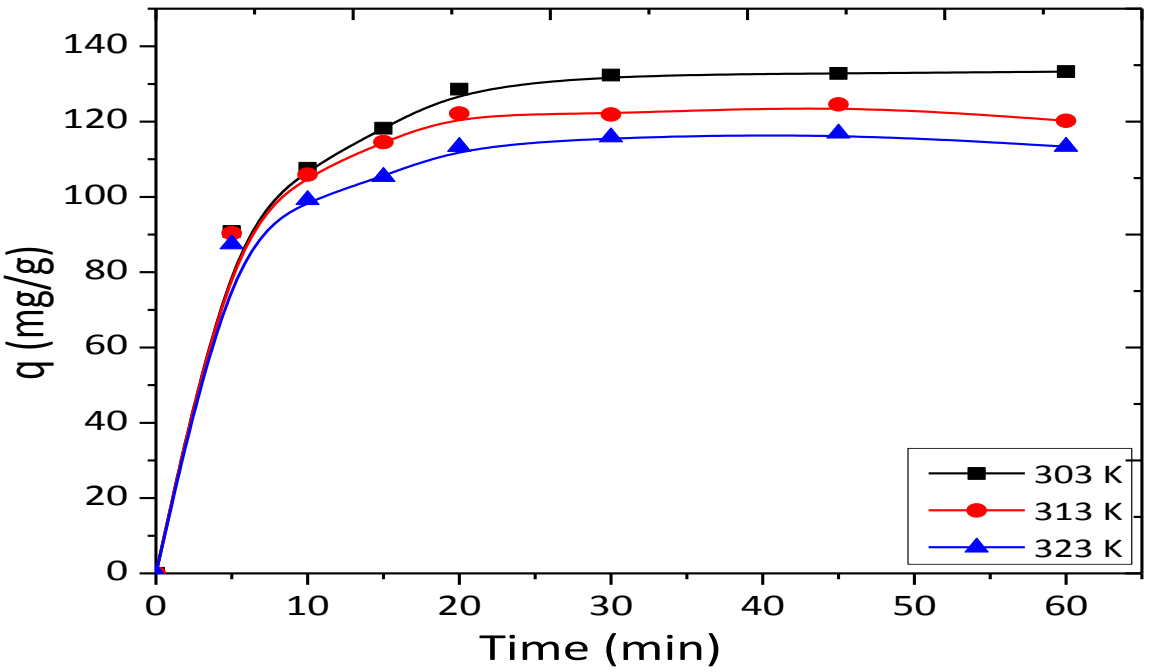

Fig. 24: Adsorption of dye FD-R H/C on GO at different temperature

The average standard enthalpy change ΔH^o and entropy change ΔS^o for the adsorption were calculated from the van't Hoff equation (Eq.11).

Table 17: 1/T vs $\ln k_d$ data of adsorption process

1/T	0.0033	0.0032	0.0031
$\ln k_d$	0.67	0.45	0.32

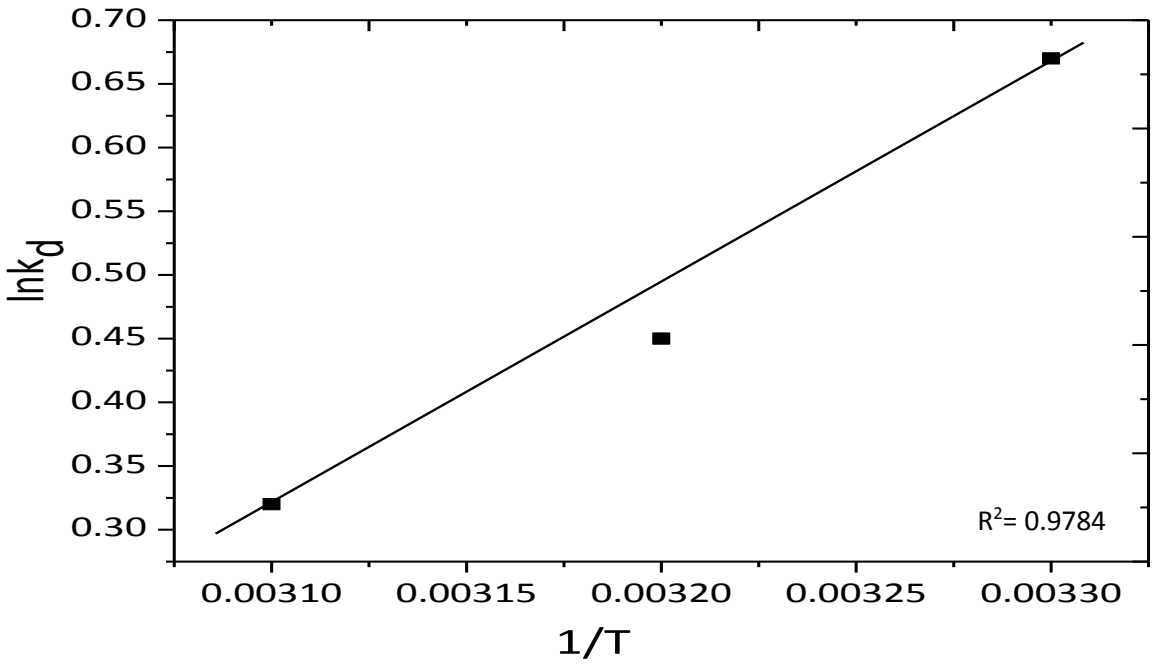

Fig. 25: Plot of van't Hoff equation for the adsorption of dye FD-R H/C on GO

A straight line was obtained by plotting $\ln k_d$ versus 1/T (Fig. 25). The standard enthalpy change ΔH^o was obtained from the slope and entropy change ΔS^o was obtained from the intercept and found to be -14.55 KJ mol^{-1} and -0.042 KJ K^{-1} mol^{-1}, respectively. The value of ΔG^o increased from -1.69 to -0.86 with the increase of the temperature from 303K to 323 K. Thus the adsorption of dye FD-R H/C on GO was spontaneous at lower temperature. Moreover, Gibb's free energy also indicates the nature of adsorption, namely physical adsorption and chemisorptions. The ΔG^o values in our experiments indicated that the adsorption of FD-R H/C on GO was a physical adsorption [32].

4.1.3.1.8. Plausible mechanism for adsorption of dye FD-R H/C on GO

Generally hydrogen bonding, electrostatic or π- π interactions are main reason of organic dye adsorption on graphene based materials. Graphene oxide possesses negative surface charge and showed higher adsorption capacity to cationic dyes compared to that of anionic dyes due to electrostatic and π- π interaction. But in our study, the prepared GO showed significant amount of anionic dye adsorption. In this case the driving forces of dye adsorption were the electrostatic interaction at lower pH and surface defects, hydrophobic association, van der walls interactions as well as π- π interaction may help in dye adsorption at higher pH [114, 115].

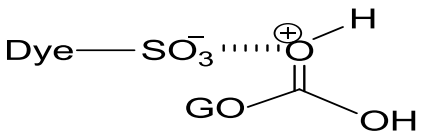

Fig. 26: Mechanism of dye FD-R H/C adsorption on GO at low pH

4.1.3.2. Adsorption of dye Turquoise GN (TGN) on GO

4.1.3.2.1. Calibration curve of dye Turquoise GN

A calibration curve was prepared using 5-200 ppm dye solutions of TURQUOISE GN by spectrophotometric method at 660 nm. Then adsorption capacity and % of removal were calculated by measuring the dye concentration before and after adsorption with respect to this calibration curve and employing Eq. (1) and Eq. (3), respectively.

Table 18: Concentration vs absorbance data of the dye TGN

Concentration (ppm)	5	10	25	50	75	100	125	150	175	200
Absorbance	0.106	0.190	0.448	0.789	1.139	1.486	2.107	2.422	2.358	2.613

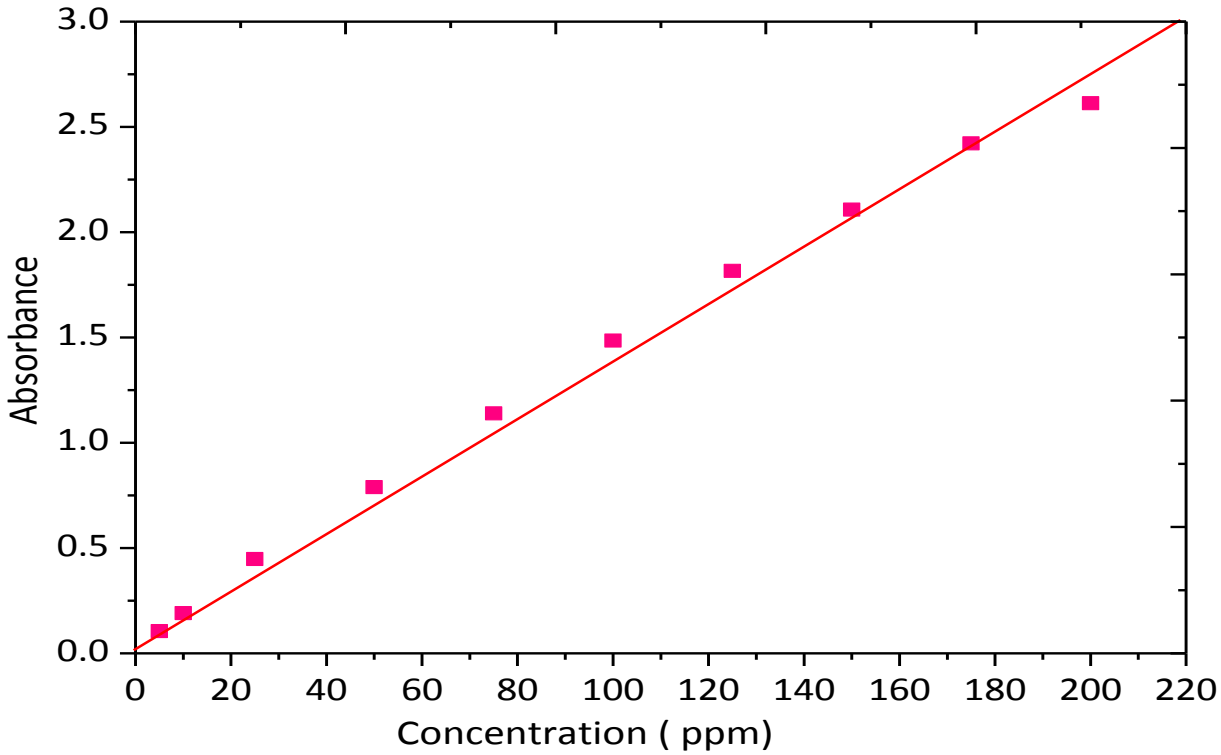

Fig. 27: Calibration curve of dye Turquoise GN

4.1.3.2.2. Effect of pH on adsorption of dye TGN by GO

The adsorption experiments of dye TGN by GO at different pH were carried out following the same procedure as 4.1.3.1.2. A set of 9 experiments were studied and 10 mg of disperse GO were added to 10 ml 200 ppm dye solutions. The mixtures were shaken for 10 minutes, filtered and absorbance of the filtrates were measured by UV-Vis spectroscopy at 660 nm. Then concentrations of the solutions after adsorption were determined with respect to standard curve (Fig. 27) and adsorption capacities were calculated. The maximum adsorption capacity of GO was 161.98 mg/g (Table-19, Fig. 28) at pH of 2 and It decreased with increasing pH.

Table 19: pH vs adsorption capacity data of GO for dye TGN

pH	2	3	4	5	6	7	8	9	10
Adsorption capacity (mg/g)	161.98	159.67	150.74	132.98	121.24	108.85	98.97	92.41	57.77

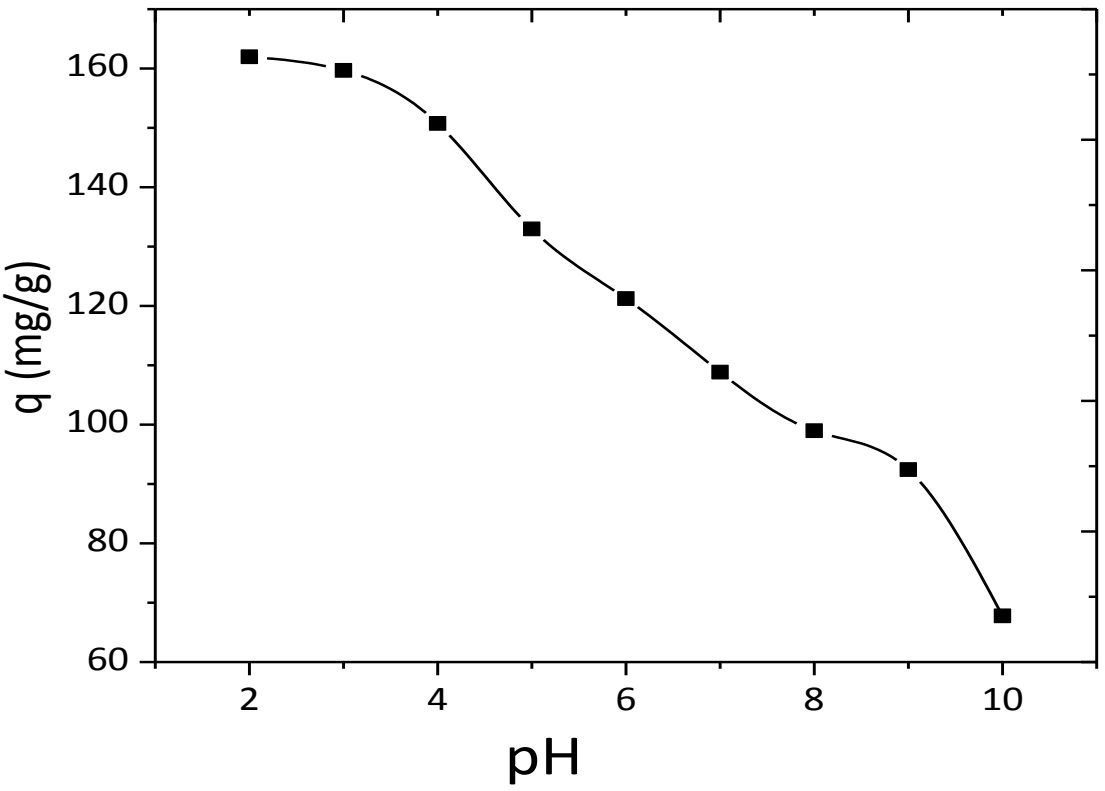

Fig. 28: Effect of pH on adsorption of dye TGN by GO

The mechanism of dye TGN adsorption on GO at low and high pH is same as **Fig. 16**.

4.1.3.2.3. Effect of adsorbent dosage on adsorption of dye TGN by GO

For the adsorption of dye TGN by GO, the optimum dosage were determined following the same procedure as 4.1.3.1.3. Here a set of 4 experiments were carried out at pH of 2 using 10 ml 300 ppm dye solutions and 5, 10, 15, 20 mg of disperse GO were added to the flasks. Then the mixtures were shaken for 10 minutes, filtered and the absorbance of the filtrates were measured by UV-Vis spectroscopy at 660 nm. Then concentrations of the solutions after adsorption were determined with respect to standard curve (Fig. 27).

Table 20: Dosage vs adsorption capacity and % removal data of GO for dye TGN

Dosage (mg)	5	10	15	20
Adsorption capacity (mg/g)	296.14	217.56	157.60	122.85
% of removal	49.35	75.52	78.80	81.90

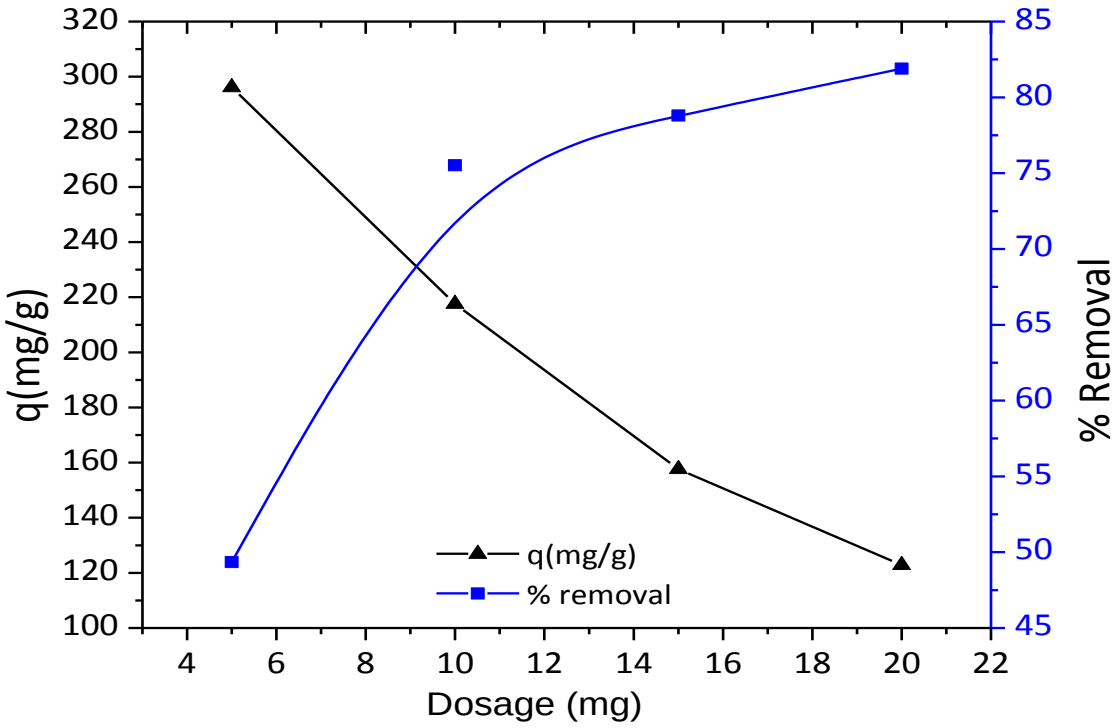

Fig. 29: Effect of adsorbent dosage on adsorption of dye TGN by GO

From Fig. 29, it was also observed that with the increase of adsorbent dosage adsorption capacity decreased but percentage removal of dye increased and 9 mg/10 ml solution demonstrate the best percentage removal as well as the best adsorption capacity (Table-20, Fig. 29). However for simplicity 10 mg/10 ml solution dosage were maintained throughout the study.

4.1.3.2.4. Effect of dye concentration and contact time on adsorption of dye TGN by GO

The adsorption experiments of dye TGN by GO at different concentrations and time were carried out following the same procedure as 4.1.3.1.4. In this case, a set of 8 experiments were carried out at pH of 2 and 10 mg of disperse GO were added to 10 ml 200 ppm dye solutions. Then the mixtures were shaken at 303 K in various intervals of time ranging from 2-60 minutes, filtered and absorbance of the filtrates were measured by UV-Vis spectroscopy at 660 nm. Then concentrations of the solutions were determined with respect to standard curve (Fig. 27). To observe the effect of dye concentration on adsorption, similar experiments were carried out using 300, 400 and 500 ppm dye solutions in the same intervals of time.

For the adsorption of TGN on GO, a set of 7 another experiments were carried out at pH of 7 following the same procedure as 3.4.3.1. For this, the experiments were carried out

using 200, 300, 400 and 600 ppm dye solutions in the intervals of time ranging from 10-60 minutes.

In these experiments due to the availability of more active sites the adsorption capacities increased (Table-21, 22 and Fig. 30, 31) with the increase in initial dye concentrations.

Table 21: Time vs adsorption capacity data of GO at different times and concentrations for dye TGN at pH of 2

Time (min)	200 ppm	300 ppm	400 ppm	500 ppm
0	0	0	0	0
2	132.14	210.48	274.23	300.60
5	150.64	216.43	277.35	321.76
10	154.54	217.56	281.56	325.00
15	156.36	224.13	286.35	328.84
20	159.89	224.78	291.35	329.75
30	162.00	225.61	291.96	347.39
45	162.03	222.43	290.95	347.39
60	161.98	221.67	287.71	352.23

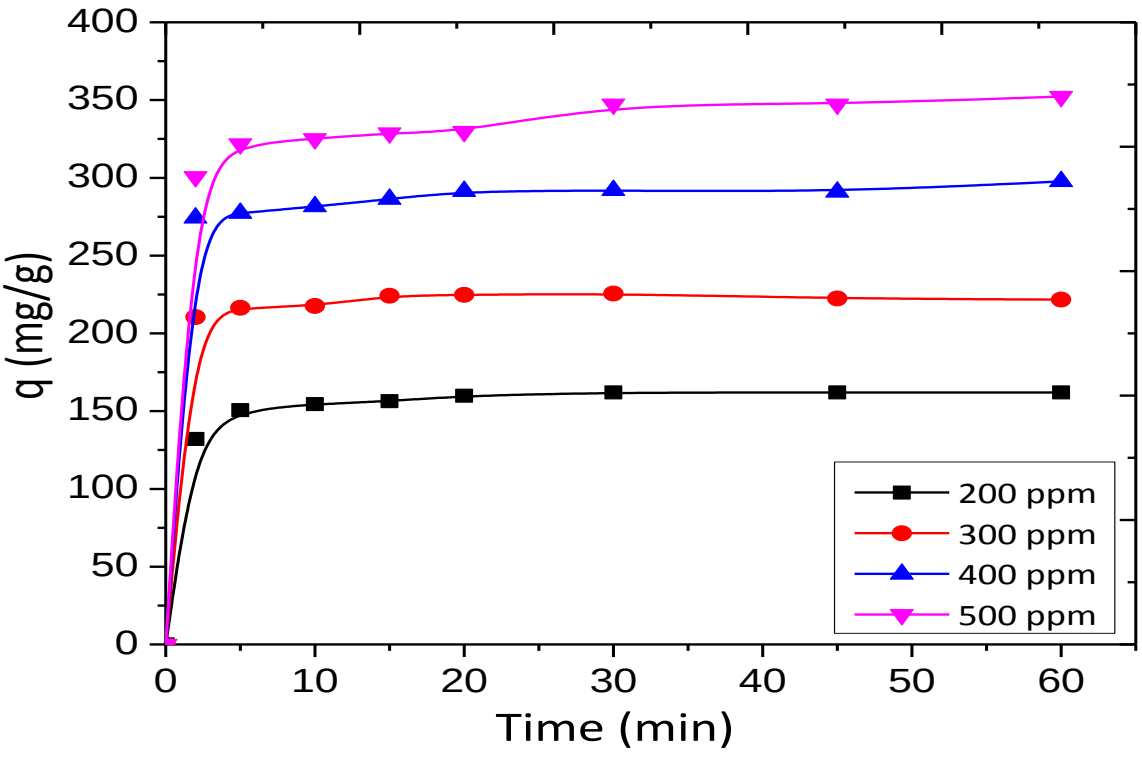

Fig. 30: Concentration and time effect on adsorption of dye TGN by GO at pH of 2

Table 22: Time vs adsorption capacity data of GO at different times and concentrations for dye TGN at pH of 7

Time (min)	200 ppm	300 ppm	400 ppm	600 ppm
0	0	0	0	0
10	89.65	108.69	137.67	143.08
15	94.68	113.13	147.02	157.17
20	95.31	118.26	156.36	170.79
25	98.67	126.36	160.54	187.29
30	102.39	136.84	165.66	202.86
45	103.36	137.41	172.26	203.51
60	108.85	139.29	162.22	206.58

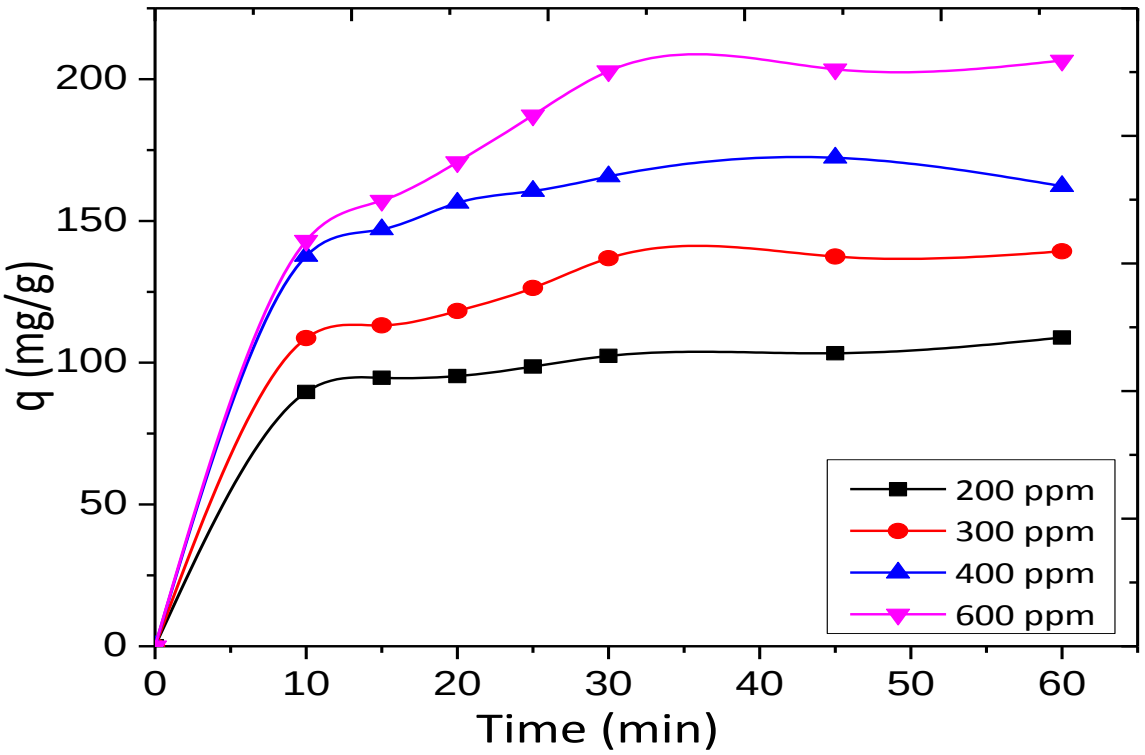

Fig. 31: Concentration and time effect on adsorption of dye TGN by GO at pH of 7

4.1.3.2.5. Adsorption isotherms for adsorption of dye TGN on GO

4.1.3.2.5.1. Langmuir adsorption isotherm

The theoretical maximum adsorption capacity q_m for the adsorption of TGN on GO was calculated following the procedure as 4.1.3.1.5.1. A linear relation between C_e/q_e and C_e were observed for both adsorptions at pH of 2 and pH of 7 (Table-23, 24 and Fig. 32, 33) with acceptable regression factor (R^2= 0.969 and 0.999, respectively).

Table 23: C_e and C_e/q_e data of GO at different concentrations for dye TGN at pH of 2

Initial concentration (ppm)	200 ppm	300 ppm	400 ppm	500 ppm
Equilibrium concentration (C_e)	38.00	74.39	108.04	152.61
C_e/q_e	0.23	0.33	0.37	0.44

Table 24: C_e and C_e/q_e data of GO at different concentrations for dye TGN at pH of 7

Initial concentration (ppm)	200 ppm	300 ppm	400 ppm	600 ppm
Equilibrium concentration (C_e)	97.61	163.16	234.34	397.14
C_e/q_e	0.95	1.19	1.42	1.96

From Langmuir isotherm ($\frac{C_e}{q_e} = \frac{1}{q_m b} + \frac{1}{q_m} c_e$) the value of slope was found 0.001768 at pH of 2. So,

$$1/q_m = 0.001768$$

$$\therefore q_m = 565.61 \text{ mg/g}$$

The value of slope was found 0.0034 at pH of 7. So,

$$1/q_m = 0.0034$$

$$\therefore q_m = 294.12 \text{ mg/g}$$

The theoretical maximum adsorption capacities q_m were calculated from the slope and found to be 565.61 mg/g and 294.12 mg/g at pH of 2 and 7, respectively. The separation factor R_L were calculated from the Eq. 5 and the values were 0.67 and 0.236 at pH of 2 and 7, respectively. These indicate very favorable monolayer adsorption process [32].

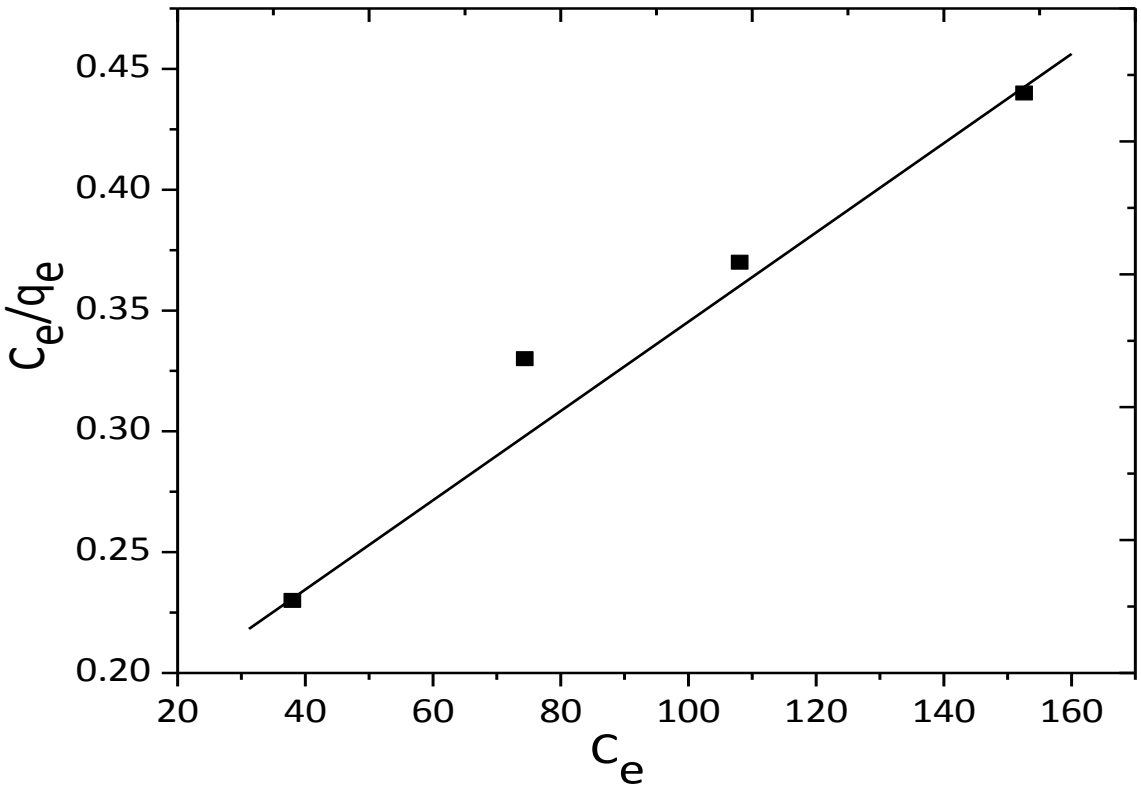

Fig. 32: Langmuir adsorption isotherm at 303 K temperature for TGN on GO at pH of 2

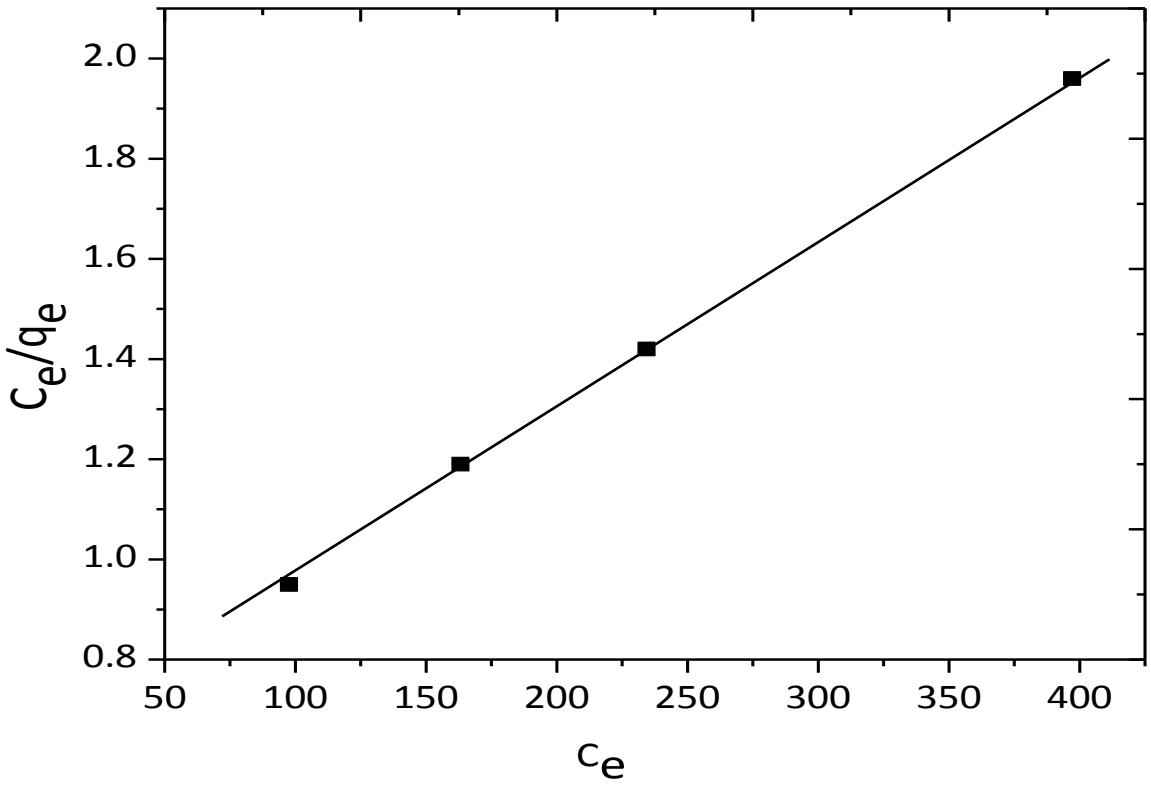

Fig. 33: Langmuir adsorption isotherm at 303 K temperature for dye TGN on GO at pH of 7

4.1.3.1.5.2. Freundlich adsorption isotherm

The experimental data were also tested for the multilayer adsorption mechanism of TGN on GO following the procedure as 4.1.3.1.5.2 (Table- 25, 26 and Fig. 34, 35). A linear relationship were observed with good regression coefficient (R^2= 0.996 and 0.993 at pH of 2 and 7, respectively). The values of n were found to be 1.81 and 2.05 at pH of 2 and pH of 7, which showed that the adsorption were moderate to good [32].

Table 25: $\ln C_e$ and $\ln q_e$ data of GO at different concentrations for dye TGN at pH of 2

Initial concentration (ppm)	200 ppm	300 ppm	400 ppm	500 ppm
$\ln C_e$	3.64	4.31	4.68	5.03
$\ln q_e$	5.09	5.42	5.68	5.85

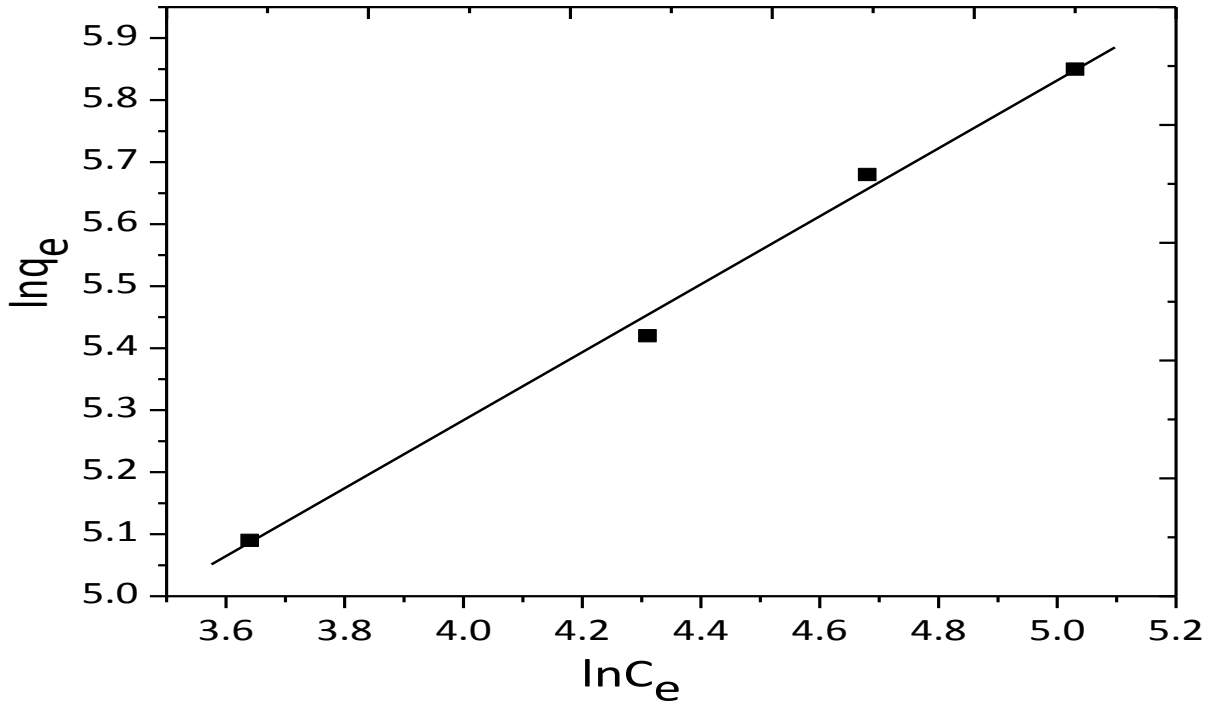

Fig. 34: Freundlich adsorption isotherm at 303 K temperature for dye TGN on GO at pH of 2

Table 26: $\ln C_e$ and $\ln q_e$ data of GO at different concentrations for dye TGN at pH of 7

Initial concentration (ppm)	200 ppm	300 ppm	400 ppm	600 ppm
$\ln C_e$	4.58	5.09	5.46	5.98
$\ln q_e$	4.63	4.92	5.11	5.31

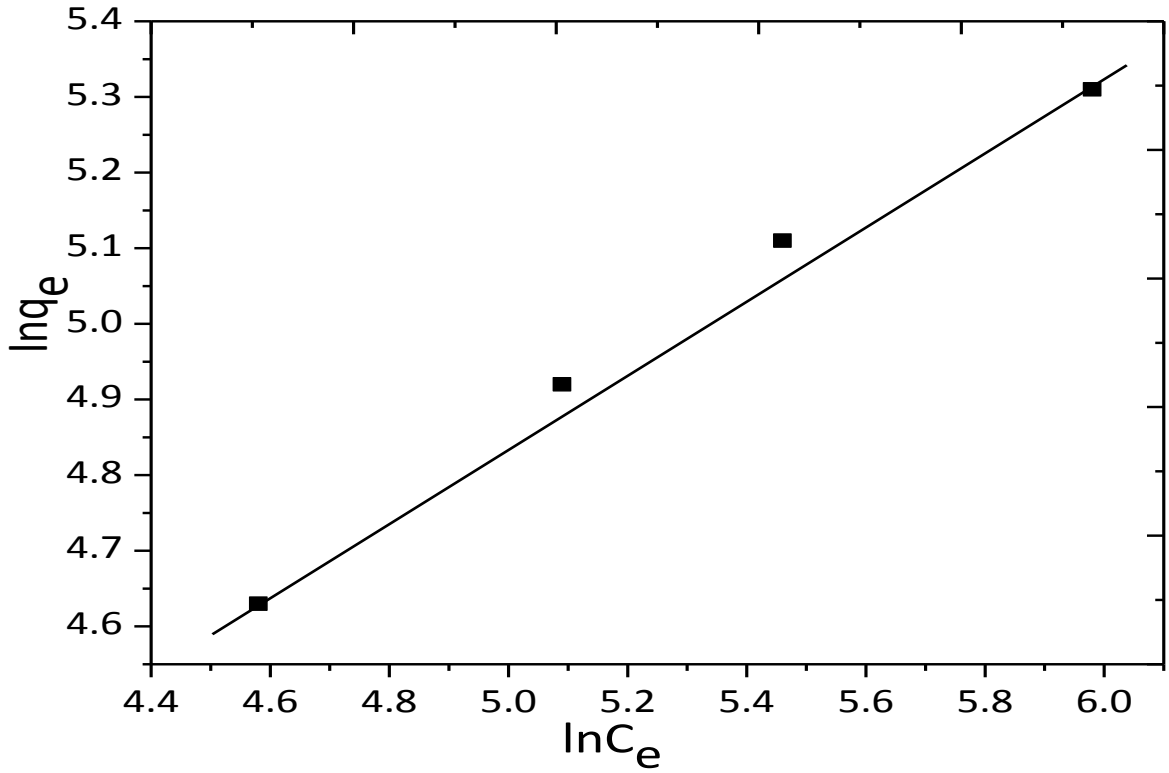

Fig. 35: Freundlich adsorption isotherm at 303 K temperature for dye TGN on GO at pH of 7

The values of different parameters of Langmuir and Freundlich models were provided in Table-27. Here, the values indicate that the adsorption of TGN on GO followed both the models but preferably the Langmuir model.

Table 27: Theoritical values of q_m,b,R_L, n, K_F and R^2 of GO for dye TGN

	Langmuir Isotherm				Freundlich Isotherm		
	q_m (mg/g)	R^2	b, Lmg^{-1}	R_L	R^2	n	K_F
At pH of 2	565.61	0.969	0.0010	0.670	0.996	1.81	21.43
At pH of 7	294.12	0.999	0.0054	0.236	0.993	2.05	11.25

4.1.3.2.6. Adsorption kinetics for adsorption of dye TGN on GO

4.1.3.2.6.1. The pseudo-first-order reaction kinetics

Pseudo-first-order model for the adsorption of TGN on GO was studied following the procedure as 4.1.3.1.6.1. The values t and $\log(q_e-q_t)$ were given in Table-28, 29 and Fig. 36, 37.

Table 28: t and log(q_e-q_t) data at different time and concentrations for adsorption of dye TGN on GO at pH of 2

Time (min)	(logq_e-q_t) at 200 ppm	(logq_e-q_t) at 300 ppm	(logq_e-q_t) at 400 ppm	(logq_e-q_t) at 500 ppm
2	1.48	1.18	1.25	1.67
5	1.06	0.96	1.16	1.41
10	0.87	0.91	1.02	1.35
15	0.70	0.17	0.75	1.27

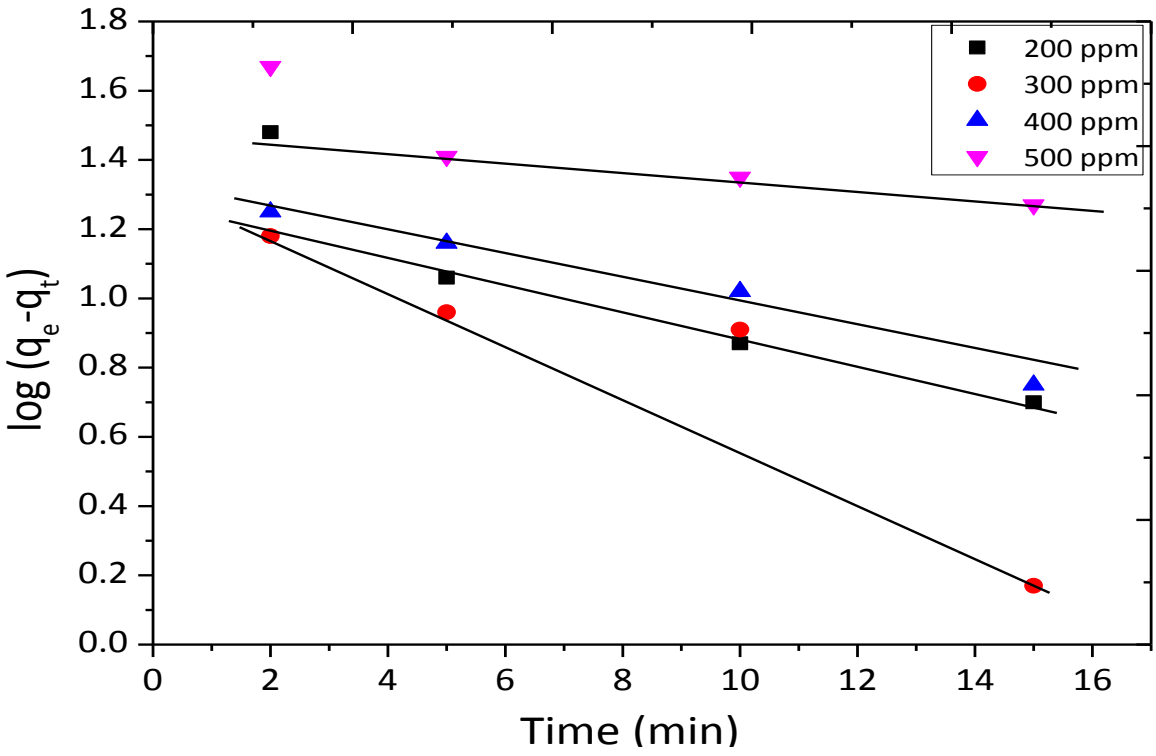

Fig. 36: Pseudo-first order adsorption kinetics for dye TGN on GO at pH of 2

Table 29: t and log(q_e-q_t) data at different time and concentrations for adsorption of dye TGN on GO at pH of 7

Time (min)	(logq_e-q_t) at 200 ppm	(logq_e-q_t) at 300 ppm	(logq_e-q_t) at 400 ppm	(logq_e-q_t) at 600 ppm
10	1.11	1.45	1.45	1.78
15	0.88	1.37	1.27	1.66
20	0.85	1.27	0.97	1.51
25	0.57	1.02	0.71	1.19

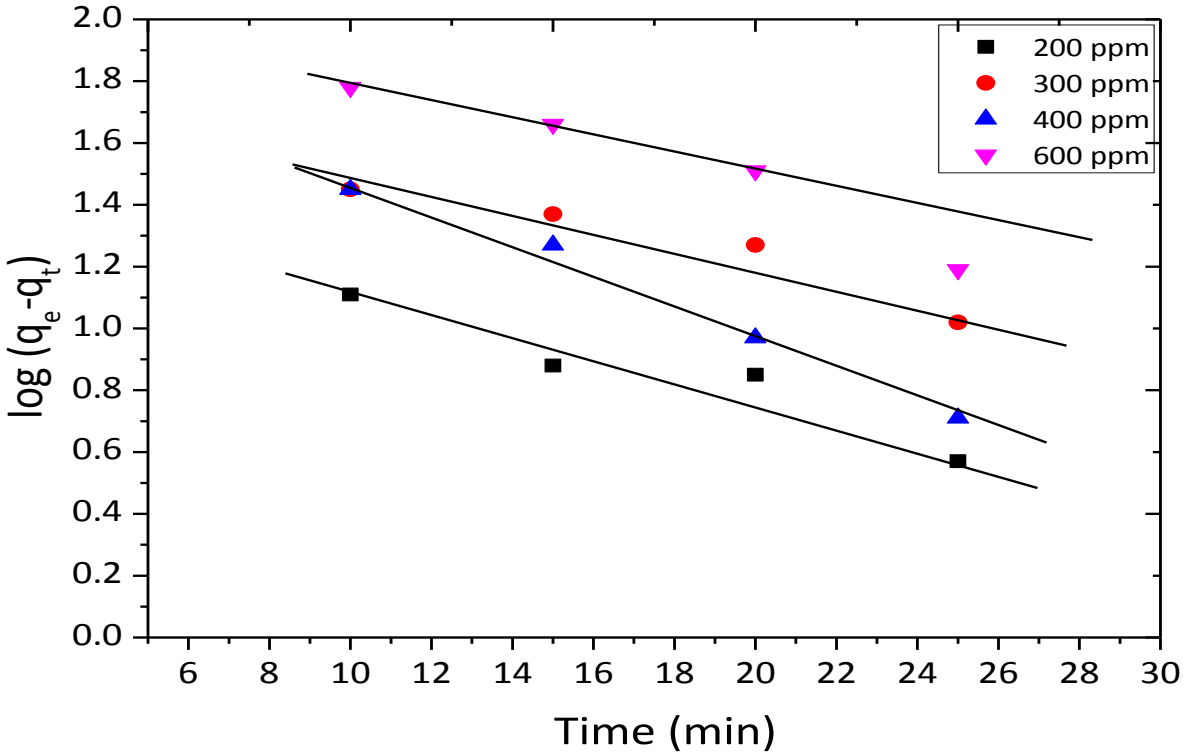

Fig. 37: Pseudo-first order adsorption kinetics for dye TGN on GO at pH of 7

4.1.3.2.6.2. The pseudo-second-order reaction kinetics

Pseudo-second-order model for the adsorption of TGN on GO was studied following the procedure as 4.1.3.1.6.2. The values t and t/q_t are given in Table-30, 31 and Fig. 38, 39.

Table 30: t and t/q_t data at different time and concentrations for adsorption of dye TGN on GO at pH of 2

Time (min)	t/q_t at 200 ppm	t/q_t at 300 ppm	t/q_t at 400 ppm	t/q_t at 500 ppm
2	0.015	0.0095	0.007	0.0067
5	0.033	0.023	0.018	0.0155
10	0.065	0.046	0.036	0.031
15	0.096	0.067	0.052	0.046
20	0.125	0.089	0.069	0.060
30	0.185	0.133	0.103	0.086
45	0.278	0.202	0.155	0.130
60	0.370	0.271	0.209	0.170

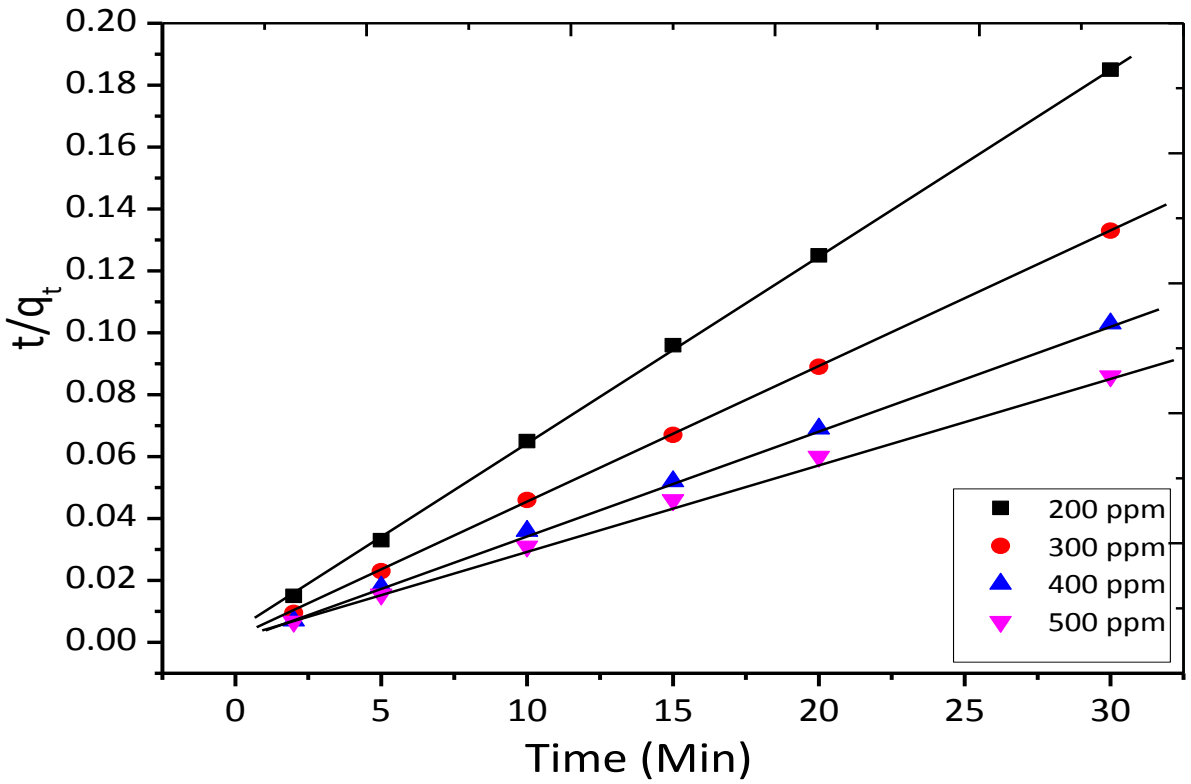

Fig. 38: Pseudo-second-order adsorption kinetics for dye TGN on GO at pH of 2

Table 31: t and t/q_t data at different time and concentrations for adsorption of dye TGN on GO at pH of 7

Time (min)	t/q_t at 200 ppm	t/q_t at 300 ppm	t/q_t at 400 ppm	t/q_t at 600 ppm
10	0.112	0.092	0.073	0.070
15	0.158	0.133	0.102	0.095
20	0.210	0.170	0.128	0.117
25	0.253	0.198	0.156	0.133
30	0.293	0.219	0.181	0.148
45	0.435	0.327	0.261	0.221
60	0.551	0.431	0.370	0.290

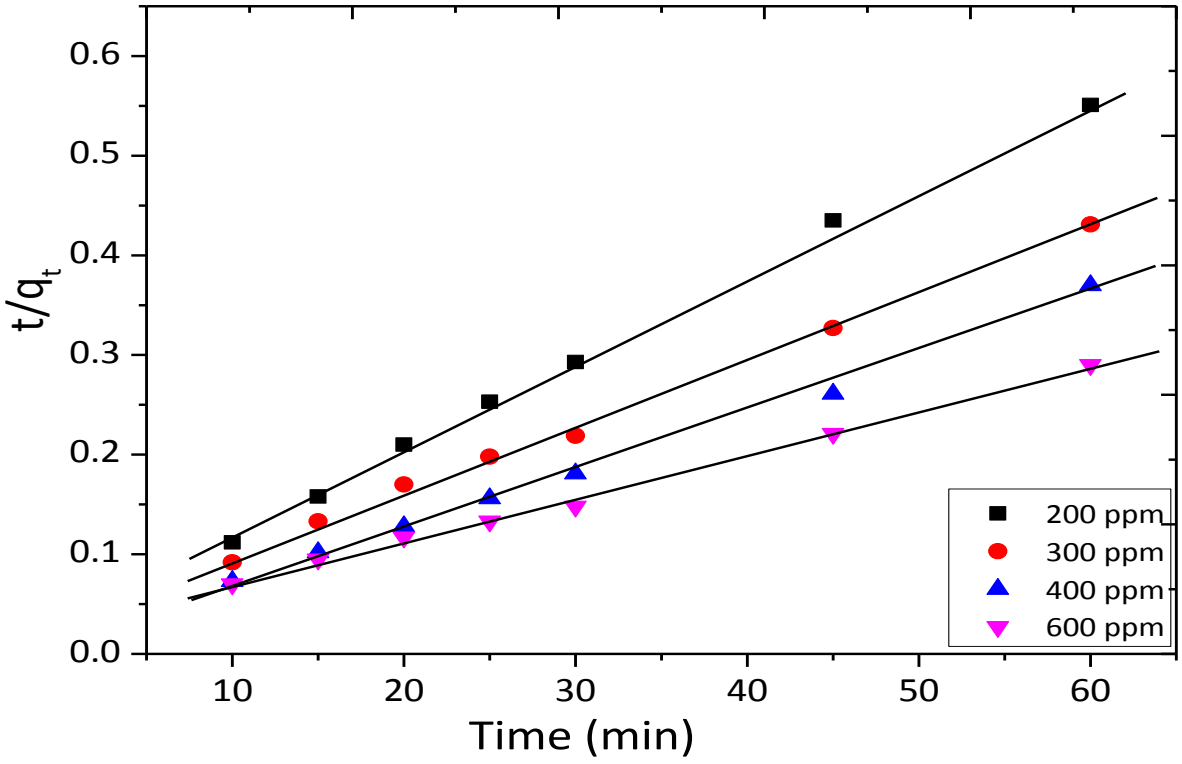

Fig. 39: Pseudo-second-order adsorption kinetics for dye TGN on GO at pH of 7

Considering the kinetic parameters stated in Table-32 at both pH of 2 and 7, it was observed that the values of correlation coefficient for second-order kinetics were much better than first-order kinetics.

Table 32: Pseudo-first-order and pseudo-second-order kinetics parameters for the adsorption of dye TGN on GO at both pH of 2 and 7

Types of kinetics model	Parameters	Results at pH of 2				Results at pH of 7			
		200 ppm	300 ppm	400 ppm	500 ppm	200 ppm	300 ppm	400 ppm	600 ppm
	$q_{e,exp}$ (mg/g)	162.00	225.61	291.96	347.39	102.39	136.84	165.66	202.86
Pseudo-first order	$q_{e,cal}$	30.27	23.55	22.18	40.18	26.92	58.08	95.94	161.06
	K_1	0.13	0.16	0.085	0.046	0.076	0.064	0.116	0.088
	R^2	0.947	0.851	0.972	0.787	0.9268	0.9229	0.99	0.9438
Pseudo-second order	$q_{e,cal}$	163.67	227.27	293.17	350.88	113.64	151.52	172.41	232.56
	K_2	0.0122	0.0173	0.043	0.01	0.0027	0.0015	0.0030	0.0007
	R^2	1.0	0.999	0.999	0.999	0.9986	0.9976	0.9955	0.9967

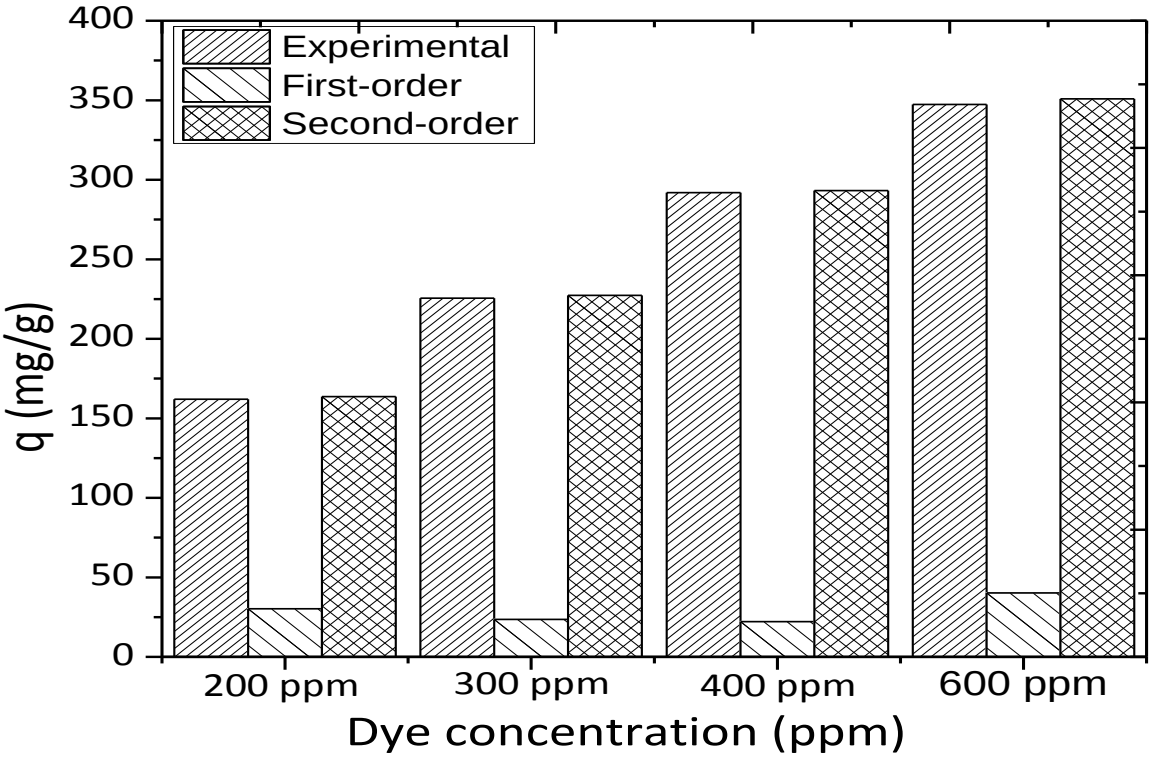

Fig. 40: Comparison of adsorption capacities of pseudo-first-order and pseudo-second-order kinetics for the adsorption of dye TGN on GO at pH of 2

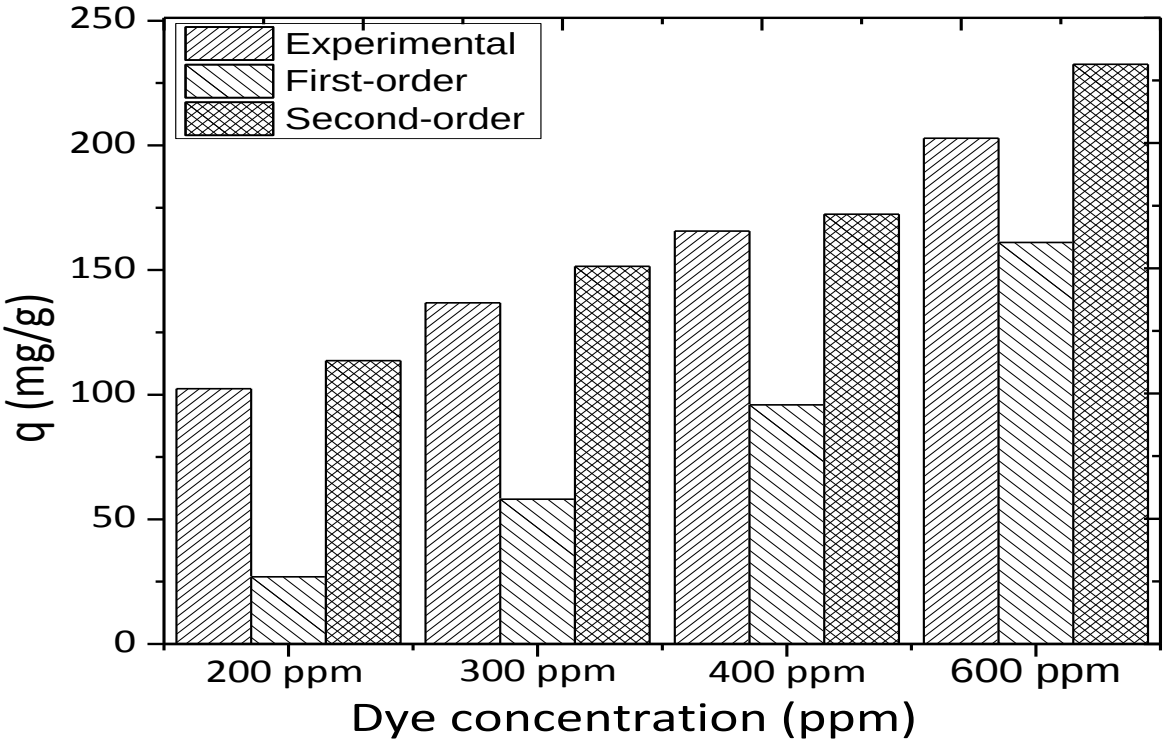

Fig. 41: Comparison of adsorption capacities of pseudo-first-order and pseudo-second-order kinetics for the adsorption of dye TGN on GO at pH of 7.

From Fig. 40 and 41, it was also observed that for TGN the calculated adsorption capacities of second-order kinetics matched well with the experimental values at both pH 2 and 7.

4.1.3.2.7. Thermodynamic analysis for adsorption of dye TGN on GO

The changes in Gibb's free energy for dye adsorption of TGN on GO at different temperatures were also studied following the procedure as 4.1.3.1.7. In this case, a set of 7 experiments were studied at pH of 2. For this, 10 mg of disperse GO were added to 10 ml of 200 ppm dye solutions and the mixtures were shaken at 303K for different time periods ranging from 5-60 minutes. After shaking the mixtures were filtered and absorbance of the filtrates were measured by UV-Vis spectroscopy at 660 nm. To observe the effect of temperature similar two sets of experiments were studied at 313K and 323K.

Table 33: Adsorption capacity data of dye TGN on GO at different time and temperatures

Time (min)	q at 303 K	q at 313 K	q at 323 K
0	0	0	0
5	150.64	134.60	128.21
10	154.54	143.38	140.79
15	156.36	147.23	141.70
20	159.89	150.20	141.65
30	162.00	149.56	141.05
45	162.03	151.14	143.07
60	161.98	150.90	142.48

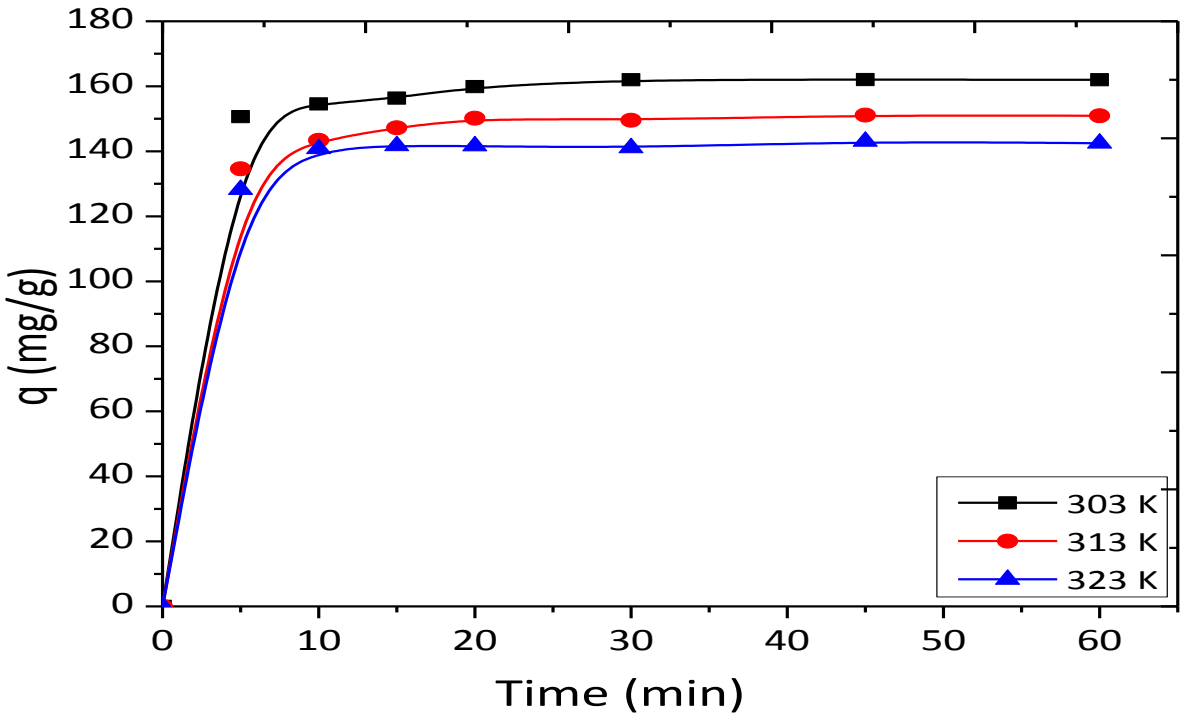

Fig. 42: Adsorption of dye TGN on GO at different temperatures

The effects of contact time and temperature on adsorption capacity of GO for TGN were plotted in Table-33 and Figure. 42. The equilibrium adsorption capacity was 162.03 mg/g at 303 K that decreased to 150.80 mg/g and 141.65 mg/g at 313 K and 323 K. The Gibb's free energies found to be -3.66, -2.92, -2.39 KJ mol^{-1} at 303K, 313K and 323K, respectively.

The average standard enthalpy change ΔH^o and entropy change ΔS^o for the adsorption of TGN on GO were also calculated. A straight line was obtained by plotting $\ln k_d$ versus 1/T (Table-34, Fig. 43).

Table 34: 1/T vs $\ln k_d$ data of adsorption process

1/T	0.0033	0.0032	0.0031
$\ln k_d$	1.45	1.12	0.89

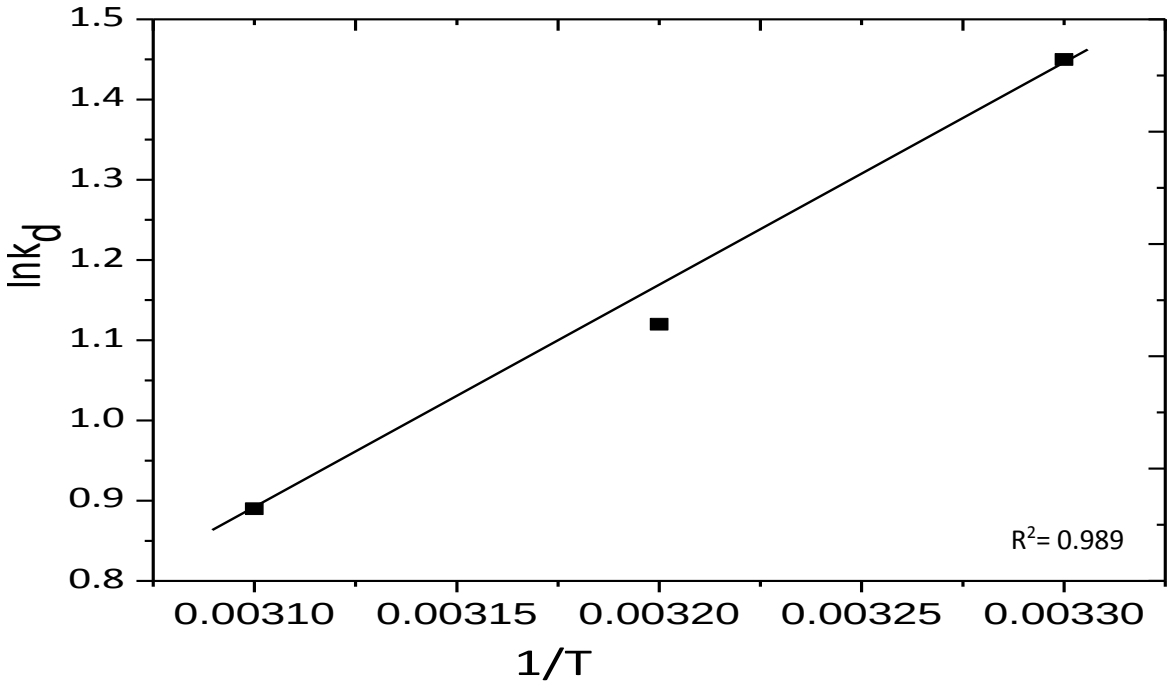

Fig. 43: Plot of van't Hoff equation for the adsorption of dye TGN on GO

The standard enthalpy change ΔH^o and entropy change ΔS^o were obtained -23.28 KJ mol^{-1} and -0.065 KJ K^{-1} mol^{-1}, respectively. The value of ΔG^o increased from -3.66 to -2.39 with increases of the temperature from 303K to 323 K. Thus the adsorption of TGN on GO was spontaneous at lower temperature and the adsorption of TGN on GO was a physical adsorption [32].

4.1.3.2.8. Plausible mechanism for adsorption of dye TGN on GO

GO shows significant adsorption capacity towards anionic dye TGN also. In this case the mechanism of dye TGN adsorption on GO is same as section **4.1.3.1.8.**

4.1.3.2.9. Regeneration of used GO

In order to check the regeneration ability 2 % HCl was added to the used GO to remove the dye. Then washed with distilled water upto pH reached to 7. Then the regenerated GO was dried and used for further adsorption.

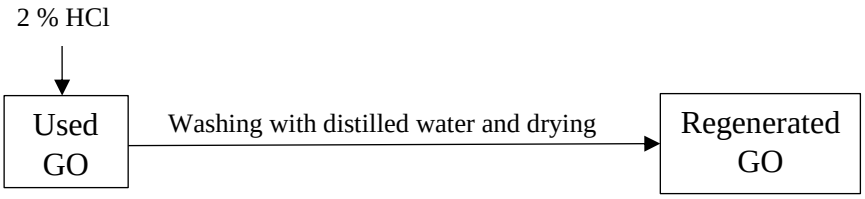

Fig. 44: Flow diagram of regeneration of used GO for dye TGN

For the adsorption study of regenerated GO, 10 mg of dispersed regenerated GO was used for10 ml 200 ppm dye solution at pH of 7 with shaking for 30 minutes. Fresh GO showed the adsorption capacity of 102.39 mg/g for 200 ppm dye solution at pH of 7 while the regenerated GO of 1st, 2nd, 3rd and 4th recycle (Table-35, Fig. 45) showed the adsorption capacities of 75.91 mg/g, 65.73 mg/g, 44.32 mg/g and 41.25 mg/g, respectively.

Table 35: Reusability of GO in the removal of dye TGN

Type of GO	Fresh GO	Recycle-1	Recycle-2	Recycle-3	Recycle-4
Adsorption capacity q (mg/g)	102.39	75.91	65.73	44.32	41.25

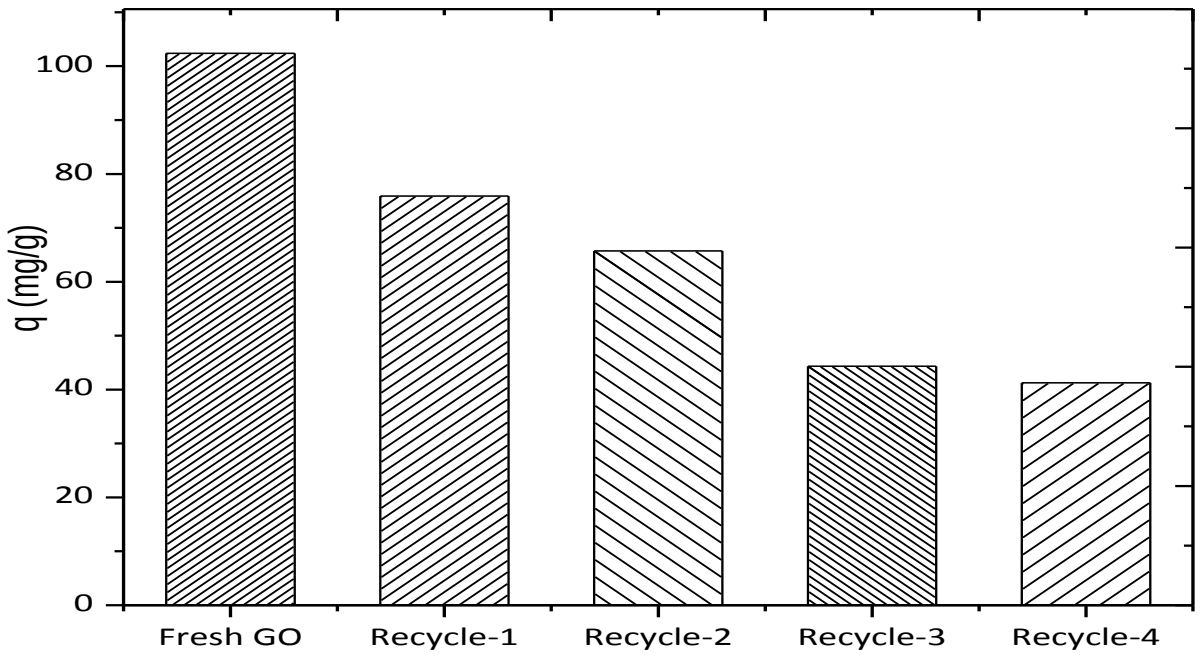

Fig. 45: Reusability of GO in the removal of dye TGN

4.1.3.3. Adsorption of dye Maxilon Blue (GRL) or MBG on GO

4.1.3.1.1. Calibration curve of dye MBG

For MBG a calibration curve was prepared using 05-75 ppm solution by spectrophotometric method at 554 nm and adsorption capacity and % of removal were calculated by measuring of the dye concentration before and after adsorption with respect to this calibration curve employing Eq. (1) and Eq. (3), respectively.

Table 36: Concentration vs absorbance data of dye MBG

Concentration (ppm)	5	10	25	50	75
Absorbance	0.1495	0.3053	0.7802	1.673	2.515

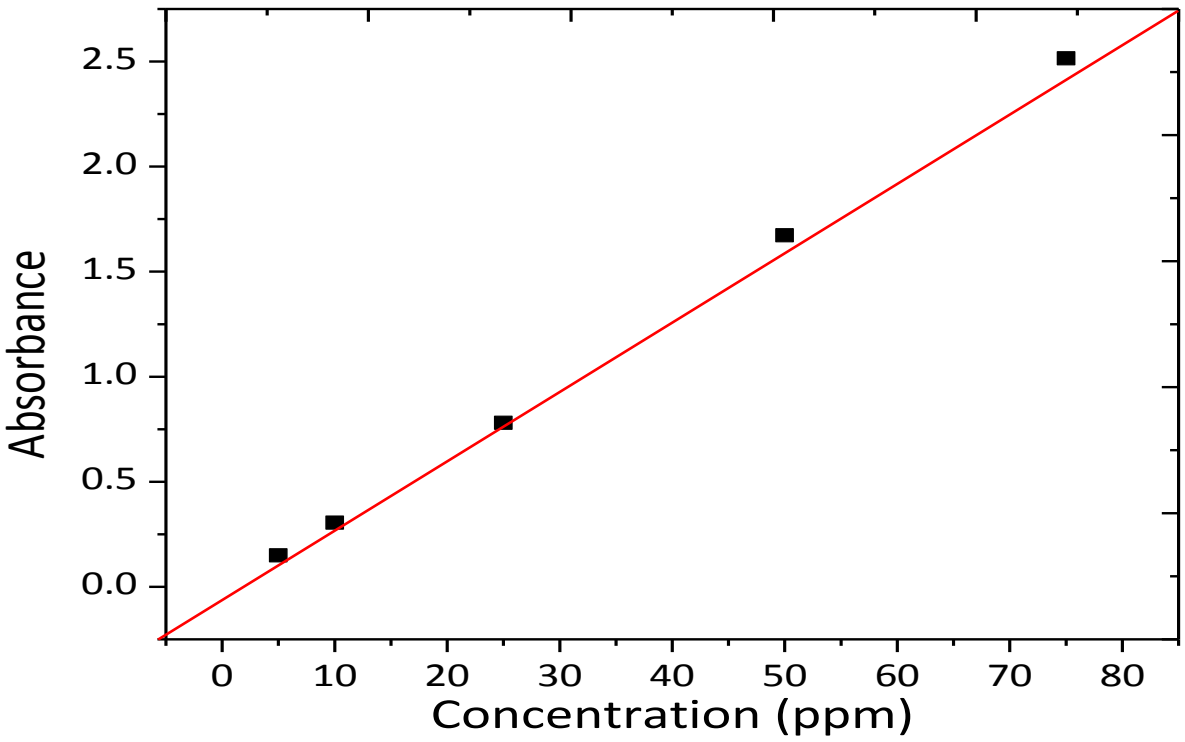

Fig. 46: Calibration curve of dye MBG

4.1.3.3.2. Effect of pH on adsorption of dye MBG by GO

The adsorption experiments of dye MBG by GO at different pH were carried out following the same procedure as 4.1.3.1.2. Here a set of 9 experiments were studied and 4 mg of disperse GO were added to 10 ml 1000 ppm dye solutions. The mixtures were shaken for 30 minutes, filtered and absorbance of the filtrates were measured by UV-Vis spectroscopy at 554 nm. Then concentrations of the solutions after adsorption were determined with respect

to standard curve (Fig. 46) and adsorption capacities were calculated. The Maximum adsorption capacity of GO for MBG was 779.80 mg/g (Table-37, Fig. 47) at pH of 10 and it decreased with a decrease in pH.

Table 37: pH vs adsorption capacity data of GO for dye MBG

pH	2	3	4	5	6	7	8	9	10
Adsorpton capacity (mg/g)	963.45	1325.25	1344.80	1370.25	1409.10	1421.10	1424.03	1517.68	1949.5

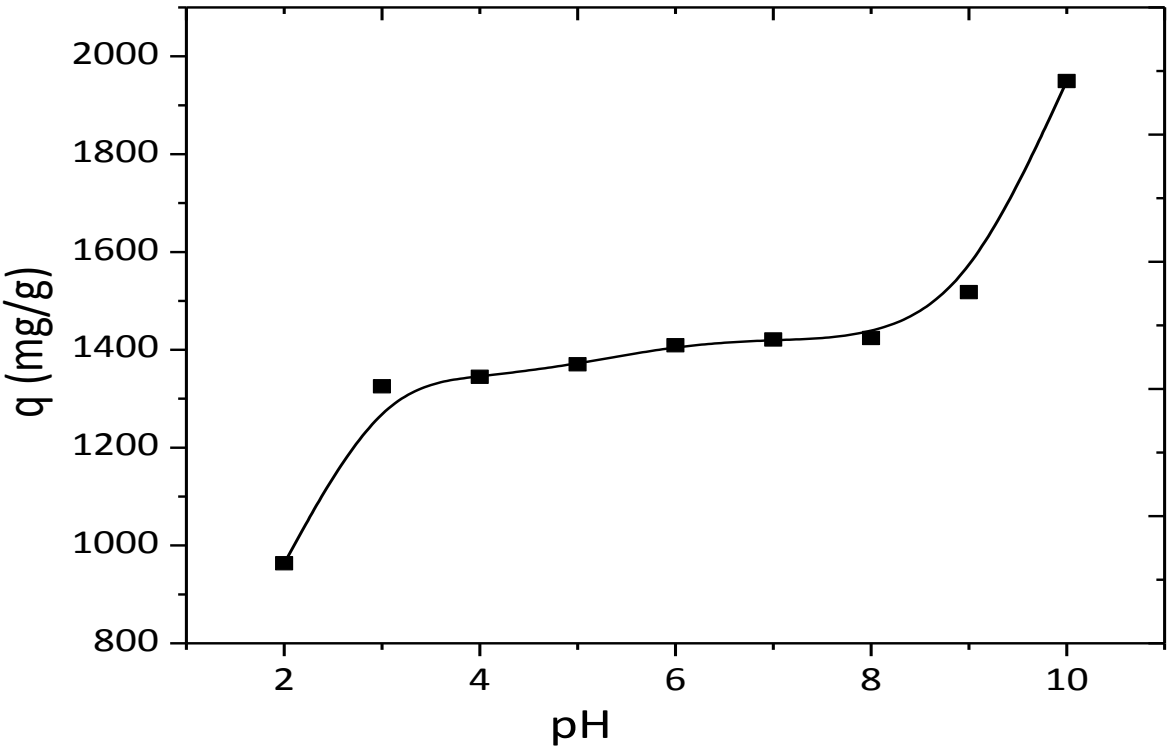

Fig. 47: Effect of pH on adsorption of dye MBG by GO

At higher pH carboxyl groups of GO dissociated extensively and surface of GO became highly negatively charged [110]. While at higher pH the dye molecule existed as cation (Dye^+) which helps in interaction between adsorbent surface and cationic dye with the increase in pH. At low pH, some of the carboxyl groups of GO was protonated and formed positive ions [111]. This demonstrated electrostatic repulsion between cationic dye and adsorbent, which led to the lower adsorption.

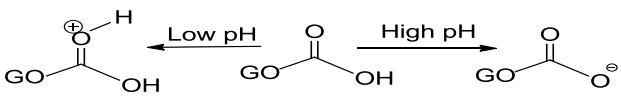

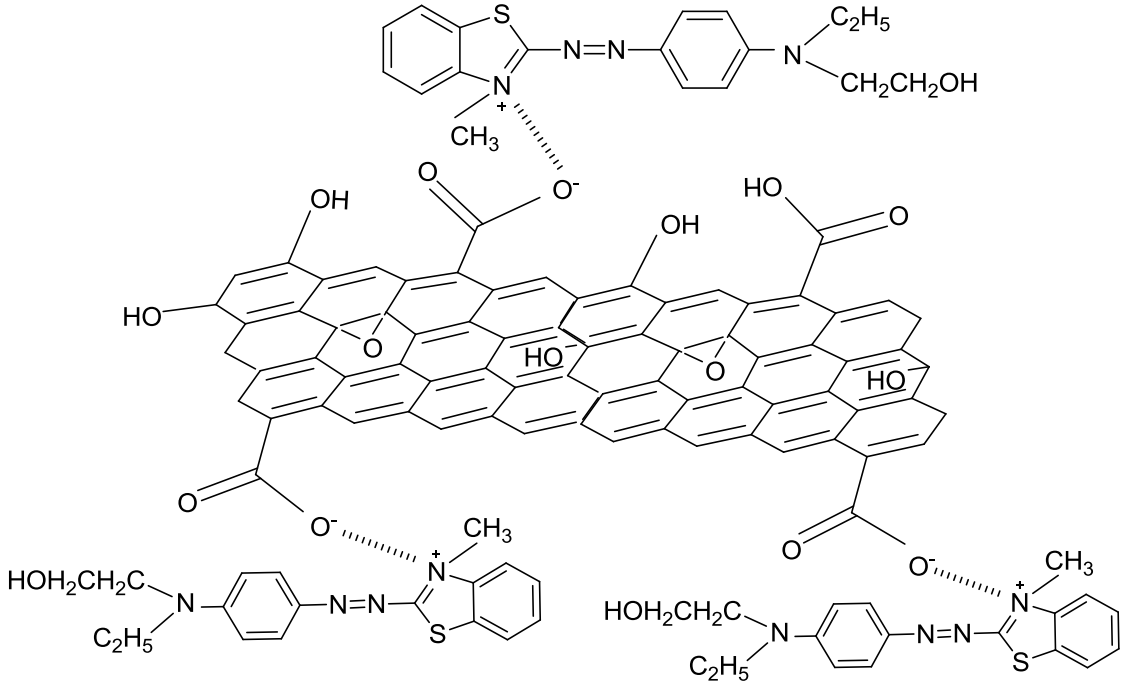

Fig. 48: Mechanism of dye MBG adsorption on GO at low and high pH

4.1.3.3.3. Effect of adsorbent dosage on adsorption of dye MBG by GO

For the adsorption of dye MBG by GO, the optimum dosage were determined following the same procedure as 4.1.3.1.3. Here a set of 4 experiments were carried out at pH of 7 using 10 ml 1000 ppm dye solutions and 2, 5, 8, 10 mg of disperse GO were added to the flasks. The mixtures were shaken for 30 minutes, filtered and the absorbance of the filtrates were measured by UV-Vis spectroscopy at 554 nm. Then concentrations of the solutions after adsorption were determined with respect to standard curve (Fig. 46).

Table 38: Dosage vs adsorption capacity and % removal data of GO for dye MBG

Dosage (mg)	2	5	8	10
Adsorption capacity (mg/g)	2513.95	1316.64	911.04	893.70
% of removal	52.28	65.83	72.88	89.37

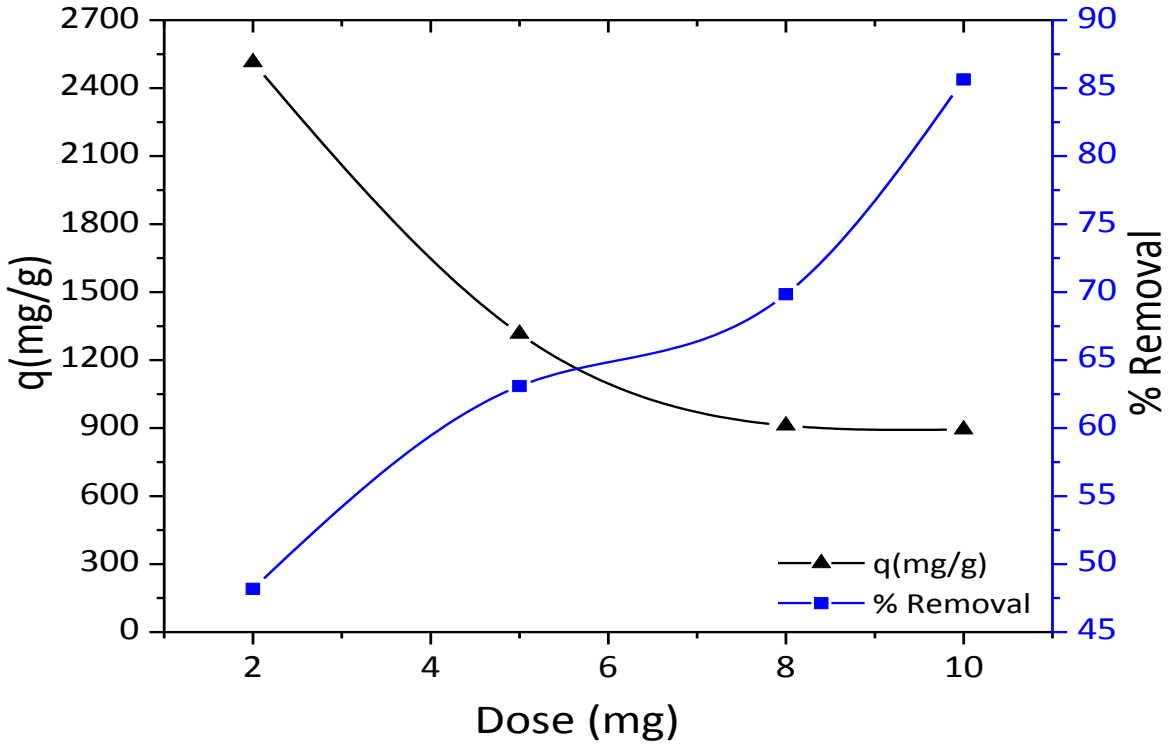

Fig. 49: Effect of adsorbent dosage on adsorption of dye MBG by GO

It was apparent that (Table-38, Fig. 49) with the increase of adsorbent dosage adsorption capacity decreased but percentage removal of dye increased. For the dosage 6 mg/10 ml solution demonstrate the best percentage removal as well as the best adsorption capacity. But at 2 or 5 mg dose the adsorption capacity and % of removal were also good. So, to reduce the use of GO 4 mg/10 ml solution dosage were maintain throughout the study.

4.1.3.3.4. Effect of dye concentration and contact time on adsorption of dye MBG by GO

The adsorption experiments of dye MBG by GO at different concentrations and time were carried out following the same procedure as 4.1.3.1.4. In this case, a set of 6 experiments were carried out at pH of 7 and 4 mg of disperse GO were used for 10 ml 500 ppm dye solutions. The mixtures were shaken at 303 K in various intervals of time ranging from 5-45 minutes, filtered and absorbance of the filtrates were measured by UV-Vis spectroscopy at 554 nm. Then concentrations of the solutions were determined with respect to standard curve (Fig. 46). To observe the effect of dye concentration on adsorption, similar experiments were carried out using 600, 800 and 1000 ppm dye solutions in the same intervals of time.

In these experiments due to the availability of more active sites the adsorption capacities increased (Table-39 and Fig. 50) with the increase in initial dye concentrations.

Table 39: Time vs adsorption capacity data of GO at different times and concentrations for dye MBG

Time (min)	500 ppm	600 ppm	800 ppm	1000 ppm
0	0	0	0	0
5	781.23	808.00	908.03	971.15
10	796.78	860.38	940.90	1074.28
15	835.38	923.38	976.63	1103.13
20	837.73	935.33	1000.20	1116.38
30	873.73	946.30	1042.85	1163.83
45	916.23	999.78	1051.05	1209.88

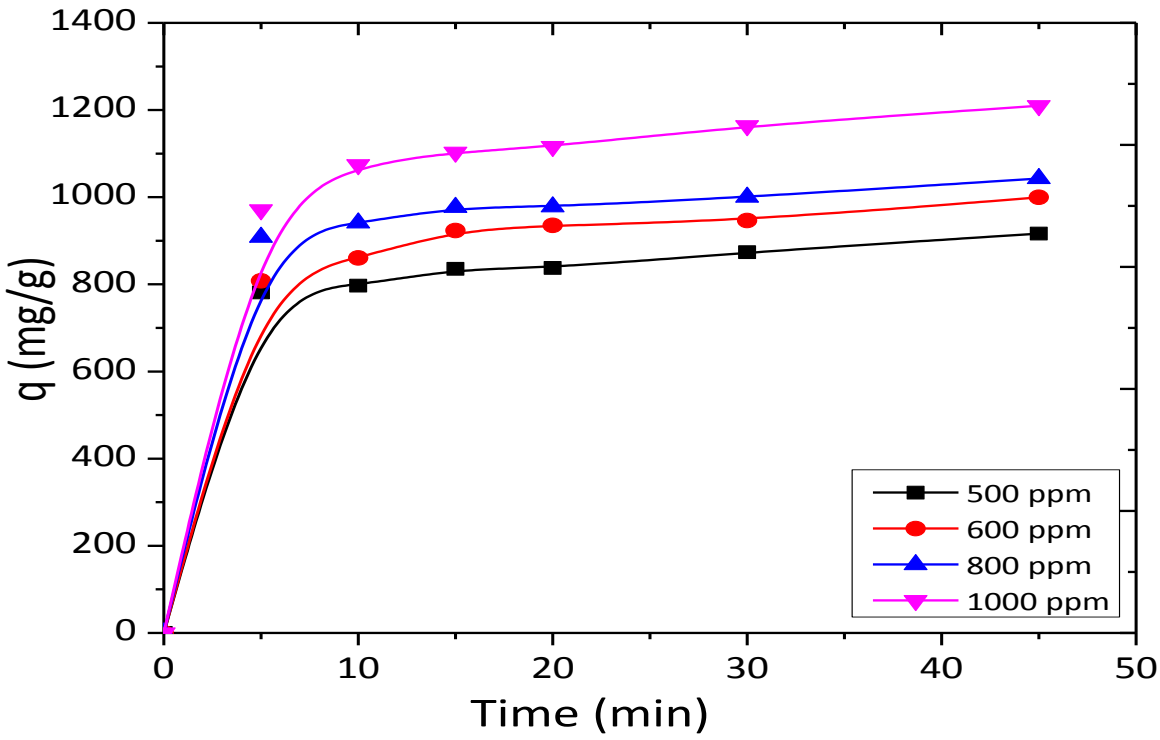

Fig. 50: Effect of dye concentration and time on adsorption of dye MBG by GO

4.1.3.3.5. Adsorption isotherms for adsorption of dye MBG on GO

4.1.3.3.5.1. Langmuir adsorption isotherm

The theoretical maximum adsorption capacity q_m for the adsorption of MBG on GO was calculated following the procedure as 4.1.3.1.5.1. A linear relation between C_e/q_e and C_e was observed (Table-40, Fig. 51) with acceptable regression factor (R^2= 0.9866).

Table 40: C_e and C_e/q_e data of GO at different concentrations for dye MBG

Initial concentration (ppm)	500 ppm	600 ppm	800 ppm	1000 ppm
Equilibrium concentration (C_e)	164.91	225.87	408.75	553.45
C_e/q_e	0.197	0.241	0.418	0.496

From Langmuir isotherm ($\frac{C_e}{q_e} = \frac{1}{q_m b} + \frac{1}{q_m} c_e$) the value of slope was found 0.000798. So,

$$1/q_m = 0.000798$$

$$\therefore q_m = 1253.13 \text{ mg/g}$$

The theoretical maximum adsorption capacity, q_m calculated from the slope was1253.13 mg/g. The value of separation factor R_L was 0.077. This indicate a very favorable monolayer adsorption process [32].

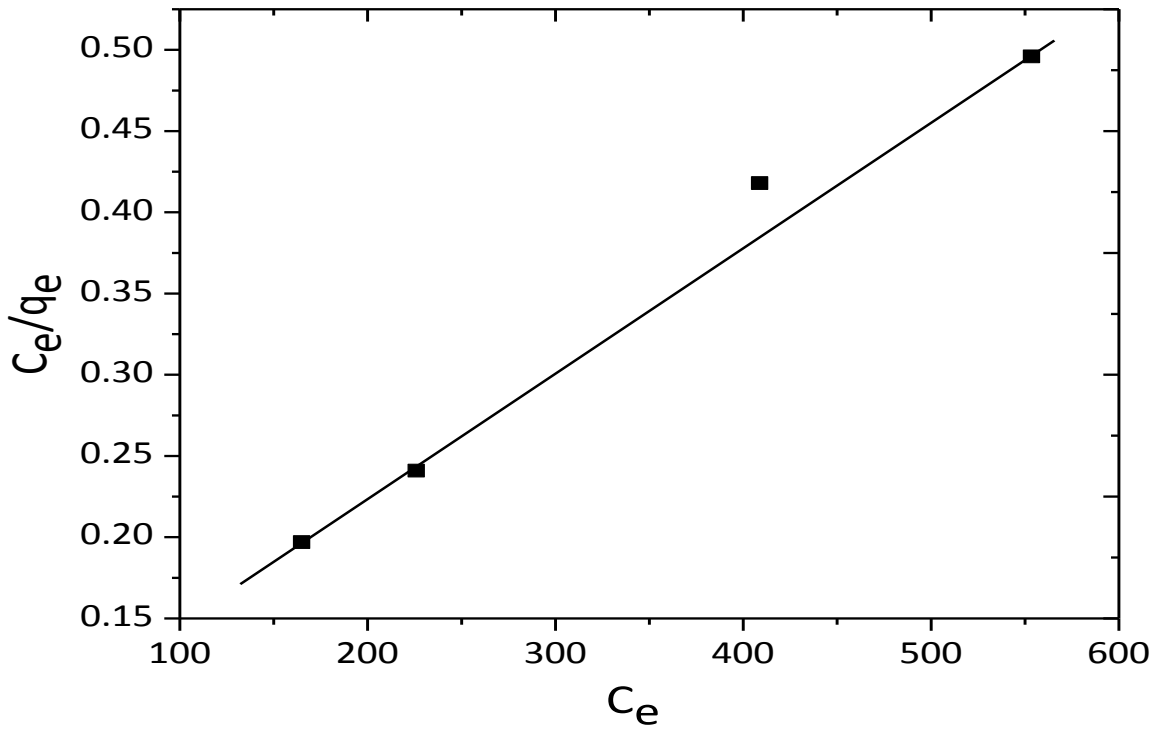

Fig. 51: Langmuir adsorption isotherm at 303 K temperature for dye MBG on GO

4.1.3.3.5.2. Freundlich adsorption isotherm

The experimental data were also tested for the multilayer adsorption mechanism of MBG on GO following the procedure as 4.1.3.1.5.2 and a linear relationship was observed (Table-41, Fig. 52) with good regression coefficient (R^2= 0.9199). The value of n was also calculated

using Eq. (6) and found to be 4.76 which showed that the adsorption were moderate to good [32].

Table 41: lnC_e and lnq_e data of GO at different concentrations for dye MBG

Initial concentration (ppm)	500 ppm	600 ppm	800 ppm	1000 ppm
lnC_e	5.11	5.42	6.01	6.32
lnq_e	6.73	6.84	6.89	7.02

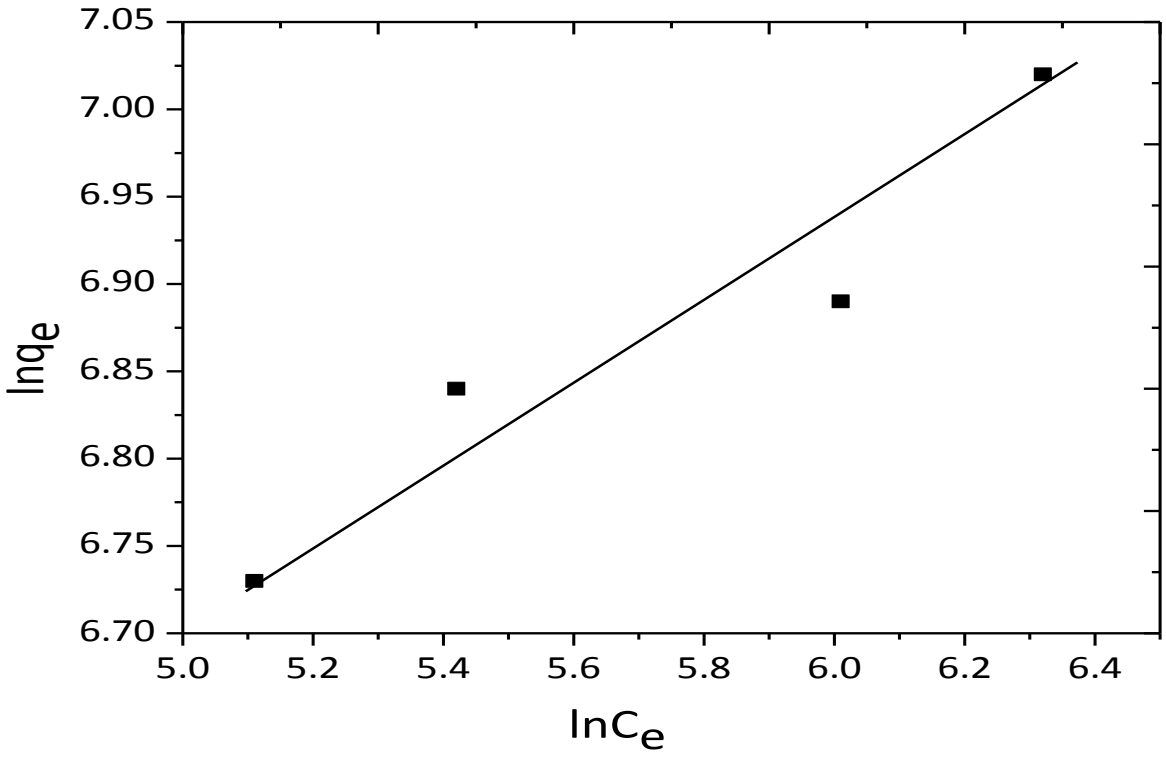

Fig. 52: Freundlich adsorption isotherm at 303 K temperature for dye MBG on GO

The values of different parameters of Langmuir isotherm and Freundlich isotherm are provided in Table-42 and it was evident that the adsorption of MBG on GO followed preferably the Langmuir isotherm model.

Table 42: Theoritical values of q_m,b,R_L, n, K_F and R^2 of GO for dye MBG

Name of isotherm	q_m(mg/g)	R^2	b, Lmg^{-1}	R_L	, n	K_F
Langmuir Isotherm	1253.13	0.9866	0.0847	0.077	-	-
Freundlich isotherm	-	0.9199	-	-	4.76	290.03

4.1.3.3.6. Adsorption kinetics for adsorption of dye MBG on GO

4.1.3.3.6.1. The pseudo-first-order reaction kinetics

Pseudo-first-order model for the adsorption of MBG on GO was studied following the procedure as 4.1.3.1.6.1. The values t and $\log(q_e-q_t)$ are given in (Table-43, Fig. 53).

Table 43: t and $\log(q_e-q_t)$ data at different time and concentrations for adsorption of dye MBG on GO

Time (min)	$(\log q_{e}-q_t)$ at 500 ppm	$(\log q_{e}-q_t)$ at 600 ppm	$(\log q_{e}-q_t)$ at 800 ppm	$(\log q_{e}-q_t)$ at 1000 ppm
5	1.75	2.10	1.85	2.16
10	1.61	1.87	1.57	1.62
15	0.37	1.08	0.18	1.12

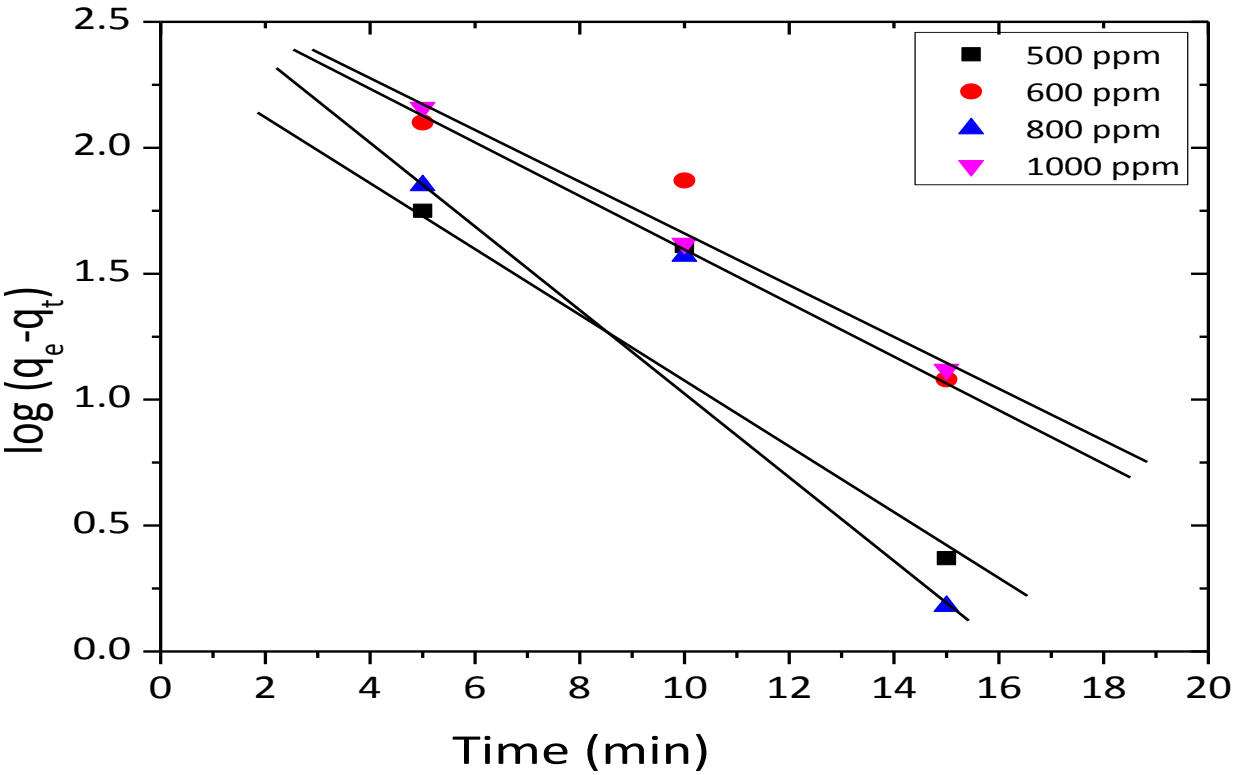

Fig. 53: Pseudo-first order adsorption kinetics for dye MBG on GO

4.1.3.3.6.2. The pseudo-second-order reaction kinetics

Pseudo-second-order model for the adsorption of MBG on GO was studied following the procedure as 4.1.3.1.6.2. The values t and t/q_t were given in Table-44 and Fig. 54.

Table 44: t and t/q_t data at different time and concentrations for adsorption of dye MBG on GO

Time (min)	t/q_t at 500 ppm	t/q_t at 600 ppm	t/q_t at 800 ppm	t/q_t at 1000 ppm
5	0.0064	0.0062	0.0055	0.0051
10	0.0126	0.0116	0.0106	0.0093
15	0.0180	0.0162	0.0154	0.0136
20	0.0239	0.0214	0.0204	0.0179
30	0.0343	0.0317	0.0300	0.0258
45	0.0491	0.0450	0.0432	0.0372

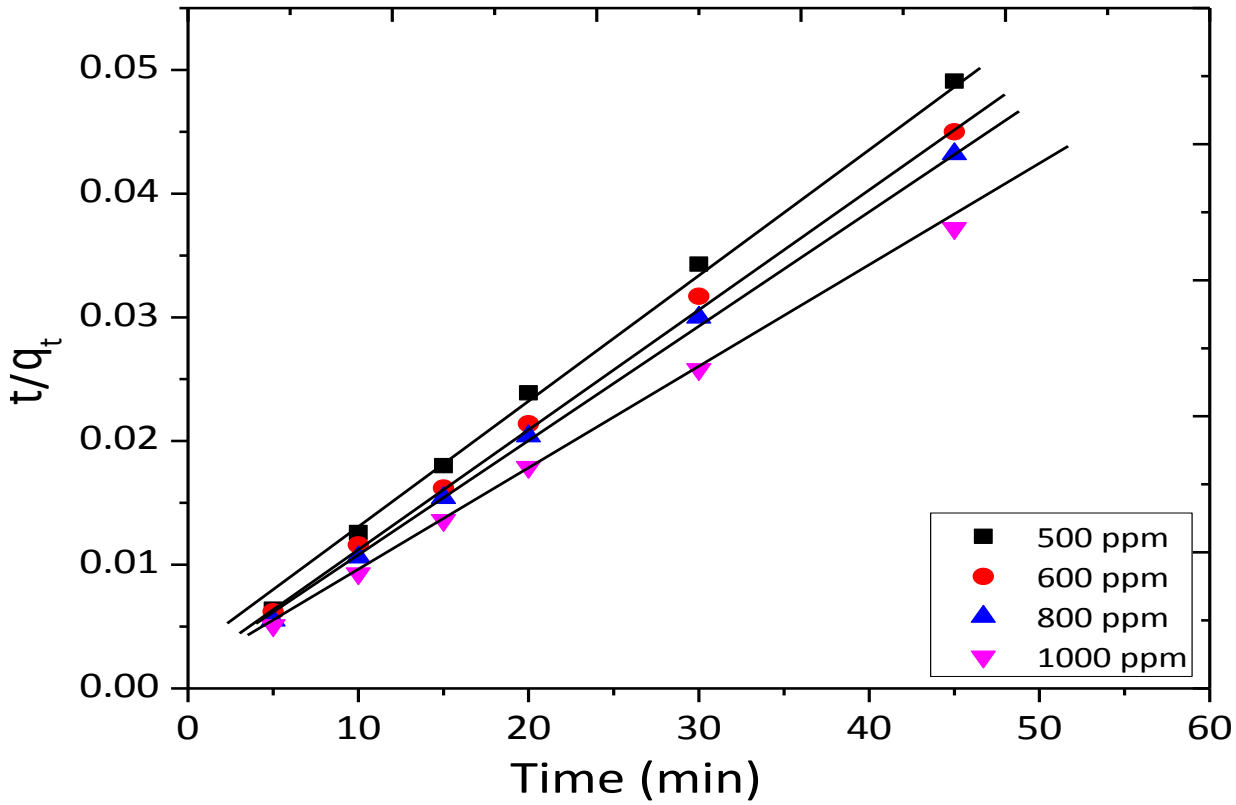

Fig. 54: Pseudo-second-order adsorption kinetics for dye MBG on GO

Considering the kinetic parameters stated in Table-45 and it was observed that the values of correlation coefficient for second-order kinetics were much better than first-order kinetics in both cases.

Table 45: Pseudo-first-order and pseudo-second-order kinetics parameters for the adsorption of dye MBG on GO

Types of kinetics model	Parameters	Initial concentration of dye			
		500 ppm	600 ppm	800 ppm	1000 ppm
	$q_{e,exp}$ (mg/g)	837.73	935.33	978.13	1116.38
Pseudo-first order	$q_{e,cal}$ (First-order)	420.05	505.01	741.31	471.30
	K_1	0.318	0.235	0.385	0.240
	R^2	0.8252	0.9087	0.8716	0.9995
Pseudo-second order	$q_{e,cal}$ (Second-order)	909.09	1000.00	1111.11	1250.00
	K_2	0.00064	0.00059	0.00068	0.00046
	R^2	0.9984	0.9989	0.9992	0.9992

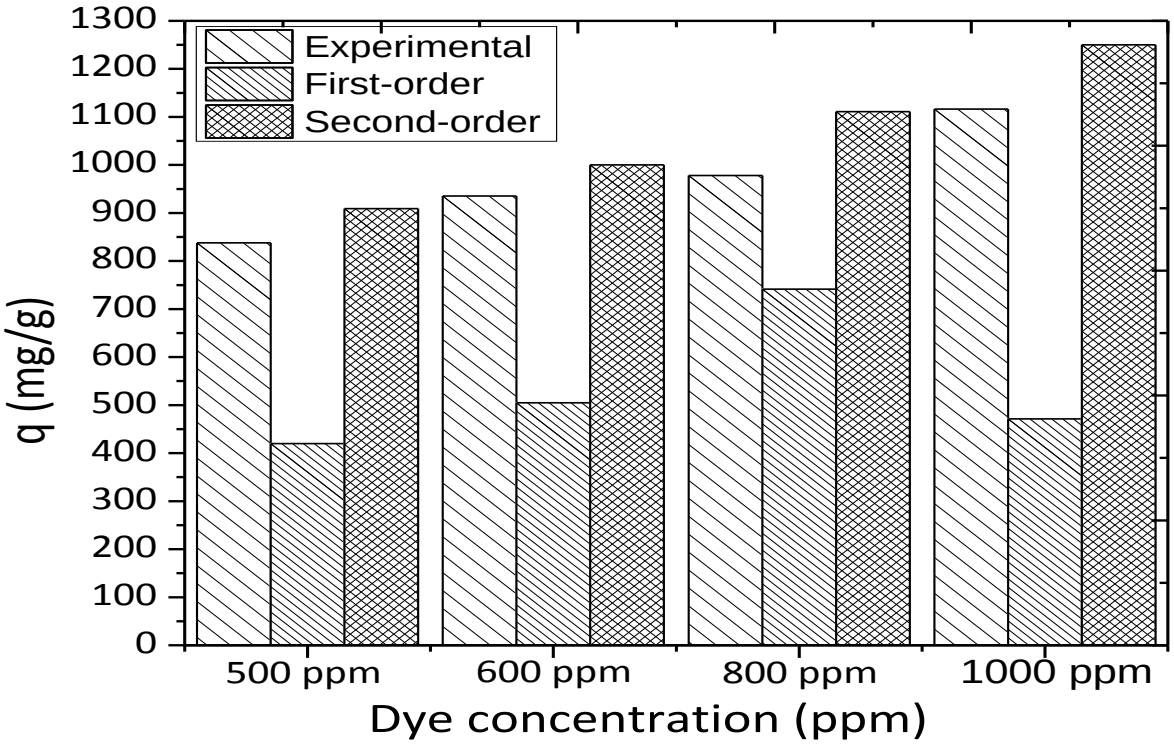

Fig. 55: Comparison of adsorption capacities of pseudo-first-order and pseudo-second-order kinetics for the adsorption of dye MBG on GO

From Fig. 55, it was also observed that the calculated adsorption capacities of second-order kinetics matched well with the experimental values. So, it was revealed that pseudo-second order kinetic model showed better correlation for the adsorption of dye MBG onto GO compared to the pseudo-first-order model.

4.1.3.3.7. Thermodynamic analysis for adsorption of dye MBG on GO

The changes in Gibb's free energy for dye adsorption of MBG on GO at different temperatures were also studied following the procedure as 4.1.3.1.7. In this case, a set of 6 experiments were studied at pH of 7. Here, 4 mg of disperse GO were added to 10 ml of 500 ppm dye solutions and the mixtures were shaken at 303K for different time periods ranging from 5-45 minutes. After shaking the mixtures were filtered and absorbance of the filtrates were measured by UV-Vis spectroscopy at 554 nm. To observe the effect of temperature on the adsorption of MBG on GO similar two sets of experiments were studied at 313K and 323K.

Table 46: Adsorption capacity data of dye MBG on GO at different time and temperatures

Time (min)	q at 303 K	q at 313 K	q at 323 K
0	0	0	0
5	781.23	701.25	618.48
10	796.78	746.68	636.00
15	835.38	782.88	654.83
20	837.73	791.00	661.75
30	873.73	806.38	674.53
45	916.23	809.63	708.20

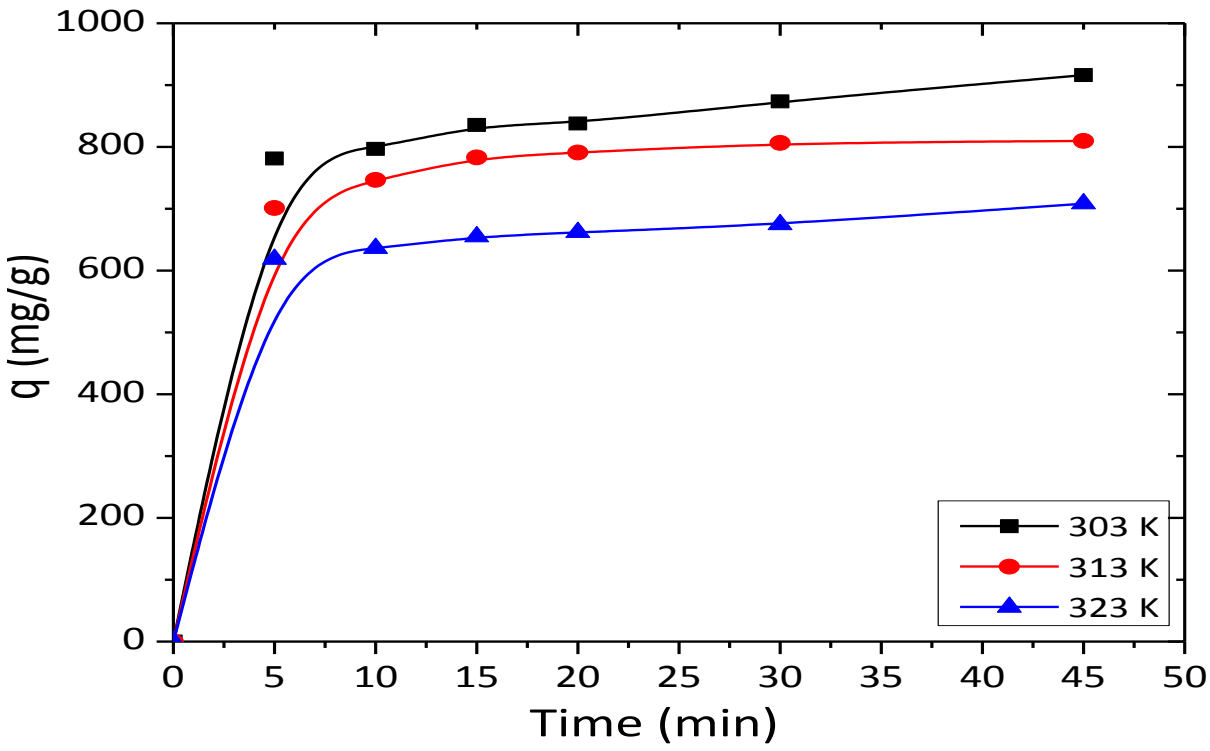

Fig. 56: Adsorption of dye MBG on GO at different temperature

The effects of contact time and temperature on adsorption capacity of GO for MBG were plotted in Table-46 and Fig. 56. The equilibrium adsorption capacity was 837.73 mg/g at 303 K that decreased to 791.00 mg/g and 661.75 mg/g at 313 K and 323 K. The Gibb's free energies were found to be -4.11, -3.80, -2.77 KJ mol^{-1} at 303K, 313K and 323K, respectively.

The average standard enthalpy change ΔH^o and entropy change ΔS^o for the adsorption of MBG on GO were also calculated from the van't Hoff equation. A straight line was obtained by plotting $\ln k_d$ versus 1/T (Table-47, Fig. 57).

Table 47: 1/T vs $\ln k_d$ data of adsorption process

1/T	0.0033	0.0032	0.0031
$\ln k_d$	1.63	1.46	1.03

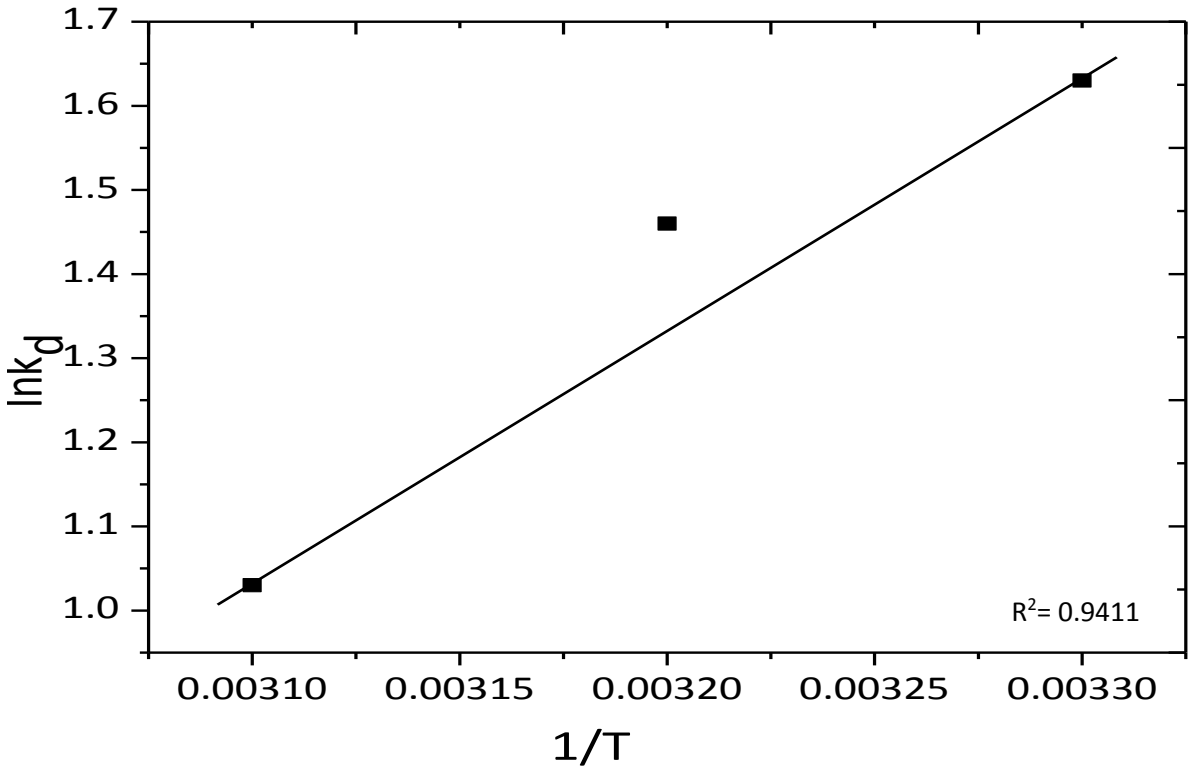

Fig. 57: Plot of van't Hoff equation for the adsorption of dye MBG on GO

The standard enthalpy change ΔH^o and entropy change ΔS^o were obtained -24.94 KJ mol^{-1} and -0.068 KJ K^{-1} mol^{-1}, respectively. The value of ΔG^o increased from -4.11 to -2.77 with increase in temperature from 303K to 323 K. Thus the adsorption of MBG on GO was spontaneous at lower temperature and the adsorption of MBG on GO was a physical adsorption [32].

4.1.3.3.8. Plausible mechanism for adsorption of dye MBG on GO

In aqueous solutions graphene oxide got dissociated, form negative ions and possess negative surface charge at all pH (Fig. 13). So, GO showed significant adsorption towards cationic dyes at all pH. But at higher pH carboxyl groups of GO dissociated extensively and surface of GO became highly negatively charged. As a result it showed higher adsorption capacity at high pH.

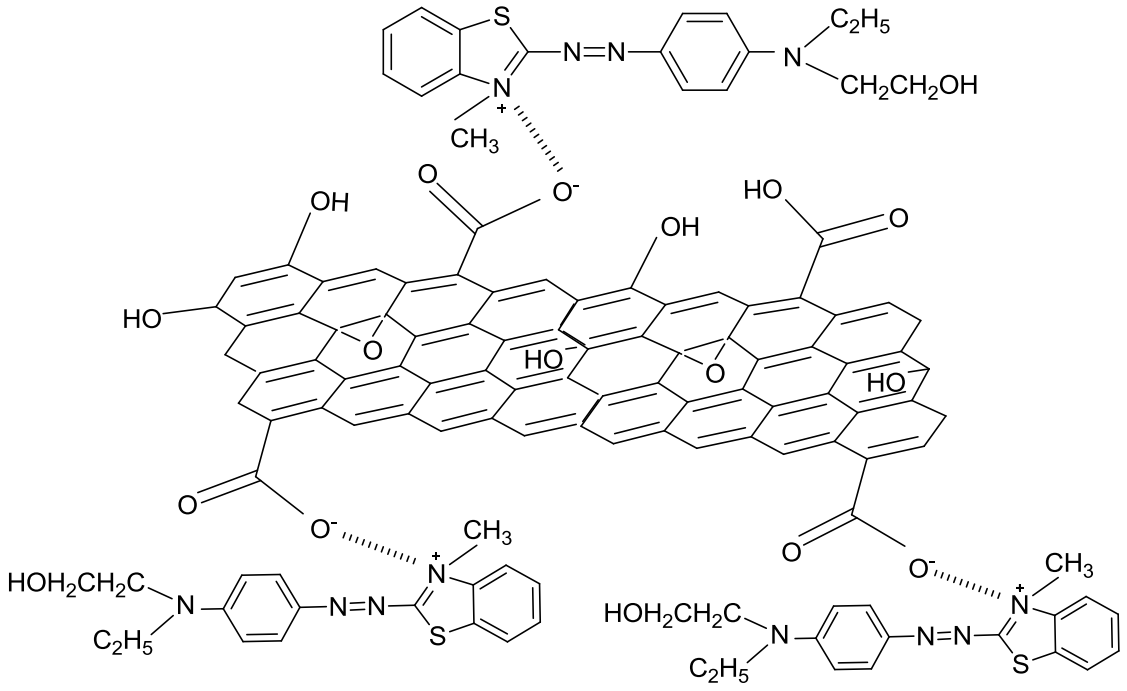

Fig. 58: Mechanism of dye MBG adsorption on GO

4.1.3.3.9. Regeneration of used GO

In order to check the regeneration ability 2 % HCl was added to the used GO to remove the dye. Then washed with distilled water upto pH reached to 7.

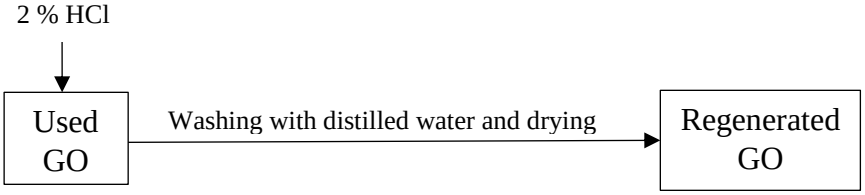

Fig. 59: Flow diagram of regeneration of used GO

Then the regenerated GO was dried and used for further adsorption. In this study, 4 mg of dispersed regenerated GO was used for10 ml 1000 ppm dye solution at pH of 7 with shaking for 30 minutes. Fresh GO showed the adsorption capacity of 1421.10 mg/g for 1000 ppm

dye solution at pH of 7 while the regenerated GO of 1st, 2nd and 3rd recycle (Table-48, Fig. 60) showed the adsorption capacities of 1066.06 mg/g, 792.50 mg/g and 713.18 mg/g, respectively.

Table 48: Reusability of GO in the removal of dye MBG

Type of GO	Fresh GO	Recycle-1	Recycle-2	Recycle-3
Adsorption capacity q (mg/g)	1421.10	1066.06	792.50	713.18

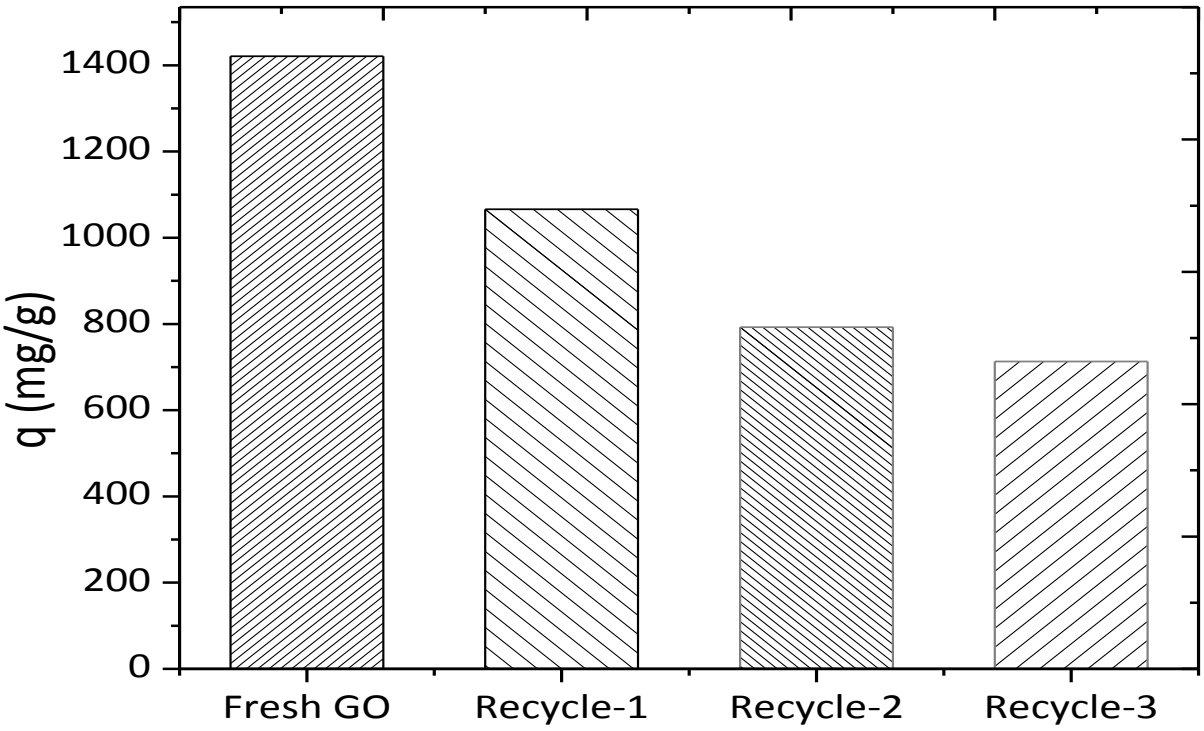

Fig. 60: Reusability of GO in the removal of dye MBG

4.2. Part 2. Synthesis and characterization of reduced graphene oxide (RGO) and its application for the removal of dye Turquoise GN (TGN) from aqueous solutions

4.2.1 Synthesis of reduced graphene oxide (RGO)

To produce RGO, graphene oxide was reduced by hydrazine hydrate. As a result in RGO, number of oxygenated functional groups (-COOH group) were reduced. This made RGO hydrophobic.

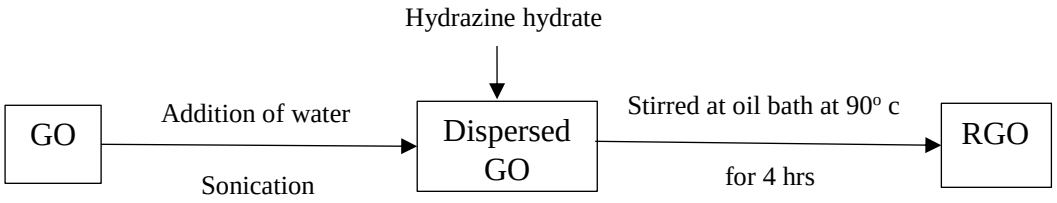

Fig. 61: Flow diagram of reduced graphene oxide (RGO) synthesis

4.2.2. Characterization of RGO

4.2.2.1. Environmental scanning electron microscopy (ESEM)

The morphology and microstructure of RGO was studied with ESEM and Fig. 62 showed randomly aggregated, thin, wrinkled sheets closely connected with each other.

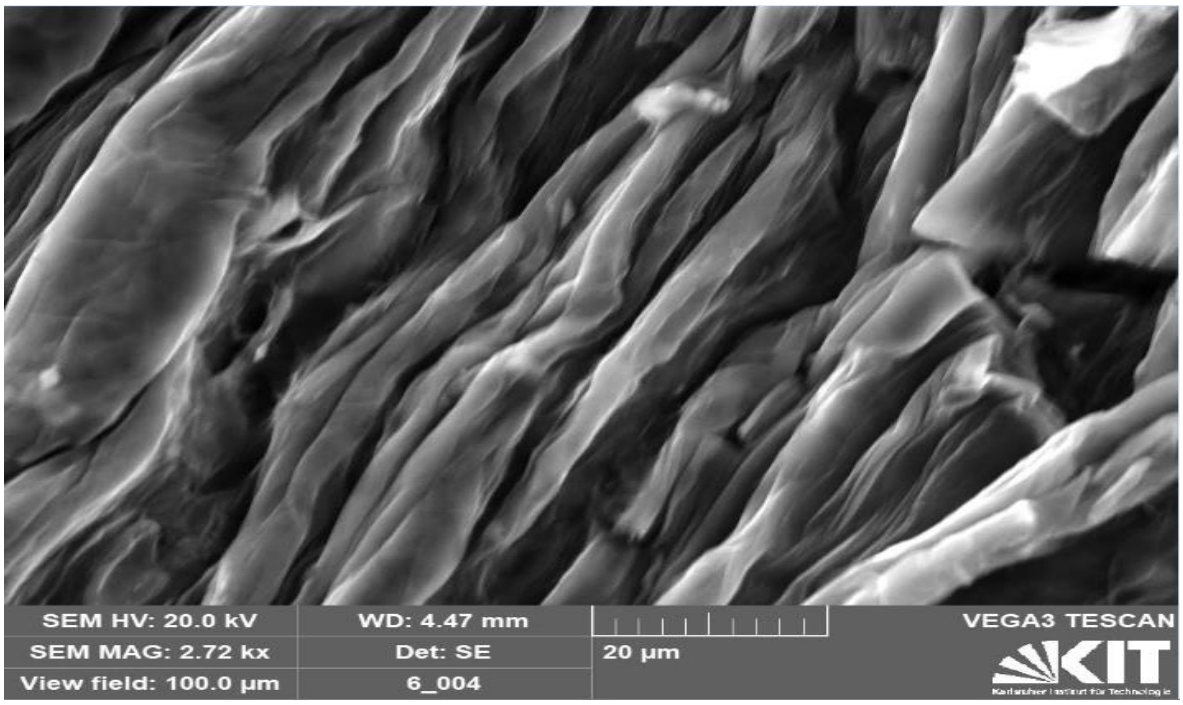

Fig. 62: ESEM image of reduced graphene oxide

4.2.2.2. Elemental analysis

Composition of RGO was determined by elemental analysis and found to contain 63.63 % C, 1.412 % H, 6.42 % N and 0.172 % S. It was also found to contain a considerable amount of oxygen (28.47 %) that was determined indirectly. The elemental analysis was in good agreement with the literature.

4.2.2.3. X-Ray diffraction (XRD) analysis of RGO

The XRD patterns of RGO was represented in Fig. 63. For RGO, the peak was observed at 2θ=23.58^{o} with interlayer spacing of 3.77 Å. The 2θ value of GO was 9.97^{o} corresponding to an interlayer spacing of 8.87 Å (Fig. 11). The shift of the peak was due to the reduction of oxygen from GO to RGO.

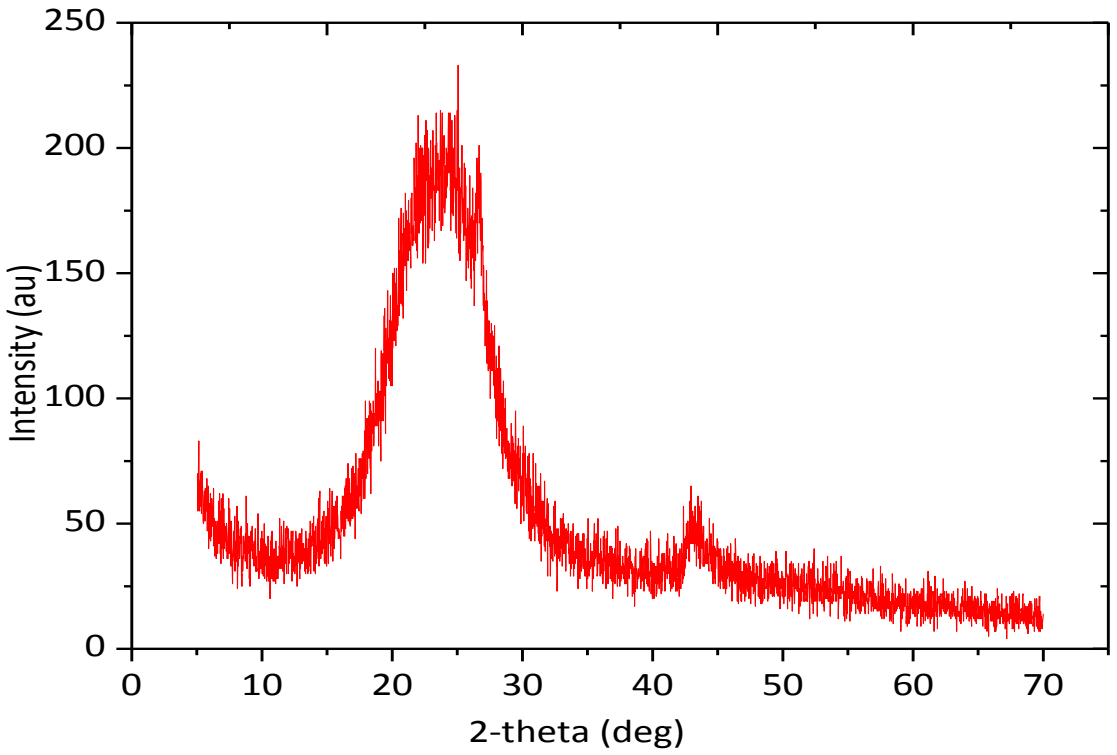

Fig. 63: XRD patterns of reduced graphene oxide

4.2.2.4. Raman spectrum analysis of RGO

Raman spectrum of RGO (Fig. 64) confirmed the existence of both D-band and G-band. The G-band was located at 1567 cm^{-1} and the D-band was located at 1332 cm^{-1}. These values were in good agreement with the documented literature. The existence of D-band revealed the presence of defect sites in the GO sheets and the size of the in-plane sp^{2} domain. The intensity ratio of the D-band and G-band, (I_D/I_G) for RGO was found to be 0.87 which was

0.74 for GO. This increase in I_D/I_G ratio indicate an increase in the average size of the sp^2 domain upon the reduction GO by hydrazine hydrate.

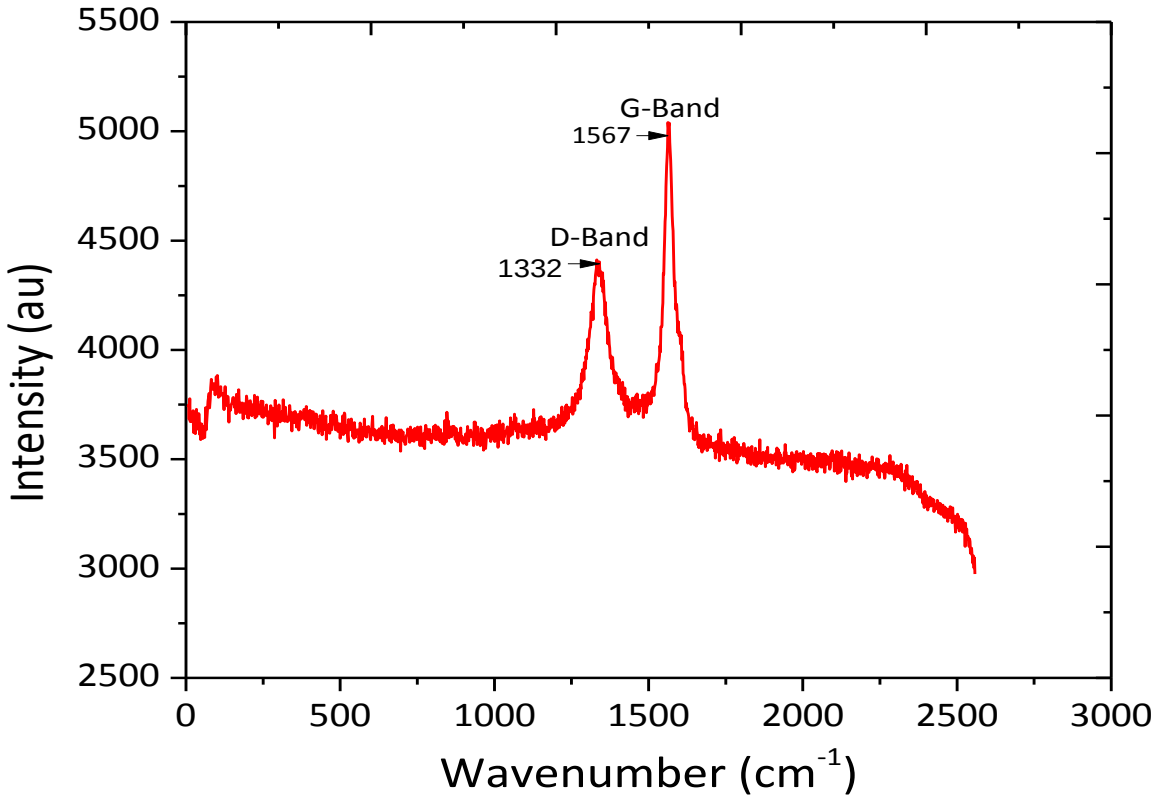

Fig. 64: Raman spectrum of reduced graphene oxide

4.2.2.5. Zeta potential value of reduced graphene oxide

Zeta potential is the potential difference existing between the surface of a solid particle immersed in a conducting liquid and the bulk of the liquid. Zeta potential determination is a significant characterization technique of nanocrystals to estimate the surface charge, which can be employed for understanding the physical stability of nanosuspensions. So, zeta potential of RGO as a function of pH was also studied. For this study RGO sample was prepared by dispersing RGO in DI water. The analysis was carried out in the pH range of 2-10. The results showed that (Table-49, Fig. 65) the zeta potential values of RGO were varied from 15.3 to -33.9 mV with an increase of pH from 2 to 10. The zeta potential values are also in good agreement with the documented literature.

Table 49: pH vs Zeta potential data of RGO

pH	2	4	6	8	10
Zeta potential (mV)	15.3	14.9	-14.3	-19.8	-33.9

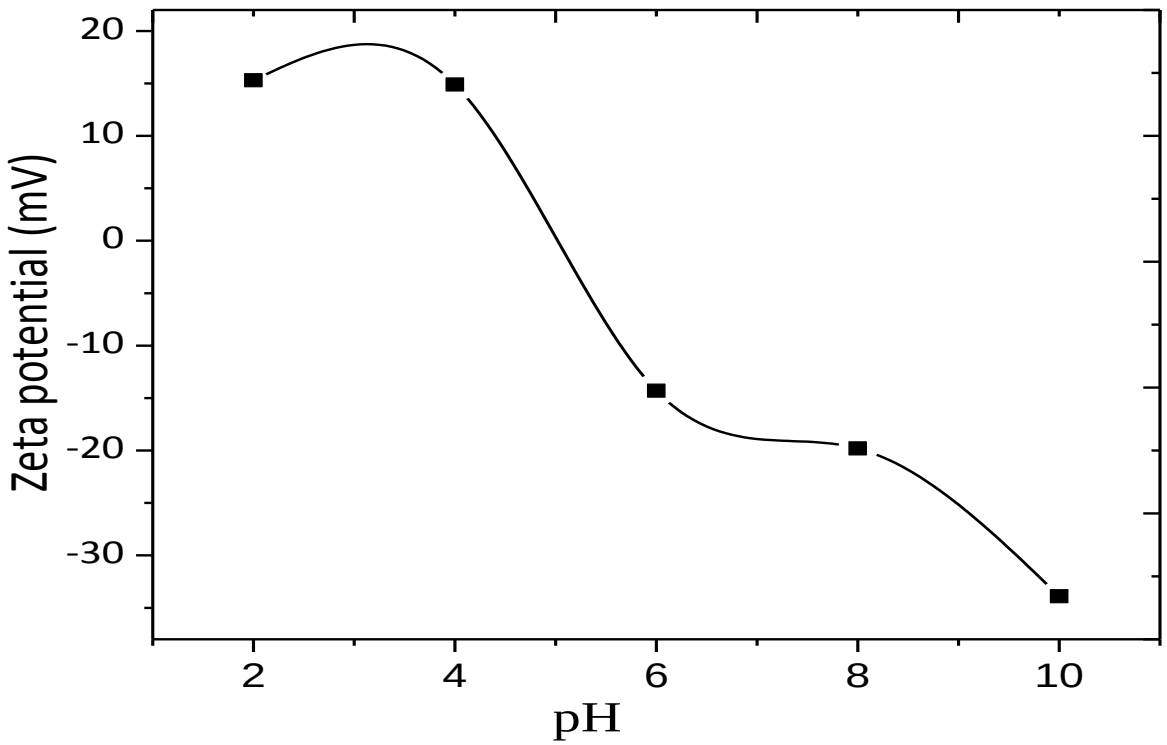

Fig. 65: Zeta potential values of RGO at different pH

4.2.3. Adsorption of dye on RGO

4.2.3.1. Adsorption of dye TGN on RGO

4.2.3.1.1. Effect of pH on adsorption of dye TGN by RGO

The adsorption experiments of dye TGN by RGO at different pH were carried out following the same procedure as 4.1.3.1.2. A set of 6 experiments were studied and 10 mg of disperse GO were added to 10 ml 700 ppm dye solutions. The mixtures were shaken for 30 minutes, filtered and absorbance of the filtrates were measured by UV-Vis spectroscopy at 660 nm. Then concentrations of the solutions after adsorption were determined with respect to standard curve (Fig. 27) and adsorption capacities were calculated. The Maximum adsorption capacity of RGO was 577.46 mg/g at pH of 2 and it slowly decreased (Table-50, Fig. 66) with an increase in pH.

Table 50: pH vs adsorption capacity data of RGO for dye TGN

pH	2	4	6	7	8	10
Adsorption capacity (mg/g)	577.46	480.80	437.65	414.80	393.80	378.69

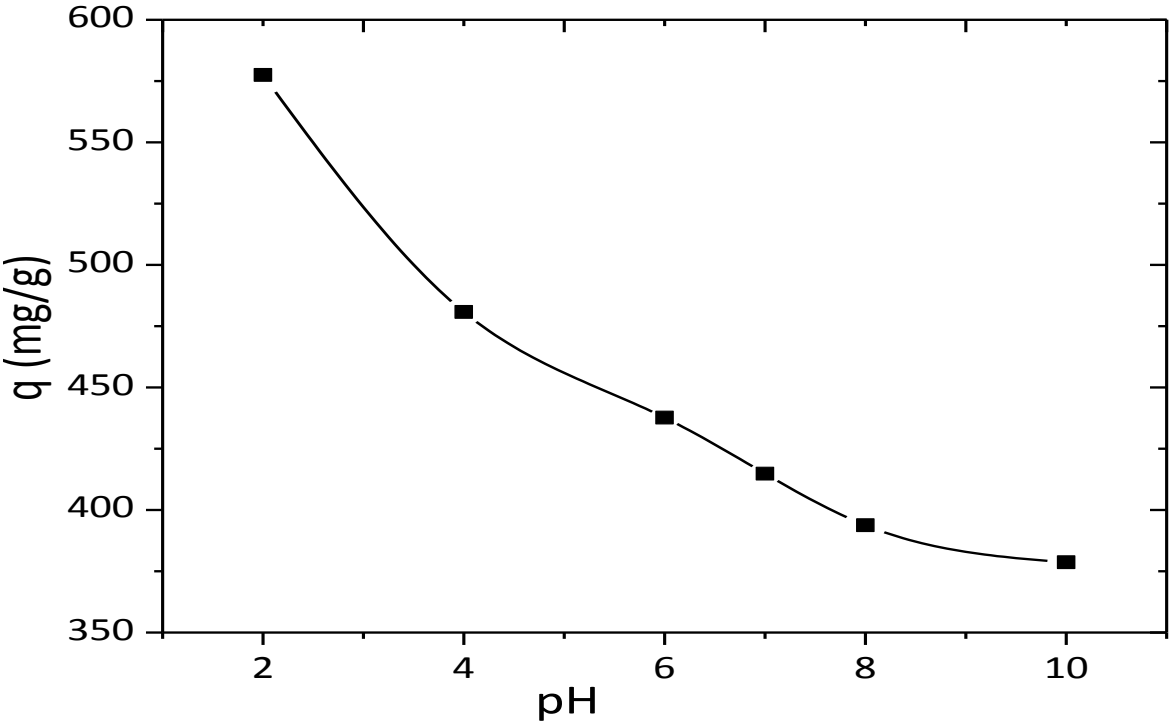

Fig. 66: Effect of pH on adsorption of dye TGN by RGO

According to Fig. 65, at pH of 2 the surface charge of RGO was positive and showed electrostatic interaction with anionic dye. But with an increase in pH carboxyl groups of RGO dissociated extensively and surface of RGO became highly negatively charged [110], while at higher pH the dye molecule existed as anion (Dye^-) and underwent electrostatic repulsion with the negatively charged surface of RGO and thus resulted lower adsorption.

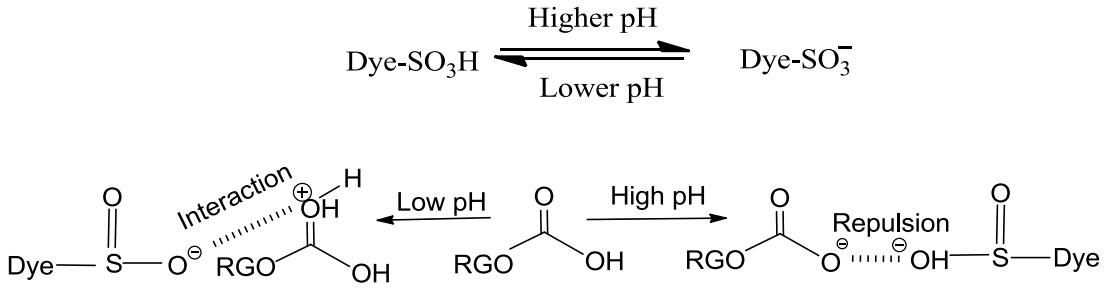

Fig. 67: Mechanism of dye TGN adsorption on RGO at low and high pH

4.2.3.1.2. Effect of adsorbent dosage on adsorption of dye TGN by RGO

For the adsorption of dye TGN by RGO, the optimum dosage were determined following the same procedure as 4.1.3.1.3. Here a set of 4 experiments were carried out at pH of 7 using 10 ml 700 ppm dye solutions and 5, 10, 15, 20 mg of disperse RGO were added to the flasks. The mixtures were shaken for 30 minutes, filtered and the absorbance of the filtrates were measured by UV-Vis spectroscopy at 660 nm. Then concentrations of the solutions after adsorption were determined with respect to standard curve (Fig. 27).

Table 51: Dosage vs adsorption capacity and % removal data of RGO for dye TGN

Dosage (mg)	5	10	15	20
Adsorption capacity (mg/g)	479.50	414.80	348.85	284.32
% of removal	39.48	64.49	79.98	86.47

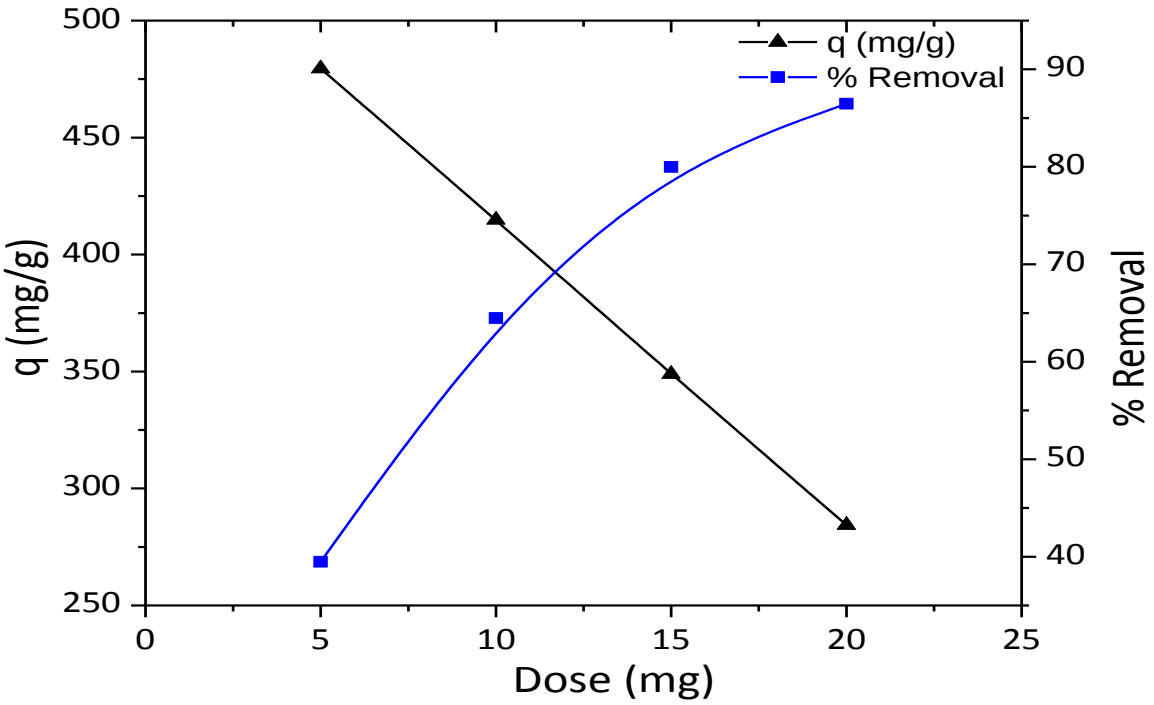

Fig. 68: Effect of adsorbent dosage on adsorption of dye TGN by RGO

It was apparent that (Table-51, Fig. 68) with the increase of adsorbent dosage adsorption capacity decreased because of the decrease of the amount of adsorbate per unit mass of adsorbent [112]. It was observed that a dosage of 11 mg/10 ml solution demonstrate the best percentage removal as well as the best adsorption capacity. However, for simplicity 10 mg/10 ml solution dosage were maintained throughout the study.

4.2.3.1.3. Effect of dye concentration and contact time on adsorption of dye TGN by RGO

The adsorption experiments of dye TGN by RGO at different concentrations and time were carried out following the same procedure as 4.1.3.1.4. In this case, a set of 7 experiments were carried out at pH of 7 and 10 mg of disperse RGO were added to 10 ml 400 ppm dye solutions. Then the mixtures were shaken at 303 K in various intervals of time ranging from 10-60 minutes, filtered and absorbance of the filtrates were measured by UV-Vis

spectroscopy at 660 nm. Then concentrations of the solutions were determined with respect to standard curve (Fig. 27). To observe the effect of dye concentration on adsorption, similar experiments were carried out using 500, 600 and 700 ppm dye solutions in the same intervals of time.

In these experiments due to the availability of more active sites the adsorption capacity increased (Table-52 and Fig. 69) with the increase in initial dye concentration.

Table 52: Time vs adsorption capacity data of RGO at different times and concentrations for dye TGN

Time (min)	400 ppm	500 ppm	600 ppm	700 ppm
0	0	0	0	0
10	346.03	352.68	419.02	482.42
15	348.65	369.54	434.72	486.14
20	350.32	376.36	448.04	495.02
25	359.86	391.00	451.26	502.30
30	360.81	401.93	458.50	512.34
45	361.79	400.78	459.28	515.38
60	356.46	398.30	460.96	519.42

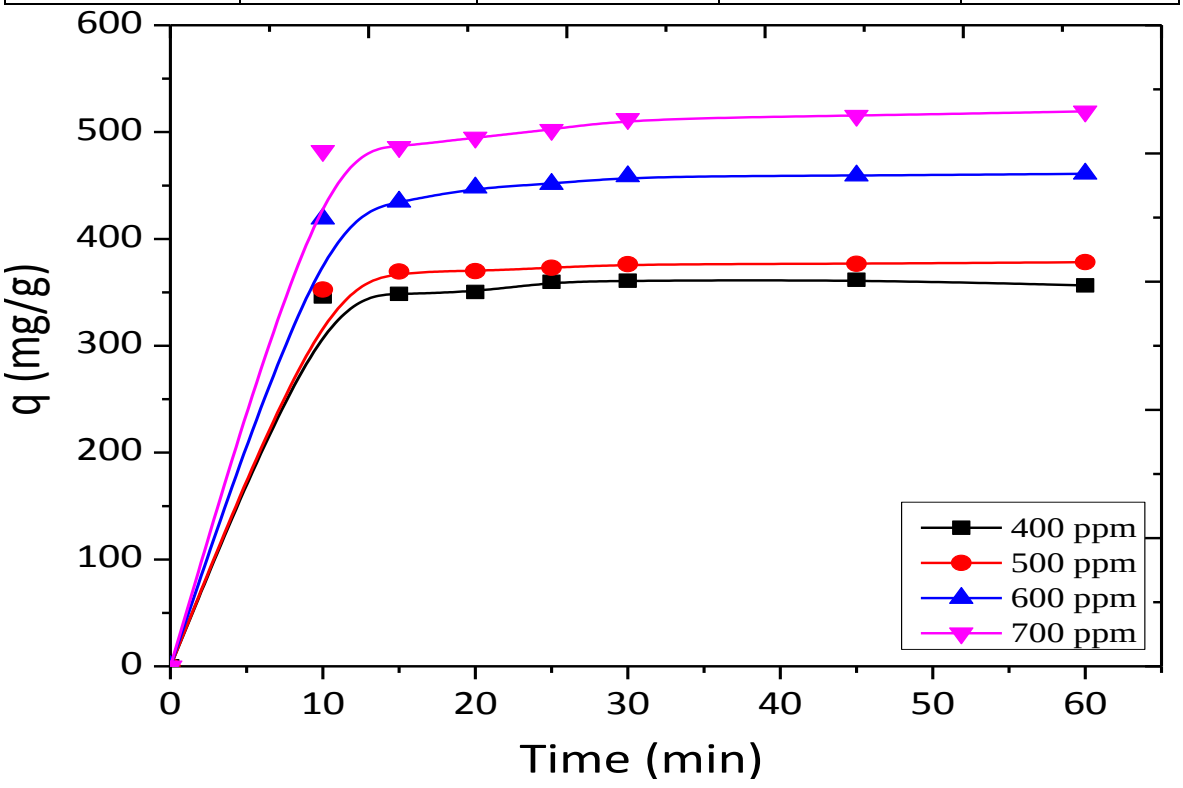

Fig. 69: Concentration and time effect on adsorption of dye TGN by RGO

4.2.3.1.4. Adsorption isotherms for adsorption of dye TGN on RGO

4.2.3.1.4.1. Langmuir adsorption isotherm

The theoretical maximum adsorption capacity q_m for the adsorption of TGN on RGO was calculated following the procedure as 4.1.3.1.5.1. A linear relation between C_e/q_e and C_e was observed (Table-53, Fig. 70) with acceptable regression (R^2= 0.9772).

Table 53: C_e and C_e/q_e data of RGO at different concentrations for dye TGN

Initial concentration (ppm)	400 ppm	500 ppm	600 ppm	700 ppm
Equilibrium concentration (C_e)	39.19	98.07	141.50	187.66
C_e/q_e	0.109	0.244	0.309	0.366

From Langmuir isotherm ($\frac{C_e}{q_e} = \frac{1}{q_m b} + \frac{1}{q_m} c_e$) the value of slope was found 0.0017. So,

$$1/q_m = 0.0017$$

$$\therefore q_m = 588.24 \text{ mg/g}$$

The theoretical maximum sorption capacities, q_m calculated from the slope was found to be 588.24 mg/g and the separation factor R_L value was 0.045 which indicates a very favorable monolayer adsorption process [32].

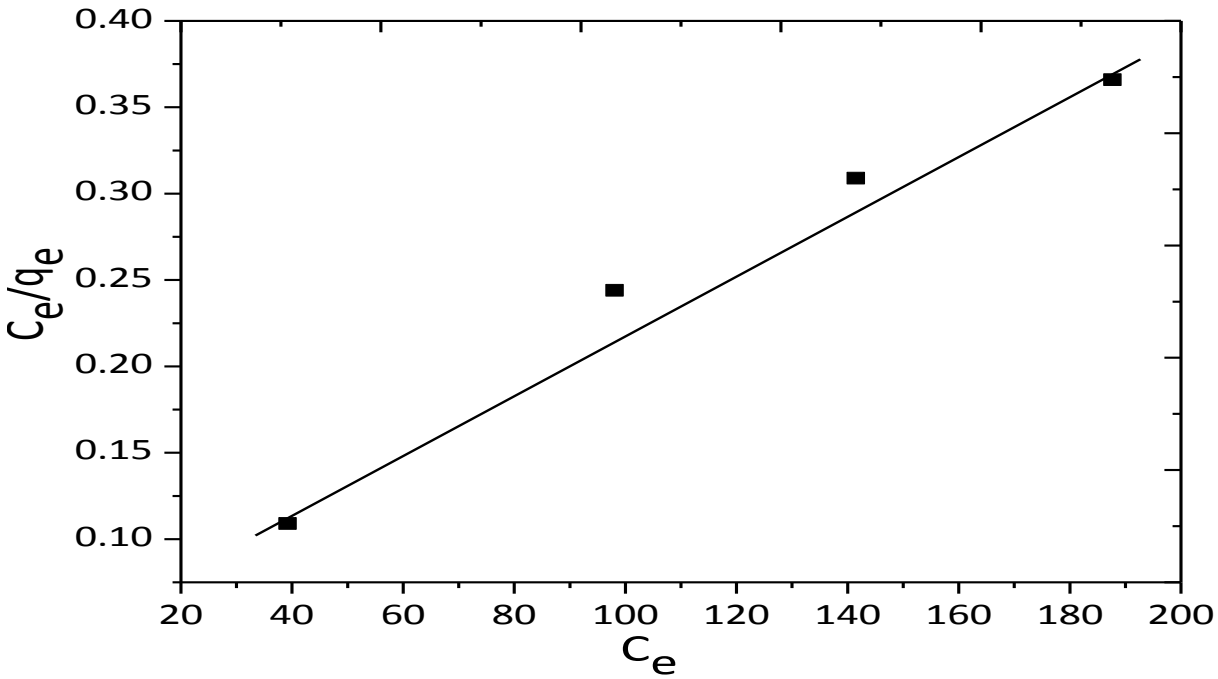

Fig. 70: Langmuir adsorption isotherm at 303 K temperature for dye TGN on RGO

4.2.3.1.4.2. Freundlich adsorption isotherm

The experimental data were also tested for the multilayer adsorption mechanism of TGN on RGO following the procedure as 4.1.3.1.5.2 and a linear relationship was observed (Table-54, Fig. 71) with good regression coefficient (R^2= 0.9107). The value of n was calculated using Eq. (6) and found to be 4.67 which showed that the adsorption was moderate to good [32].

Table 54: $\ln C_e$ and $\ln q_e$ data of RGO at different concentrations for dye TGN

Initial concentration (ppm)	400 ppm	500 ppm	600 ppm	700 ppm
$\ln C_e$	3.67	4.59	4.95	5.23
$\ln q_e$	5.89	6.00	6.13	6.24

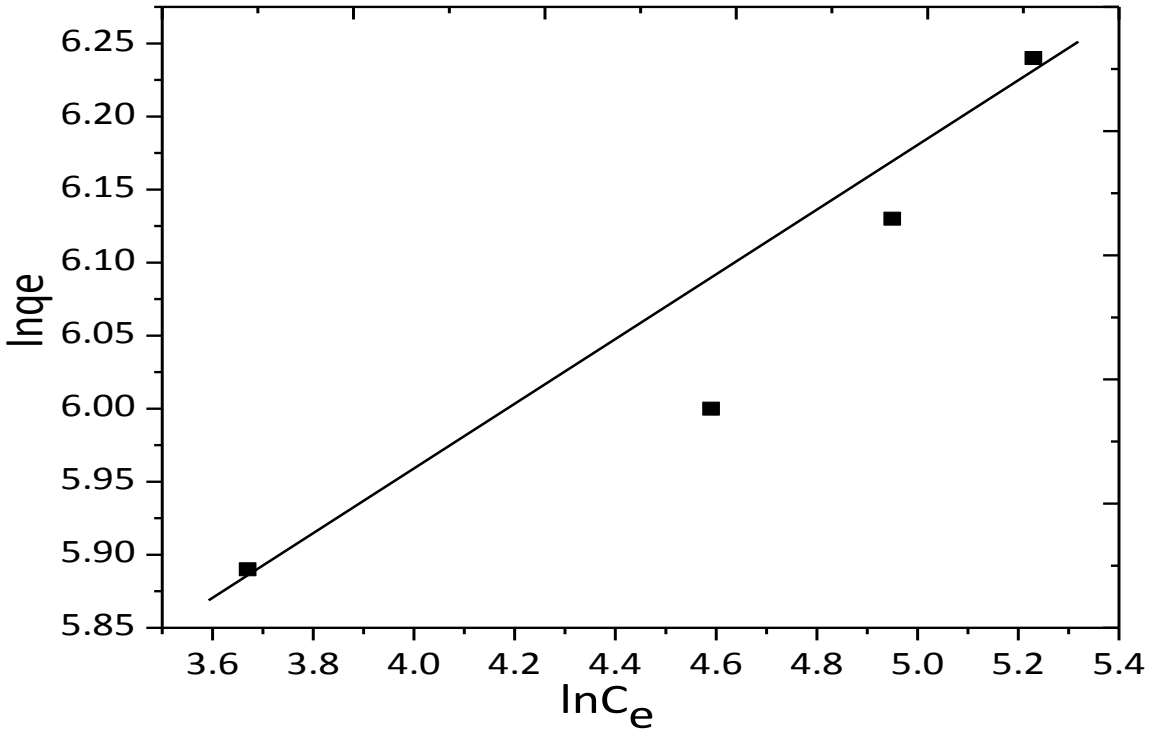

Fig. 71: Freundlich adsorption isotherm at 303 K temperature for dye TGN on RGO

The values of different parameters of Langmuir isotherm and Freundlich isotherm were provided in Table-55 and it was evident that the adsorption of dye TGN on RGO followed both the models but preferably the Langmuir isotherm model.

Table 55: Theoritical values of q_m,b,R_L, n, K_F and R^2 of RGO for dye TGN

Name of isotherm	q_m(mg/g)	R^2	b, Lmg^{-1}	R_L	, n	K_F
Langmuir Isotherm	588.24	0.9772	0.03	0.045	-	-
Freundlich isotherm	-	0.9107	-	-	4.67	160.40

4.2.3.1.5. Adsorption kinetics for adsorption of dye TGN on RGO

4.2.3.1.5.1. The pseudo-first-order reaction kinetics

Pseudo-first-order model for the adsorption of TGN on RGO was studied following the procedure as 4.1.3.1.6.1. The values t and $\log(q_e-q_t)$ were given in Table-56 and Fig. 72.

Table 56: t and $\log(q_e-q_t)$ data at different time and concentrations for adsorption of dye TGN on RGO

Time (min)	$(\log q_e-q_t)$ at 400 ppm	$(\log q_e-q_t)$ at 500 ppm	$(\log q_e-q_t)$ at 600 ppm	$(\log q_e-q_t)$ at 700 ppm
10	1.17	1.69	1.60	1.48
15	1.08	1.51	1.38	1.42
20	1.02	1.41	1.02	1.24
25	0.95	1.04	0.86	1.01

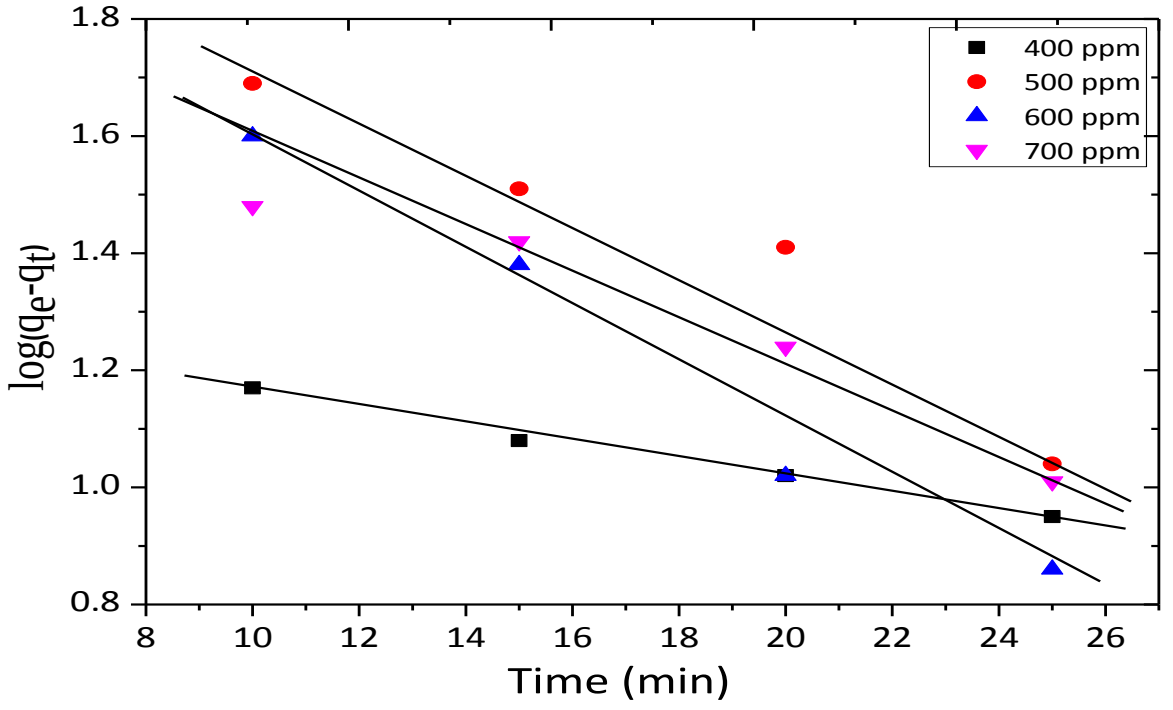

Fig. 72: Pseudo-first order adsorption kinetics for dye TGN on RGO

4.2.3.1.5.2. The pseudo-second-order reaction kinetics

Pseudo-second-order model for the adsorption of TGN on RGO was studied following the procedure as 4.1.3.1.6.2. The values t and t/q_t were given in Table-57 and Fig. 73.

Table 57: t and t/q_t data at different time and concentrations for adsorption of dye TGN on RGO

Time (min)	t/q_t at 400 ppm	t/q_t at 500 ppm	t/q_t at 600 ppm	t/q_t at 700 ppm
10	0.029	0.028	0.023	0.021
15	0.043	0.041	0.035	0.031
20	0.057	0.053	0.045	0.040
25	0.070	0.064	0.055	0.050
30	0.083	0.075	0.065	0.059
45	0.124	0.112	0.098	0.087
60	0.170	0.151	0.130	0.116

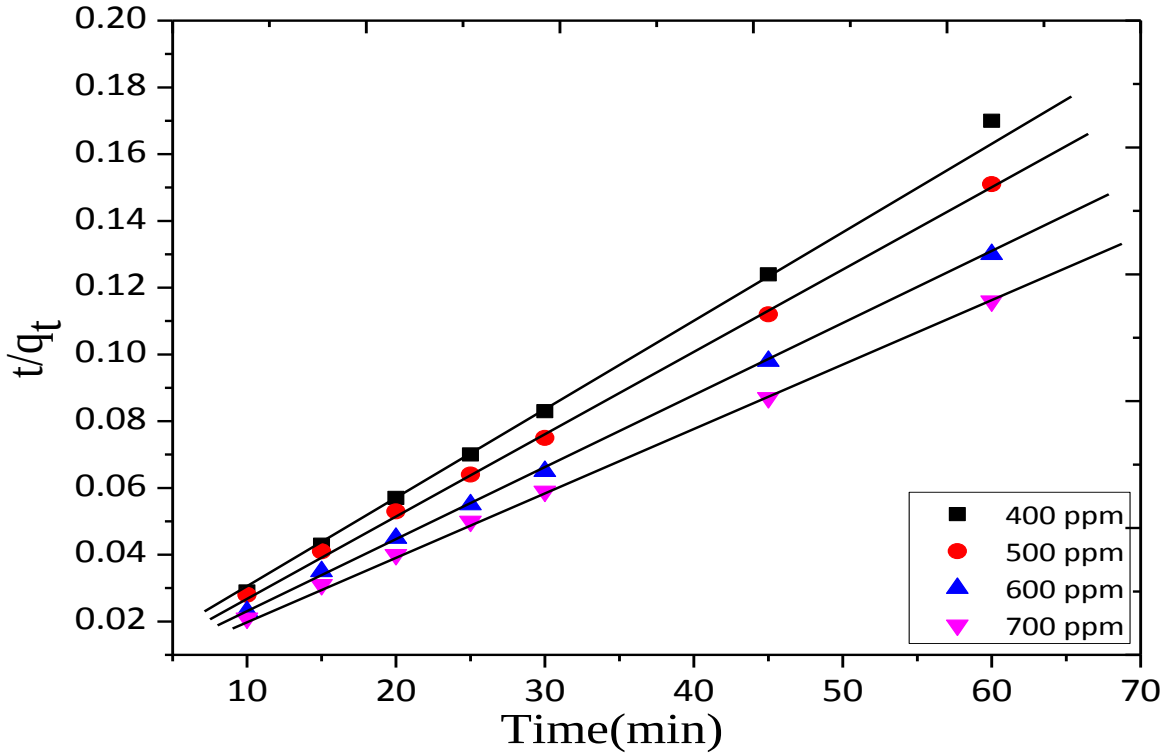

Fig. 73: Pseudo-second-order adsorption kinetics for dye TGN on RGO

Considering the kinetic parameters stated in Table-58 orders of the adsorption processes were studied and it was observed that the values of correlation coefficient for second-order kinetics were much better than first-order kinetics in both cases.

Table 58: Pseudo-first-order and pseudo-second-order kinetics parameters for the adsorption of dye TGN on RGO

Types of kinetics model	Parameters	Initial concentration of dye			
		400 ppm	500 ppm	600 ppm	700 ppm
	$q_{e,exp}$ (mg/g)	360.81	401.93	458.50	512.34
Pseudo-first order	$q_{e,cal}$ (First-order)	20.28	134.90	131.22	69.82
	K_1	0.033	0.094	0.119	0.073
	R^2	0.9931	0.9327	0.9803	0.9442
Pseudo-second order	$q_{e,cal}$ (Second-order)	357.14	416.67	476.19	526.32
	K_2	0.0157	0.0016	0.0021	0.0016
	R^2	0.9992	0.9993	0.9997	0.999

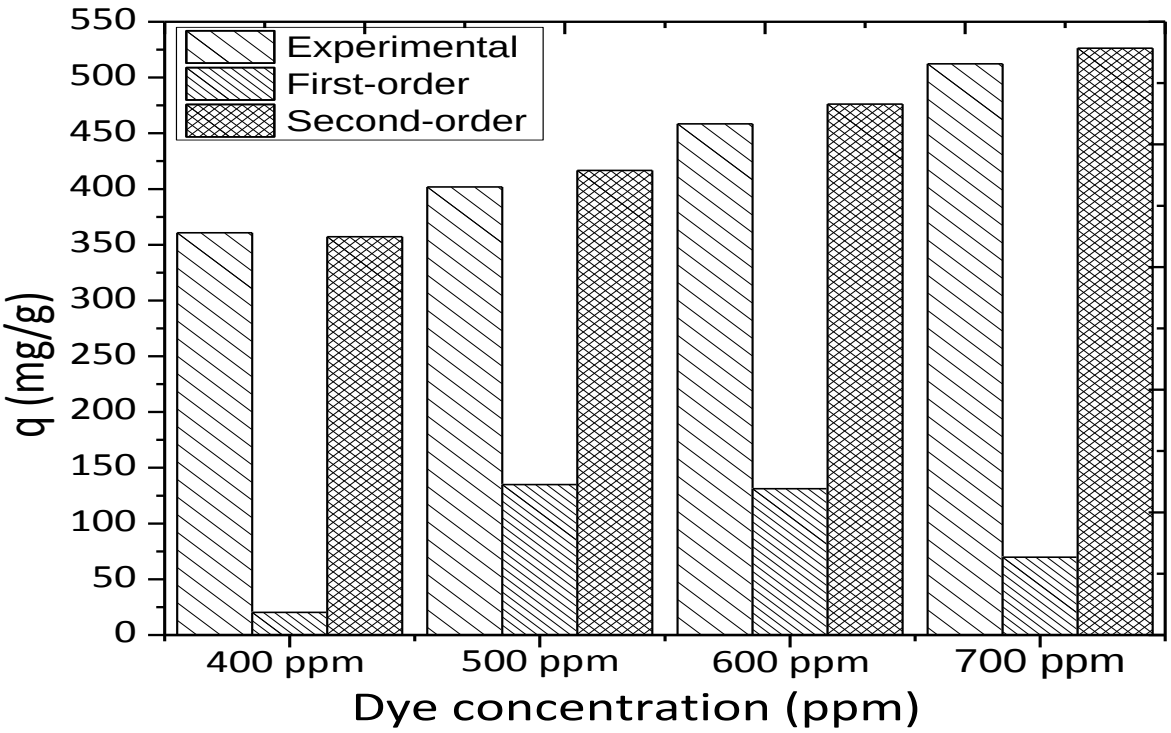

Fig. 74: Comparison of adsorption capacities of pseudo-first-order and pseudo-second-order kinetics for the adsorption of dye TGN on RGO

From Fig. 74, it was also observed that the calculated adsorption capacities of second-order kinetics matched well with the experimental values. So, it is revealed that pseudo-second order kinetic model showed better correlation for the adsorption of TGN onto RGO compared to the pseudo-first-order model.

4.2.3.1.6. Plausible mechanism for adsorption of dye TGN on RGO

In our study, the prepared RGO showed significant amount of anionic dye adsorption. In this case the driving forces of dye adsorption are the electrostatic interaction at low pH and surface defects, hydrophobic association, van der walls interactions as well as π- π interaction at higher pH [114, 115].

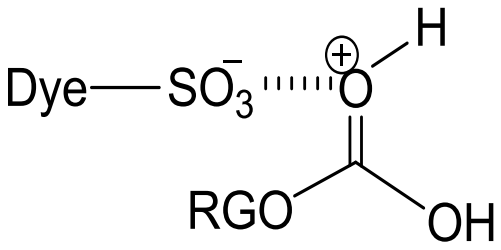

Fig. 75: Mechanism of dye TGN adsorption on RGO at low pH

4.2.3.1.7. Regeneration of used RGO

In order to check the regeneration ability used RGO was washed with 2 % HCl to remove the dye. Then the RGO was washed with distilled water up to pH reached to 7.

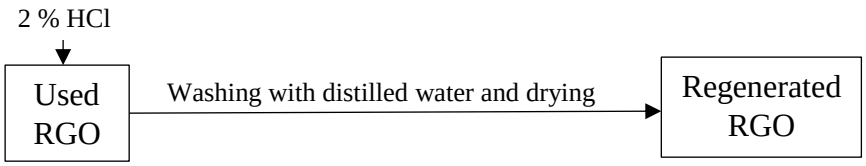

Fig. 76: Flow diagram of regeneration of used RGO

Finally, the regenerated RGO was dried and 10 mg of dispersed regenerated RGO was used for10 ml 700 ppm dye solution at pH of 7. Fresh RGO showed the adsorption capacity of 414.80 mg/g for 700 ppm dye solution at pH of 7 while the regenerated RGO of 1st, 2nd, 3rd and 4th recycle (Table-59, Fig. 77) showed the adsorption capacities of 143.03 mg/g, 135.23 mg/g, 111.28 mg/g and 82.53 mg/g, respectively. From the result it was understood that the regenerated RGO showed moderate adsorption capacity.

Table 59: Reusability of RGO in the removal of dye TGN

Type of RGO	Fresh RGO	Recycle-1	Recycle-2	Recycle-3	Recycle-4
Adsorption capacity q (mg/g)	414.80	143.03	135.23	111.28	82.53

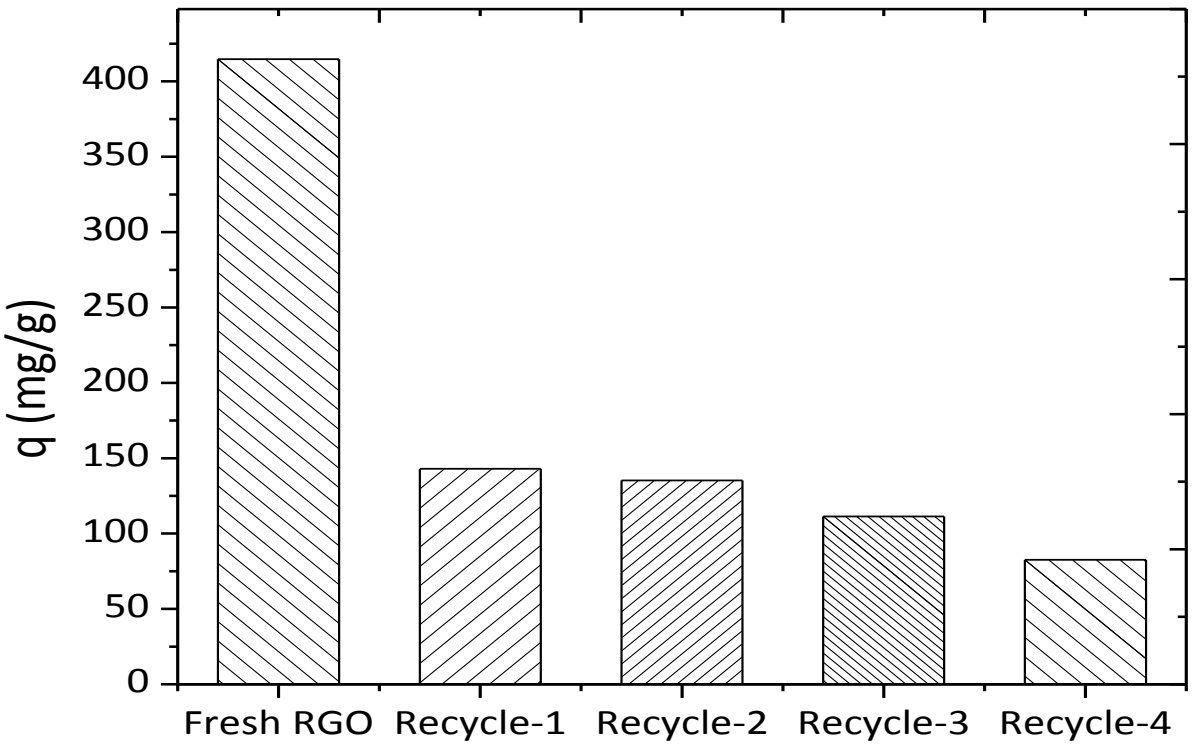

Fig. 77: Reusability of RGO in the removal of dye TGN

4.3. Part 3. Preparation and characterization of composite of sodium-alginate (SA) and GO (SA-GO) and its application for the removal of dye Maxilon Blue (GRL) from aqueous solutions

4.3.1 Preparation of SA-GO composite

To prepare SA-GO composite, a mixture of Na-alginate, GO and $CaCO_3$ was added dropwise into 2 % HCl and a composite of SA-GO was produced. Here, hydrogen bonding took place between sodium alginate and GO [116]. During the reaction CO_2 gas was produced which make the composite porous.

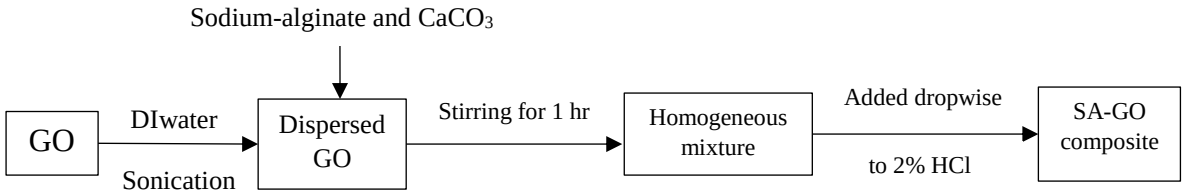

Fig. 78: Flow diagram of SA-GO composite preparation

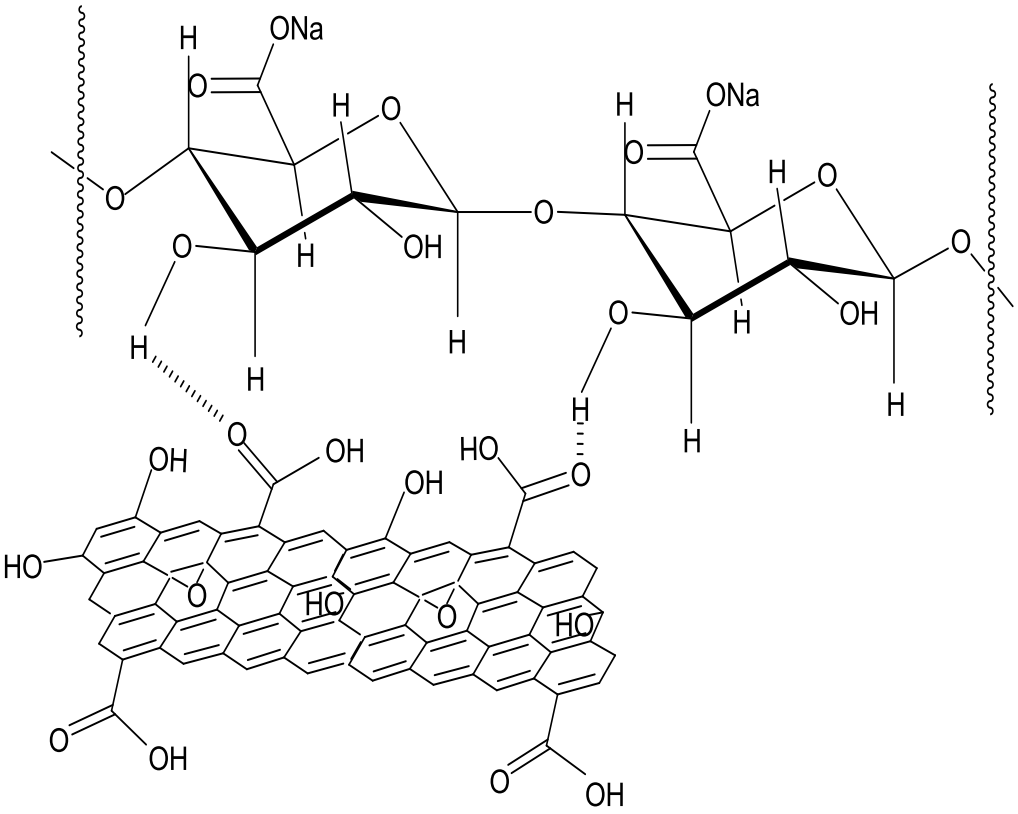

Fig. 79: Interaction between graphene oxide and sodium alginate

4.3.2. Characterization of SA-GO composite

4.3.2.1. Scanning electron microscopy (SEM) of SA and SA-GO composite

The morphology of SA and SA-GO composite was studied with scanning electron microscopy (SEM). Here, rod like shape was observed in SA (Fig. 80). But wrinkled GO sheets were observed in SA-GO composite (Fig. 81).

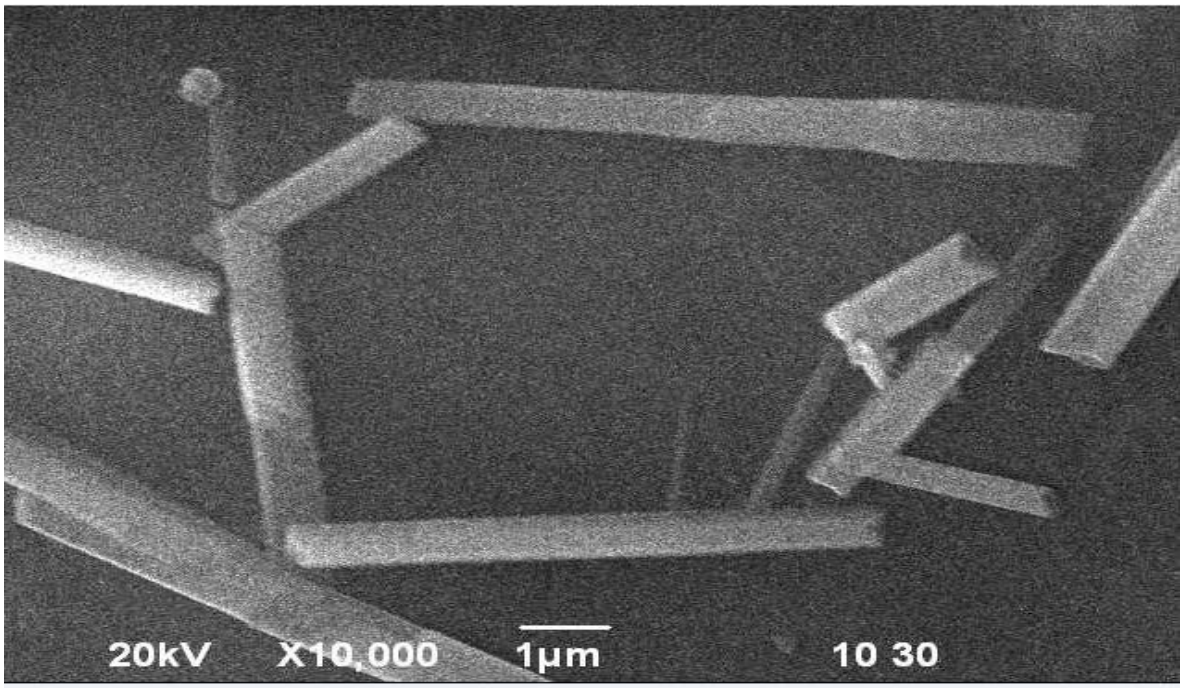

Fig. 80: SEM image of sodium alginate

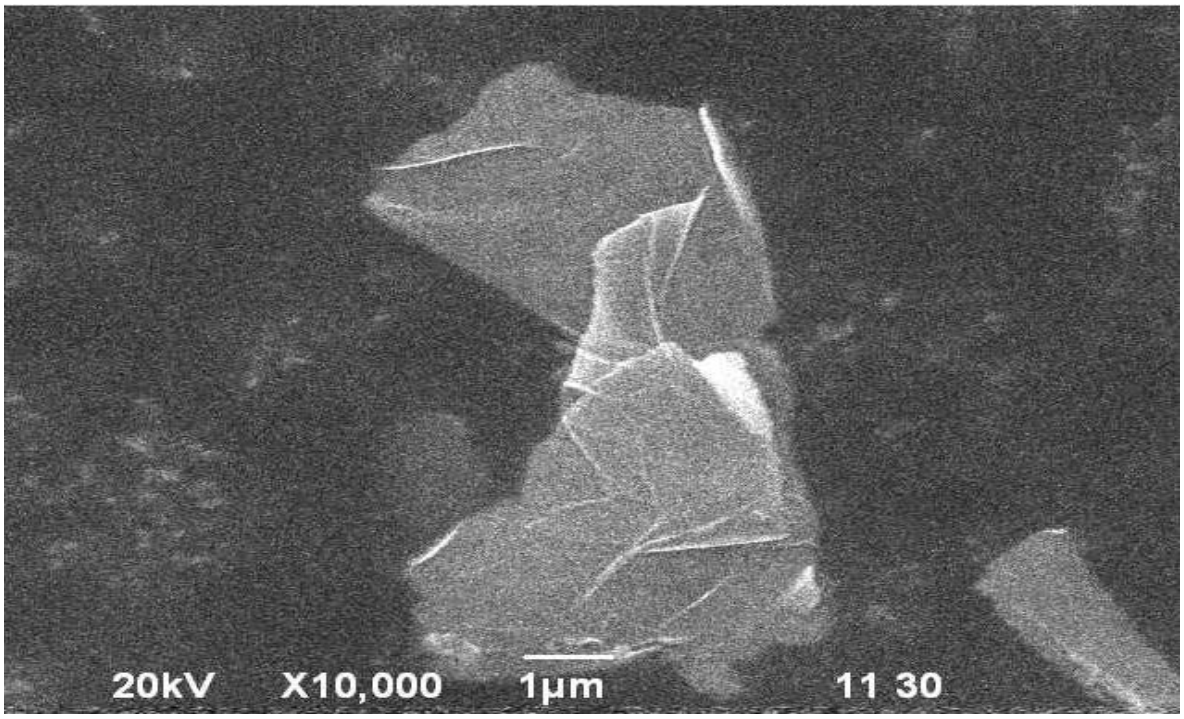

Fig. 81: SEM image of SA-GO composite

4.3.2.2. X-Ray diffraction (XRD) analysis of SA and SA-GO composite

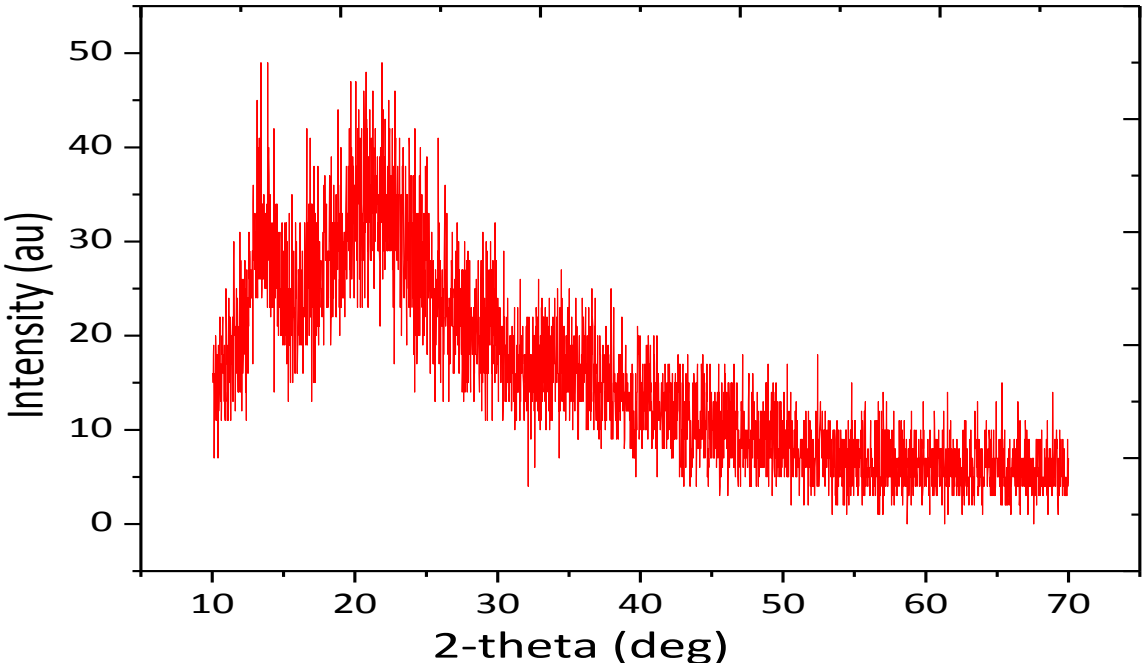

Fig. 82: XRD patterns of sodium alginate

The XRD patterns of sodium alginate (SA) is represented in Fig. 82. The XRD pattern of Na-alginate presented two weak and broad peaks at 2θ=13.38^o and 20.98^o corresponding to interlayer spacing of 6.61 and 4.23 Å indicating a rather amorphous structure.

For SA-GO composite, the peak was observed at 2θ=22.10^o corresponding to interlayer spacing of 4.02 Å (Fig. 83). For GO the value of 2θ was 9.97^o corresponding to an interlayer spacing of 8.87 Å (Fig.11). These results revealed that the diffraction as well as interlayer spacing of composite became closer to sodium alginate.

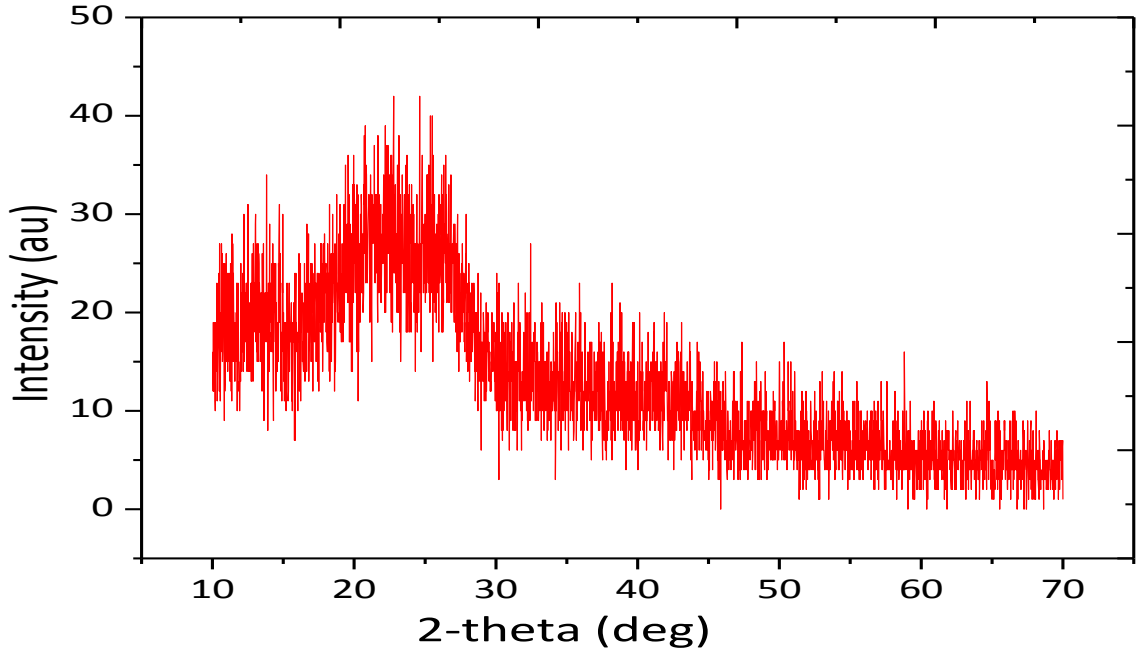

Fig. 83: XRD patterns of composite SA-GO composite

4.3.2.3. FT-IR spectrum of SA-GO composite

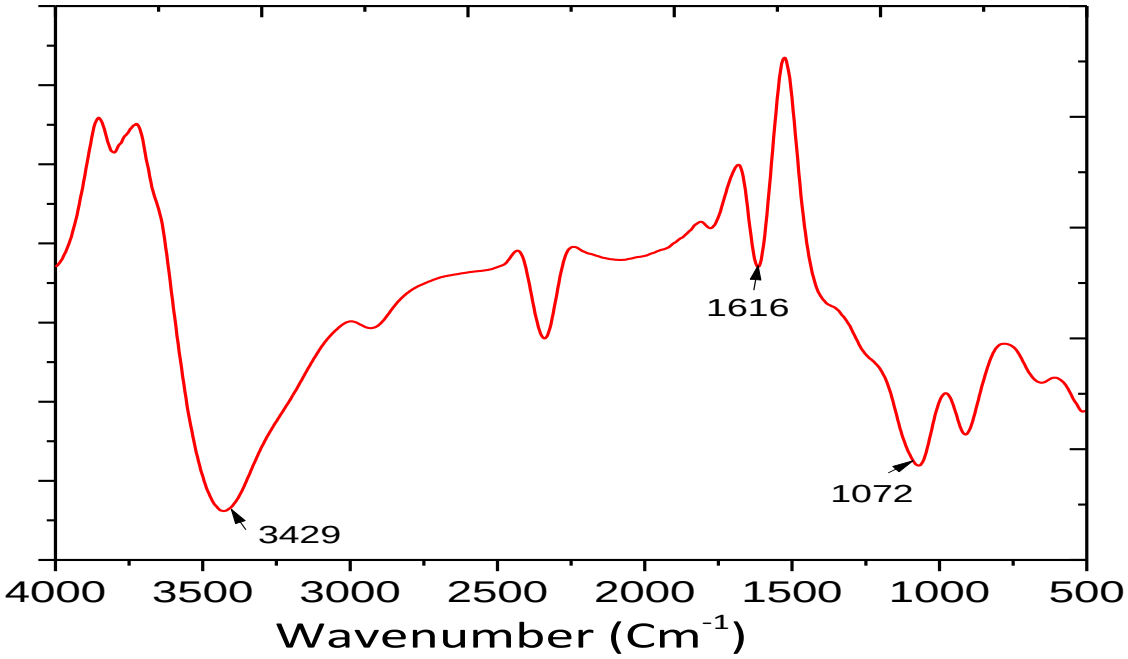

Fig. 84: FT-IR spectrum of SA-GO composite

For SA-GO composite peak was observed at 3429 cm^{-1}, 1616 cm^{-1} and 1072 cm^{-1} (Fig. 84) corresponding to -OH stretching, aromatic C=C and C-O groups, respectively. In GO spectrum, the peak observed at 1080 cm^{-1}, 1412 cm^{-1}, 1620 cm^{-1}, 1708 cm^{-1}, 2919 cm^{-1} and 3408 cm^{-1} which are attributable to C-O, C-O-H , aromatic C=C, carbonyl C=O, C-H streching and –OH groups, respectively.

4.3.2.4. Zeta potential value of SA-GO composite

Zeta potential is the potential difference existing between the surface of a solid particle immersed in a conducting liquid and the bulk of the liquid. Zeta potential determination is a significant characterization technique of nanocrystals to estimate the surface charge, which can be employed for understanding the physical stability of nanosuspensions. So. Zeta potential of SA-GO composite as a function of pH was also studied. For this study SA-GO composite was dispersed in DI water. The analysis was carried out in the pH range of 2-10. The results showed that (Table-60, Fig. 85) the zeta potential values of composite were negative over the whole pH range and the values varied from -4.93 to -45.9 mV with an increase of pH from 2 to 10.

Table 60: pH vs Zeta potential data of SA-GO composite

pH	2	4	6	8	10
Zeta potential (mV)	-4.93	-28.2	-40.5	-43.8	-45.9

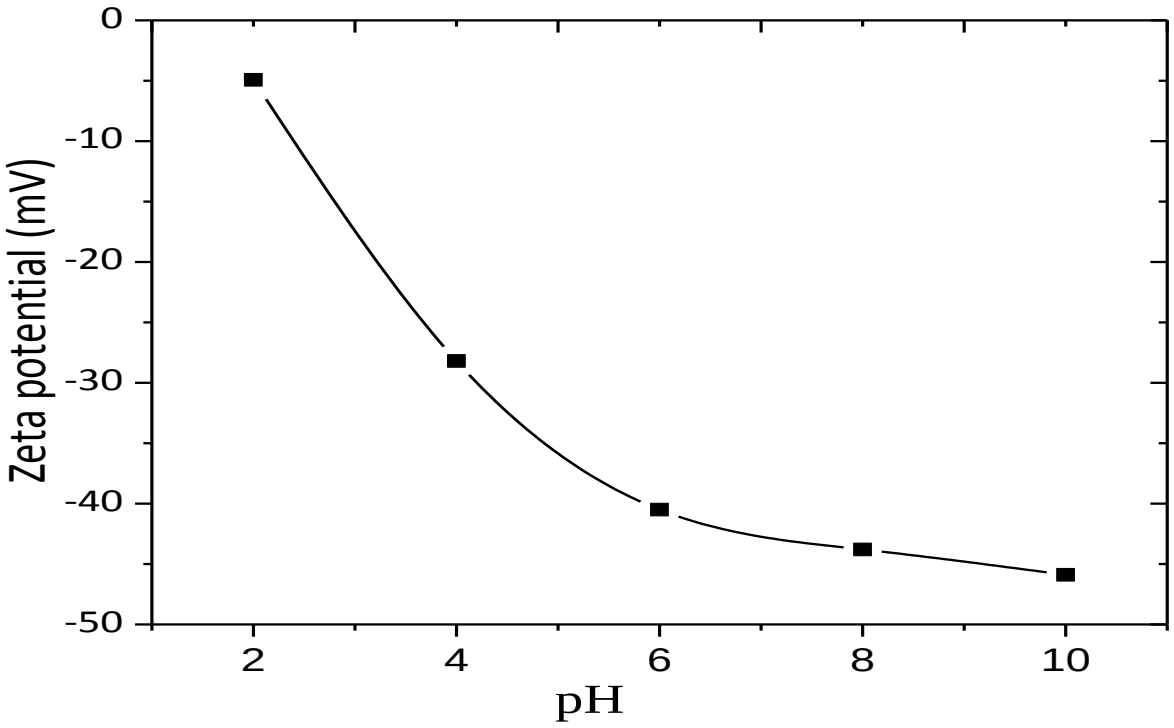

Fig. 85: Zeta potential value of SA-GO composite at different pH

4.3.3. Adsorption of dye on SA-GO composite

4.3.3.1. Adsorption of dye MBG on SA-GO composite

4.3.3.1.1. Effect of pH on adsorption of dye MBG by SA-GO composite

The adsorption experiments of dye MBG by SA-GO composite at different pH were carried out following the same procedure as 4.1.3.1.2. A set of 5 experiments were studied and 9 mg of SA-GO composite were added to 10 ml 700 ppm dye solutions. The mixtures were shaken for 60 minutes, filtered and absorbance of the filtrates were measured by UV-Vis spectroscopy at 554 nm. Then concentrations of the solutions after adsorption were determined with respect to standard curve (Fig. 46) and adsorption capacities were calculated. The minimum adsorption capacity of SA-GO was 338.57 mg/g at pH of 2. The adsorption capacity sharply increased at pH of 4 and remain almost constant up to pH of 10. The maximum adsorption capacity was 795.10 mg/g at pH of 10 (Table-61, Fig. 86).

.**Table 61:** pH vs adsorption capacity data of SA-GO composite for dye MBG

pH	2	4	6	8	10
Adsorption capacity (mg/g)	338.57	749.68	770.64	780.40	795.10

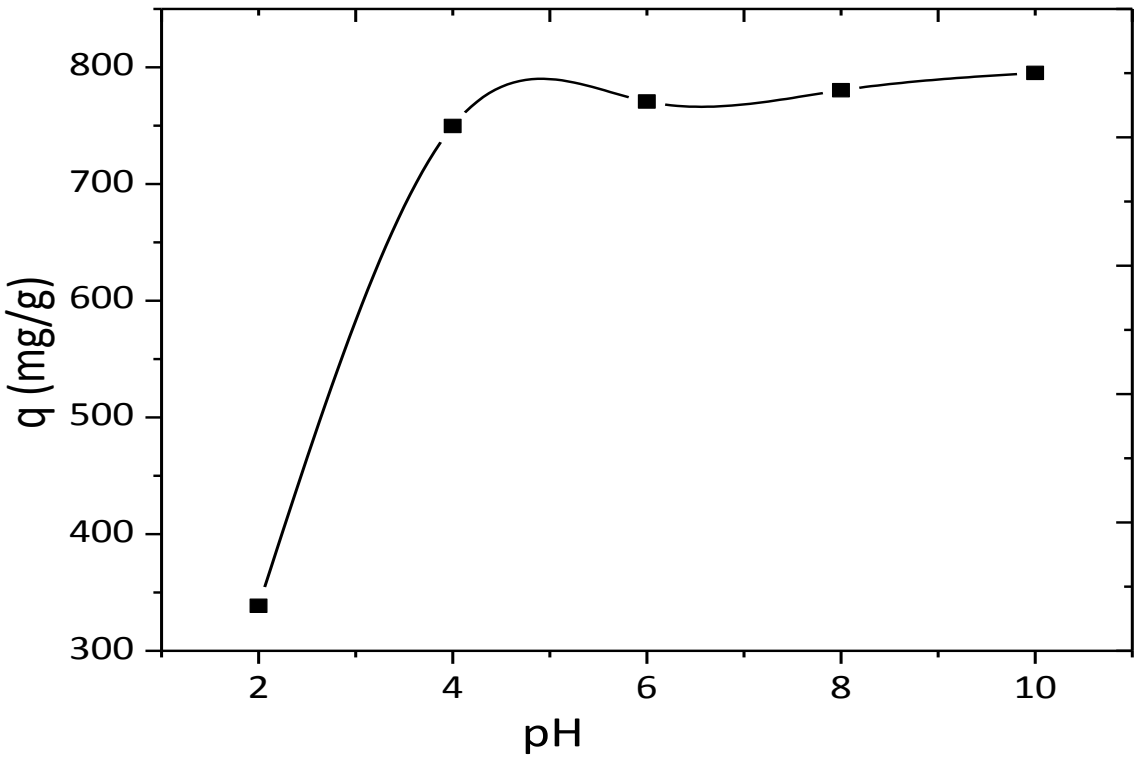

Fig. 86: Effect of pH on adsorption of dye MBG by SA-GO composite

At low pH, some of the carboxyl groups of GO as well as of sodium alginate of the composite got protonated and formed positively charged surface [111] which demonstrated electrostatic repulsion with the cationic dye MBG, and thus led to lower adsorption. With the increase in pH, carboxyl groups of GO as well as of sodium alginate of the composite got dissociated extensively [110] and surface became highly negatively charged. These led to electrostatic interaction between composite and cationic dye MBG. As a result adsorption capacity increased sharply with increasing pH.

However, the maximum adsorption was achieved at pH of 4. It was assumed that at pH of 4 carboxyl groups of GO and of sodium alginate mostly exists as deprotonated form ($–COO^-$) and showed the maximum adsorption. As most of the carboxyl groups are deprotonated at pH of 4, further increase of pH didn't affect the deprotonation (117] and thus adsorption remained almost constant.

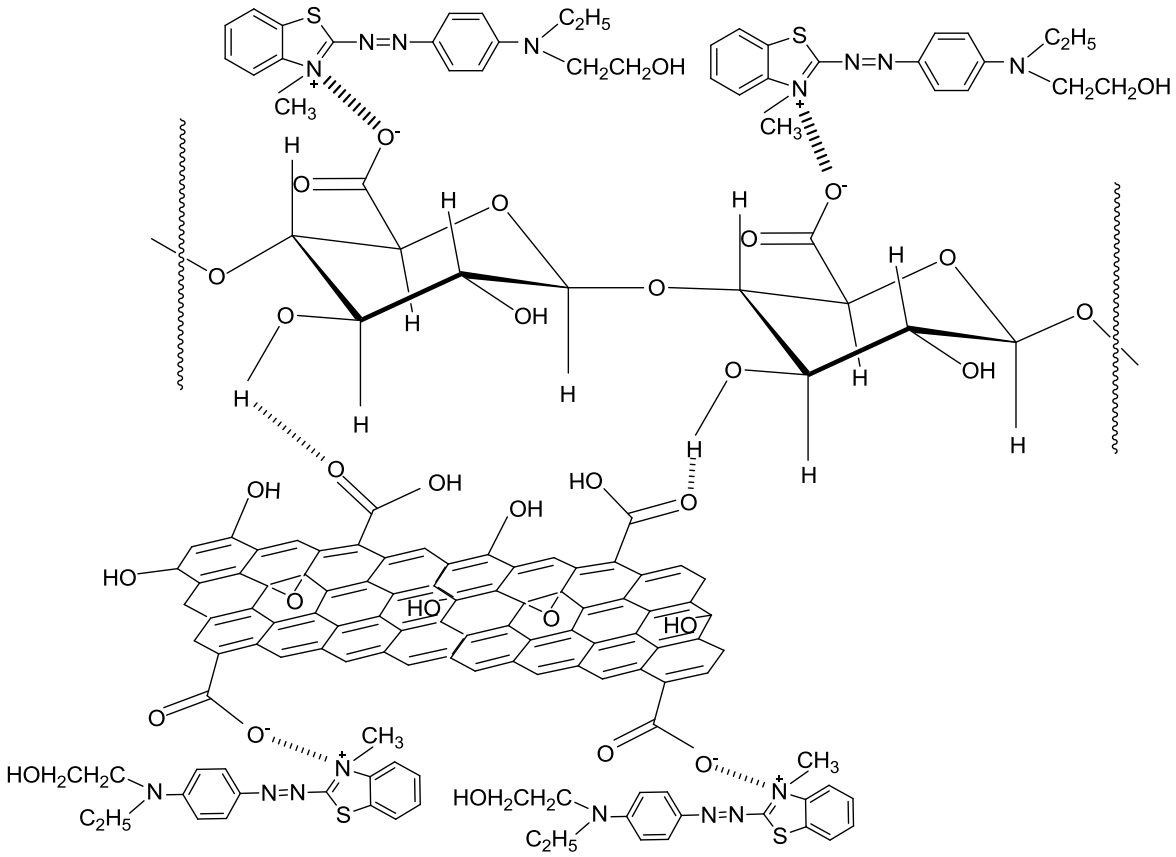

Fig. 87: Mechanism of dye MBG adsorption on SA-GO composite at high pH

4.3.3.1.2. Effect of adsorbent dosage on adsorption of dye MBG by SA-GO composite

For the adsorption of dye MBG by SA-GO composite, the optimum dosage were determined following the same procedure as 4.1.3.1.3. Here a set of 4 experiments were carried out using 10 ml 1000 ppm dye solutions at pH of 7 and 5, 10, 15, 20 mg of SA-GO composite were added to the flasks. Then the mixtures were shaken for 60 minutes, filtered and the absorbance of the filtrates were measured by UV-Vis spectroscopy at 554 nm. Then concentrations of the solutions after adsorption were determined with respect to standard curve (Fig. 46).

It is apparent that (Table-62, Fig. 88) with the increase of adsorbent dosage adsorption capacity decreased but percentage removal of dye increased. For the dosage 9 mg/10 ml solution demonstrate the best percentage removal as well as the best adsorption capacity. So, 9 mg dosage for 10 ml dye solution were maintain throughout the study.

Table 62: Dosage vs adsorption capacity and % removal data of SA-GO composite for dye MBG

Dosage (mg)	5	10	15	20
Adsorption capacity (mg/g)	1268.72	867.47	646.30	493.23
% of removal	63.43	86.75	96.95	98.65

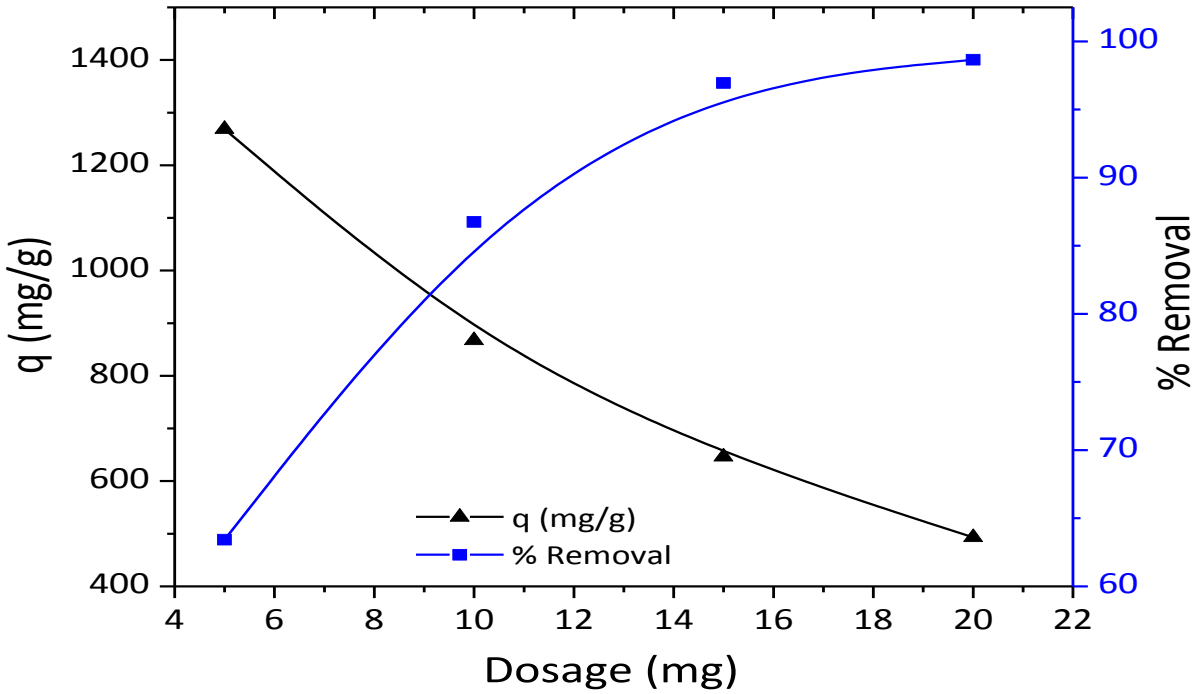

Fig. 88: Effect of adsorbent dosage on adsorption of dye MBG by SA-GO composite

4.3.3.1.3. Effect of dye concentration and contact time on adsorption of dye MBG by SA-GO composite

The adsorption experiments of dye MBG by SA-GO composite at different concentrations and time were carried out following the same procedure as 4.1.3.1.4. In this case, a set of 7 experiments were carried out at pH of 7 and 9 mg of SA-GO composite were added to 10 ml 500 ppm dye solutions. Then the mixtures were shaken at 303 K in various intervals of time ranging from 10-90 minutes, filtered and absorbance of the filtrates were measured by UV-Vis spectroscopy at 554 nm. Then concentrations of the solutions were determined with respect to standard curve (Fig. 46). To observe the effect of dye concentration on adsorption, similar experiments were carried out using 600, 800 and 900 ppm dye solutions in the same intervals of time.

In these experiments due to the availability of more active sites the adsorption capacity increased with an increase of time (Table-63 and Fig. 89) and with the increase in initial dye concentration.

Table 63: Time vs adsorption capacity data of SA-GO composite at different times and concentrations for dye MBG

Time (min)	500 ppm	600 ppm	800 ppm	900 ppm
0	0	0	0	0
10	478.48	472.62	650.71	782.87
20	491.86	539.10	694.29	791.63
30	517.22	618.84	719.42	822.36
45	520.26	621.79	762.02	843.00
60	520.56	622.10	796.94	874.26
75	520.33	624.37	800.24	875.81
90	518.96	629.10	810.81	879.11

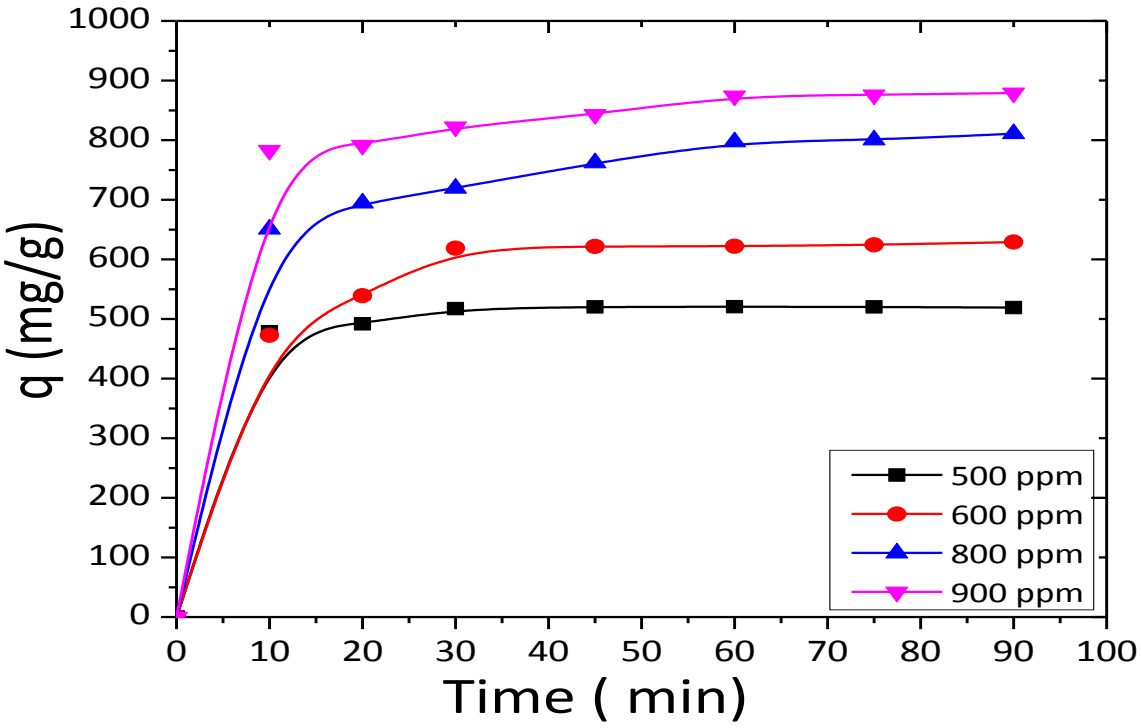

Fig. 89: Effect of dye concentration and time on adsorption of dye MBG by SA-GO composite

4.3.3.1.4. Adsorption isotherms for adsorption of dye MBG on SA-GO composite

4.3.3.1.4.1. Langmuir adsorption isotherm

The theoretical maximum adsorption capacity q_m for the adsorption of MBG on SA-GO composite was calculated following the procedure as 4.1.3.1.5.1. A linear relation between C_e/q_e and C_e was observed (Table-64, Fig. 90) with acceptable regression factor (R^2= 0.9982).

Table 64: C_e and C_e/q_e data of SA-GO composite at different concentrations for dye MBG

Initial concentration (ppm)	500 ppm	600 ppm	800 ppm	900 ppm
Equilibrium concentration (C_e)	31.50	41.11	82.75	113.17
C_e/q_e	0.061	0.066	0.104	0.129

From Langmuir isotherm ($\frac{C_e}{q_e} = \frac{1}{q_m b} + \frac{1}{q_m} c_e$) the value of slope was found 0.0009. So,

$$1/q_m = 0.0009$$

$$\therefore q_m = 1111.11 \text{ mg/g}$$

The theoretical maximum adsorption capacities, q_m calculated from the slope and found to be 1111.11 mg/g. The value of separation factor R_L was 0.040. This indicates a very favorable monolayer adsorption process [32].

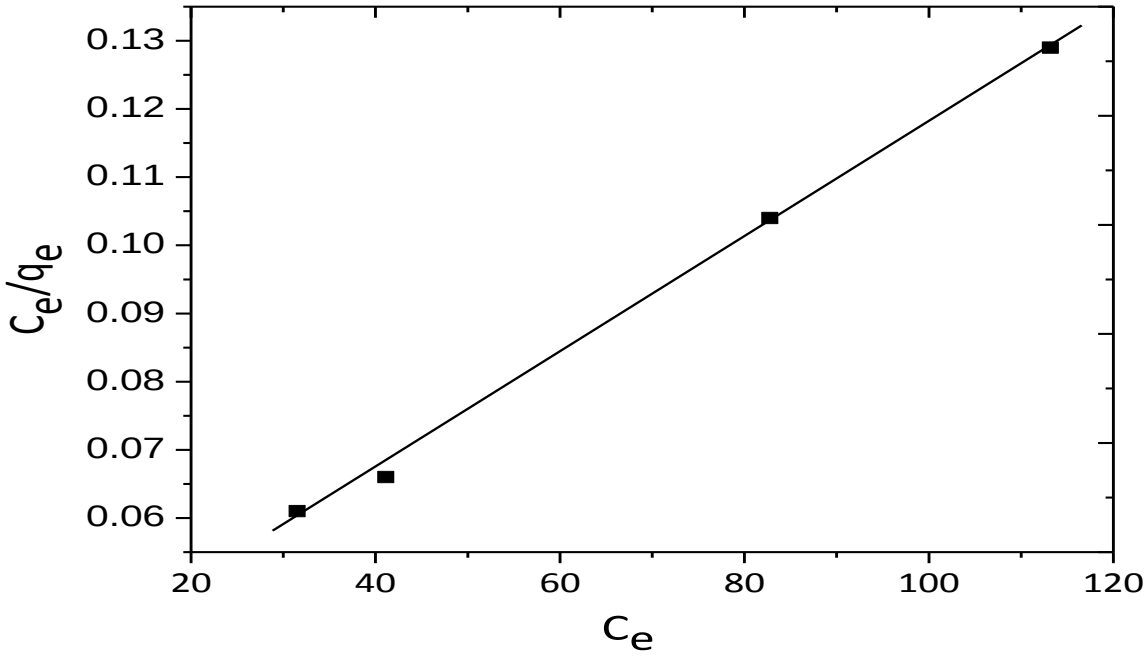

Fig. 90: Langmuir adsorption isotherm at 303 K temperature for dye MBG on SA-GO composite

4.3.3.1.4.2. Freundlich adsorption isotherm

The experimental data were also tested for the multilayer adsorption mechanism of MBG on SA-GO composite following the procedure as 4.1.3.1.5.2 and a linear relationship was observed (Table-65, Fig. 91) with good regression coefficient (R^2= 0.984). The value of n was also calculated using Eq. (6) and found to be 2.58 which showed that the adsorption were moderate to good [32].

Table 65: lnC_e and lnq_e data of SA-GO composite at different concentrations for dye MBG

Initial concentration (ppm)	500 ppm	600 ppm	800 ppm	900 ppm
lnC_e	3.45	3.72	4.42	4.73
lnq_e	6.26	6.43	6.68	6.71

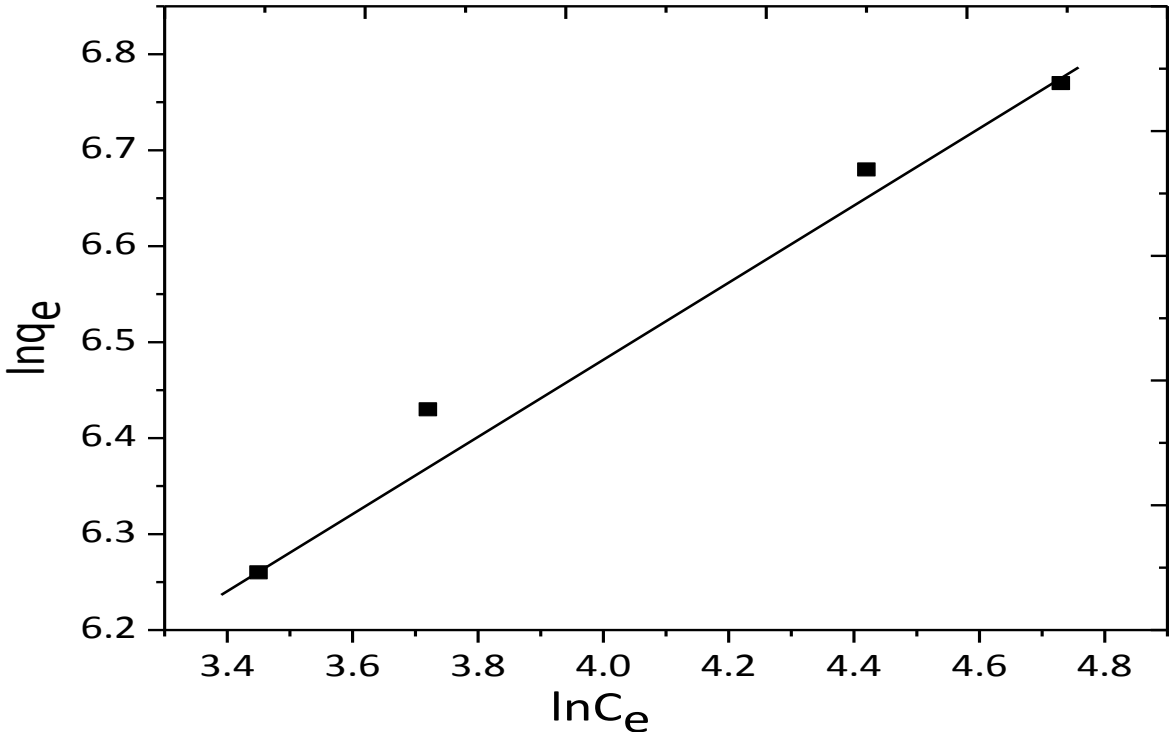

Fig. 91: Freundlich adsorption isotherm at 303 K temperature for dye MBG on SA-GO composite

The values of different parameters of Langmuir isotherm and Freundlich isotherm were provided in Table-66 and it was evident that the adsorption of dye MBG on SA-GO followed both the models but preferably the Langmuir isotherm model.

Table 66: Theoritical values of q_m,b,R_L, n, K_F and R^2 of SA-GO composite for dye MBG

Name of isotherm	q_m(mg/g)	R^2	b, Lmg^{-1}	R_L	, n	K_F
Langmuir Isotherm	1111.11	0.9982	0.027	0.040	-	-
Freundlich isotherm	-	0.9840	-	-	2.58	141.43

4.3.3.1.5. Adsorption kinetics for adsorption of dye MBG on SA-GO composite

4.3.3.1.5.1. The pseudo-first-order reaction kinetics

Pseudo-first-order model for the adsorption of MBG on SA-GO was studied following the procedure as 4.1.3.1.6.1. The values t and $\log(q_e-q_t)$ are given in Table-67, Fig. 92.

Table 67: t and $\log(q_e-q_t)$ data at different time and concentrations for adsorption of dye MBG on SA-GO composite

Time (min)	$(\log q_e-q_t)$ at 500 ppm	$(\log q_e-q_t)$ at 600 ppm	$(\log q_e-q_t)$ at 800 ppm	$(\log q_e-q_t)$ at 900 ppm
10	1.62	2.17	2.17	1.96
20	1.46	1.92	2.01	1.92
30	0.52	0.51	1.89	1.72
45	-0.52	-0.51	1.54	1.49

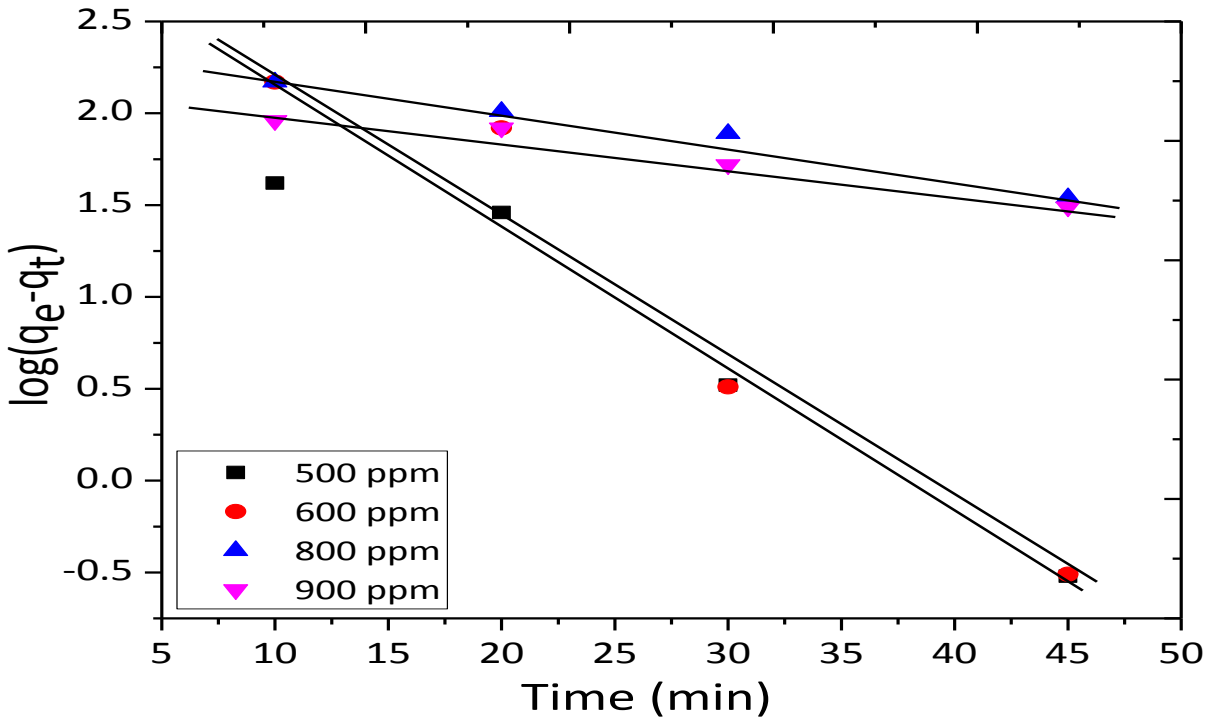

Fig. 92: Pseudo-first order adsorption kinetics for dye MBG on SA-GO composite

4.3.3.1.5.2. The pseudo-second-order reaction kinetics

Pseudo-second-order model for the adsorption of dye MBG on SA-GO composite was studied following the procedure as 4.1.3.1.6.2. The values t and t/q_t are given in Table-68 and Fig. 93.

Table 68: t and t/q_t data at different time and concentrations for adsorption of dye MBG on SA-GO composite

Time (min)	t/q_t at 500 ppm	t/q_t at 600 ppm	t/q_t at 800 ppm	t/q_t at 900 ppm
10	0.021	0.021	0.0154	0.0128
20	0.041	0.037	0.0288	0.0253
30	0.058	0.048	0.0417	0.0365
45	0.086	0.072	0.0591	0.0534
60	0.115	0.096	0.0753	0.0686
75	0.144	0.120	0.0937	0.0856
90	0.173	0.143	0.1110	0.1024

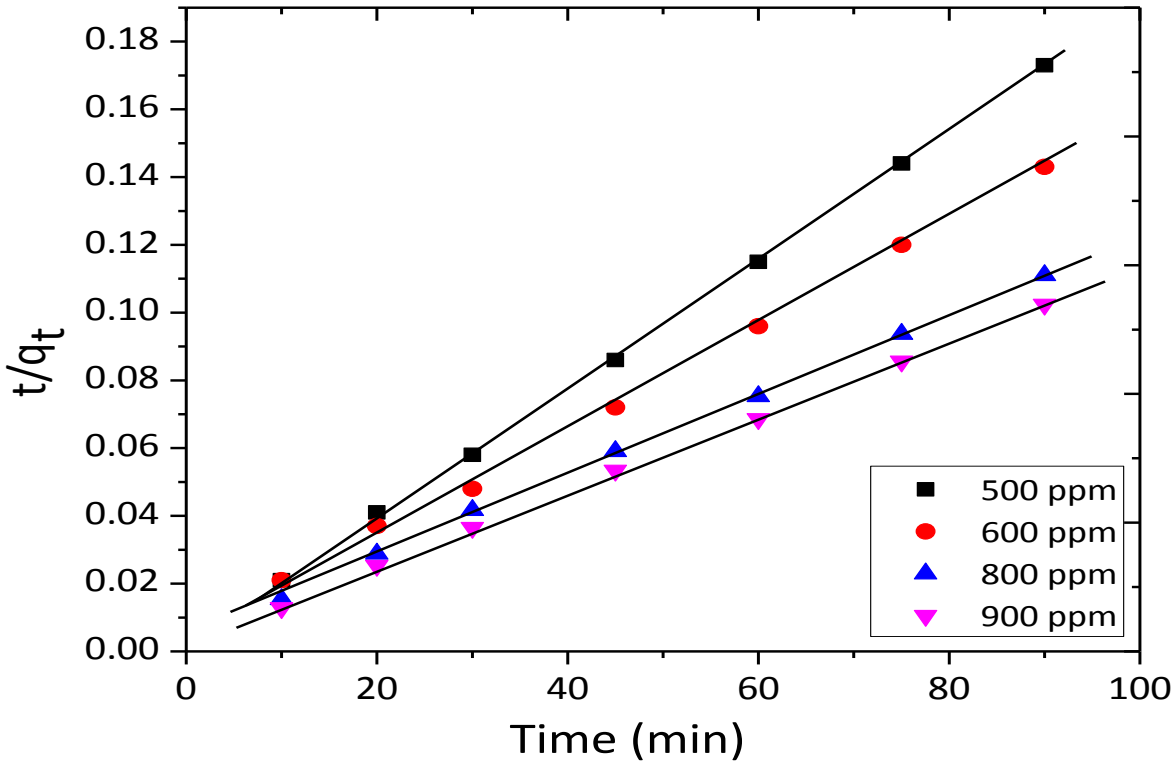

Fig. 93: Pseudo-second-order adsorption kinetics for dye MBG on SA-GO composite

Considering the kinetic parameters stated in Table-69 it was observed that the values of correlation coefficient for second-order kinetics were much better than first-order kinetics.

Table 69: Pseudo-first-order and pseudo-second-order kinetics parameters for the adsorption of dye MBG on SA-GO composite

Types of kinetics model	Parameters	Initial concentration of dye			
		500 ppm	600 ppm	800 ppm	900 ppm
	$q_{e,exp}$ (mg/g)	520.56	622.10	796.94	874.26
Pseudo-first-order	$q_{e,cal}$ (First-order)	293.56	266.26	233.40	139.28
	K_1	0.149	0.189	0.040	0.033
	R^2	0.9562	0.9526	0.9802	0.96
Pseudo-second order	$q_{e,cal}$ (Second-order)	526.32	666.67	833.33	909.09
	K_2	0.0019	0.00049	0.00029	0.00045
	R^2	0.9998	0.9989	0.9993	0.9996

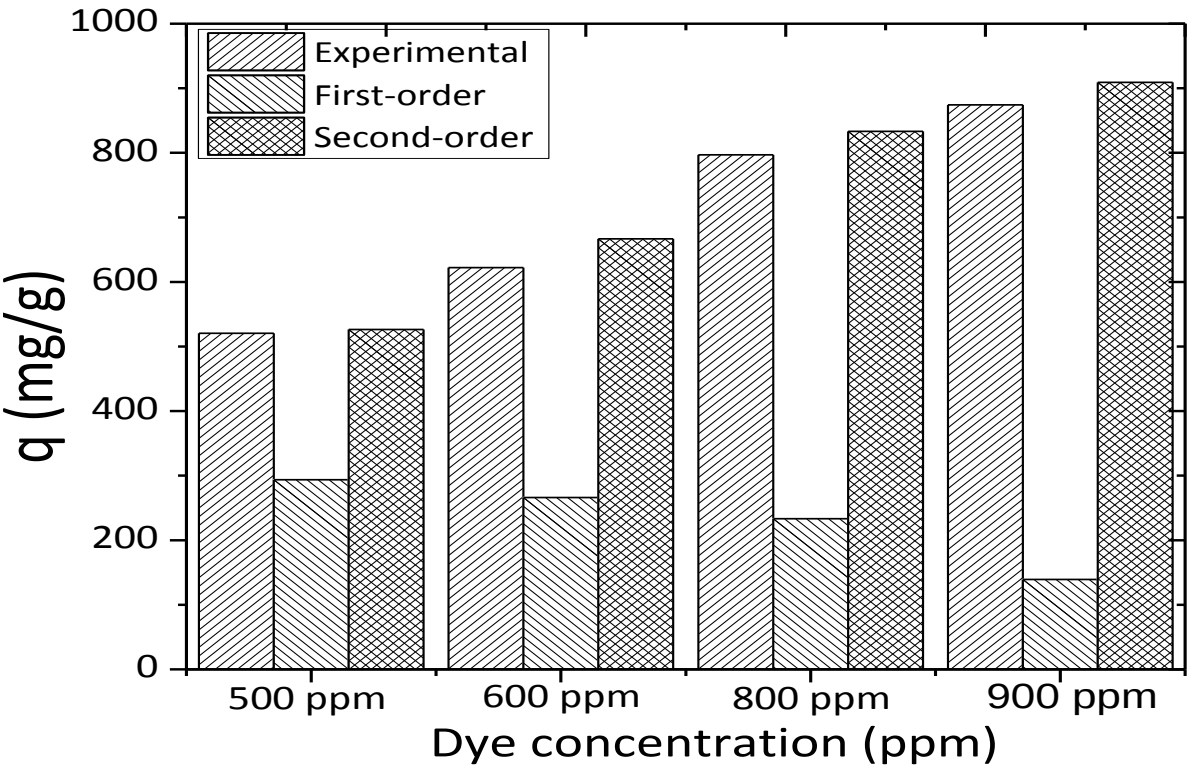

Fig. 94: Comparison of adsorption capacities of pseudo-first-order and pseudo-second-order kinetics for the adsorption of dye MBG on SA-GO composite

From Fig. 94, it was also observed that the calculated adsorption capacities of second-order kinetics matched well with the experimental values. So, it was revealed that pseudo-second order kinetic model showed better correlation for the adsorption of dye MBG onto SA-GO composite compared to the pseudo-first-order model.

4.3.3.1.6. Thermodynamic analysis for adsorption of dye MBG on SA-GO composite

The changes in Gibb's free energy for dye MBG adsorption on SA-GO composite at different temperatures were also studied following the procedure as 4.1.3.1.7. In this case, a set of 7 experiments were studied at pH of 7. Here, 9 mg of composite were added to10 ml of 900 ppm dye solutions and the mixtures were shaken at 303K for different time periods ranging from 10-90 minutes. After shaking the mixtures were filtered and absorbance of the filtrates were measured by UV-Vis spectroscopy at 554 nm. To observe the effect of temperature similar two sets of experiments were studied at 313K and 323K.

Table 70: Adsorption capacity data of dye MBG on SA-GO composite at different time and temperatures

Time (min)	q at 303 K	q at 313 K	q at 323 K
0	0	0	0
10	782.87	423.89	309.56
20	791.63	487.54	398.74
30	822.36	611.22	583.98
45	843.00	703.78	645.10
60	874.26	791.30	699.29
75	875.81	798.43	708.11
90	879.11	805.64	710.07

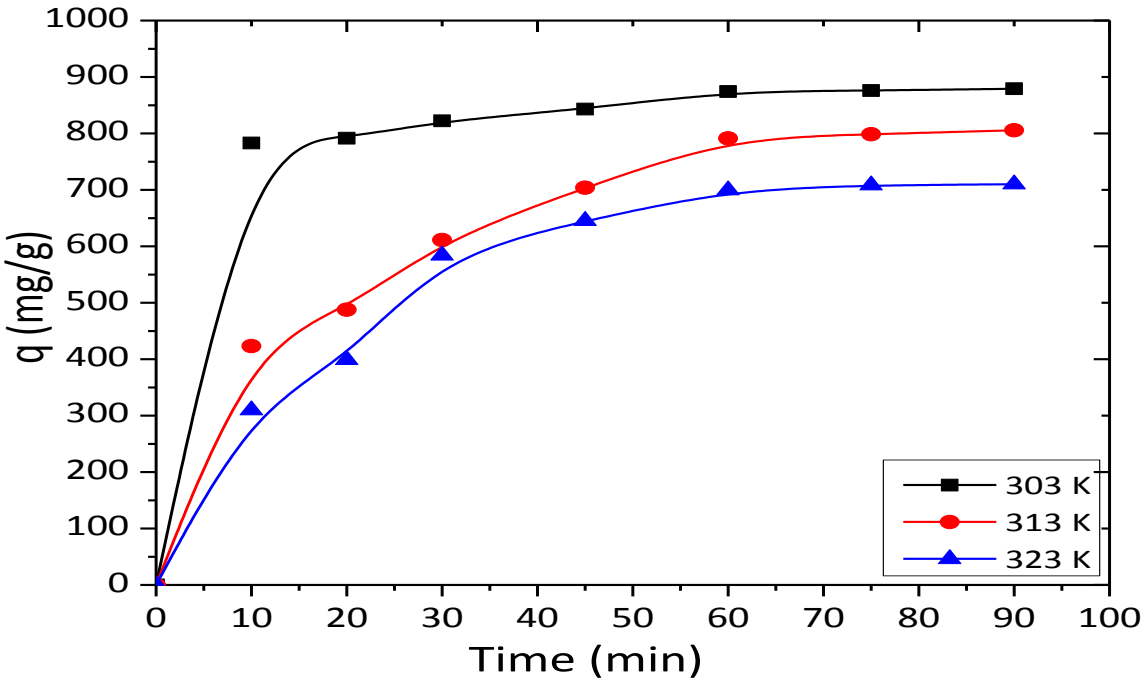

Fig. 95: Adsorption of dye MBG on SA-GO composite at different temperature

The effects of contact time and temperature on adsorption capacity of SA-GO composite for MBG were plotted in Table-70 and Fig. 95. The equilibrium adsorption capacity was 874.26 mg/g at 303 K that decreased to 791.30 mg/g and 699.29 mg/g at 313 K and 323 K. The Gibb's free energies were found to be -5.27, -3.75, -2.55 KJ mol^{-1} at 303K, 313K and 323K, respectively.

The average standard enthalpy change ΔH^o and entropy change ΔS^o for the adsorption of MBG on SA-GO composite were calculated from the van't Hoff equation. A straight line was obtained by plotting $\ln k_d$ versus 1/T (Table-71, Fig. 96).

Table 71: 1/T vs $\ln k_d$ data of adsorption process

1/T	0.0033	0.0032	0.0031
$\ln k_d$	2.09	1.44	0.95

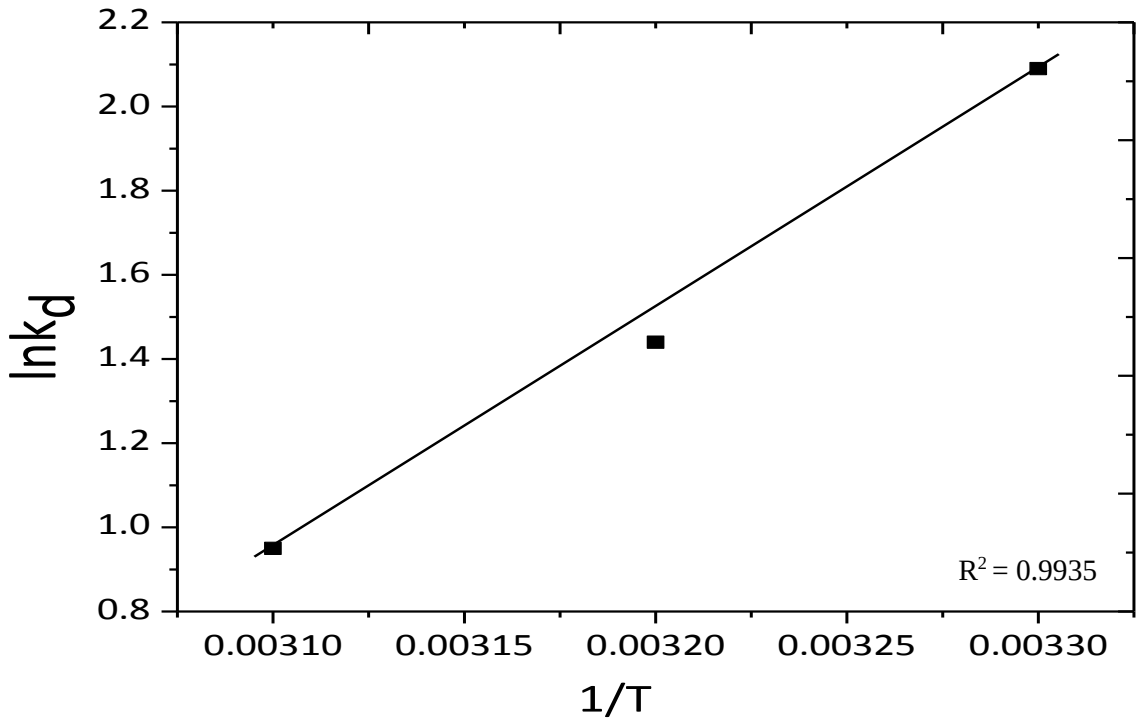

Fig. 96: Plot of van't Hoff equation for the adsorption of dye MBG on SA-GO composite

The standard enthalpy change ΔH^o and entropy change ΔS^o were obtained -47.39 KJ mol^{-1} and -0.139 KJ K^{-1} mol^{-1}, respectively. The value of ΔG^o increased from -5.27 to -2.55 with an increase of temperature from 303K to 323 K. Thus the adsorption of MBG on SA-GO composite was spontaneous at lower temperature and the adsorption of MBG on SA-GO composite was physical adsorption [32].

4.3.3.1.7. Plausible mechanism for adsorption of dye MBG on SA-GO composite

In aqueous solutions carboxyl groups of GO as well as of sodium alginate of the composite got dissociated and form negatively charged surface. As a result the composite showed significant adsorption towards cationic dyes.

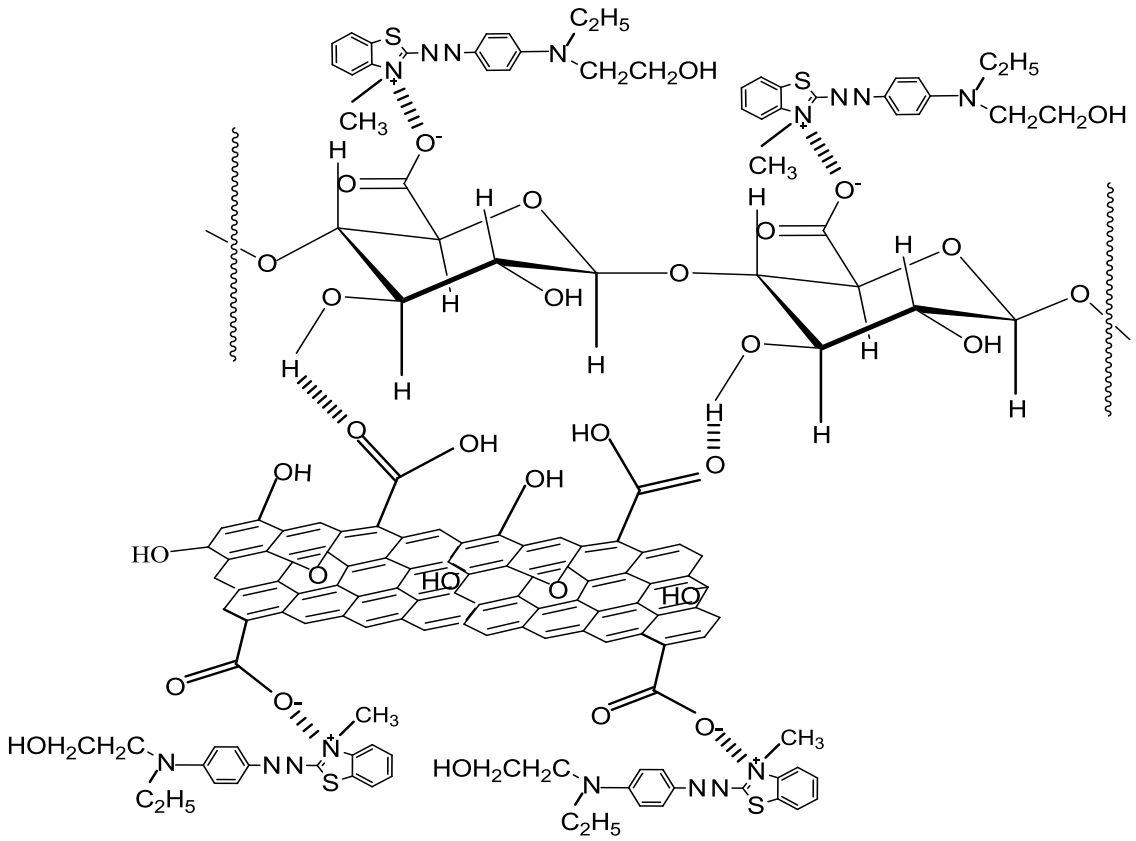

Fig. 97: Mechanism of dye MBG adsorption on SA-GO composite

4.3.3.1.8. Regeneration of used SA-GO composite

In order to check the regeneration ability 2% HCl was added to the used SA-GO composite to remove the dye. Then washed with distilled water upto pH reached to 7.

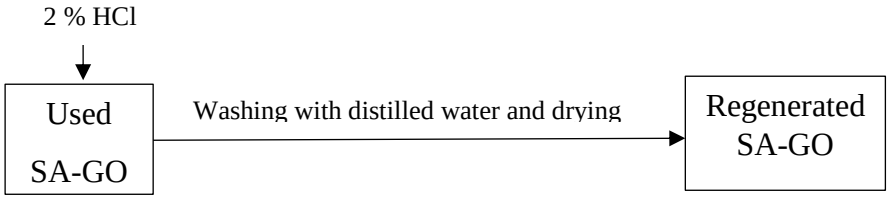

Fig. 98: Flow diagram of regeneration of used SA-GO composite

The regenerated SA-GO composite was dried and used for further adsorption. In this study, 9 mg of dispersed regenerated SA-GO was used for10 ml 900 ppm dye solution at pH of 7 with shaking for 60 minutes. Fresh SA-GO composite showed the adsorption capacity of

874.26 mg/g for 900 ppm dye solution at pH of 7 while the regenerated SA-GO composite of 1st, 2nd , 3rd , 4thand 5th recycle (Table-72, Fig. 99) showed the adsorption capacities of 683.27 mg/g, 667.84 mg/g, 664.31 mg/g, 653.43 mg/g and 657.38 mg/g, respectively.

Table 72: Reusability of SA-GO composite in the removal of dye MBG

Type of SA-GO	Fresh SA-GO	Recycle-1	Recycle-2	Recycle-3	Recycle-4	Recycle-5
Adsorption capacity q (mg/g)	786.83	683.27	667.84	664.31	653.43	657.38

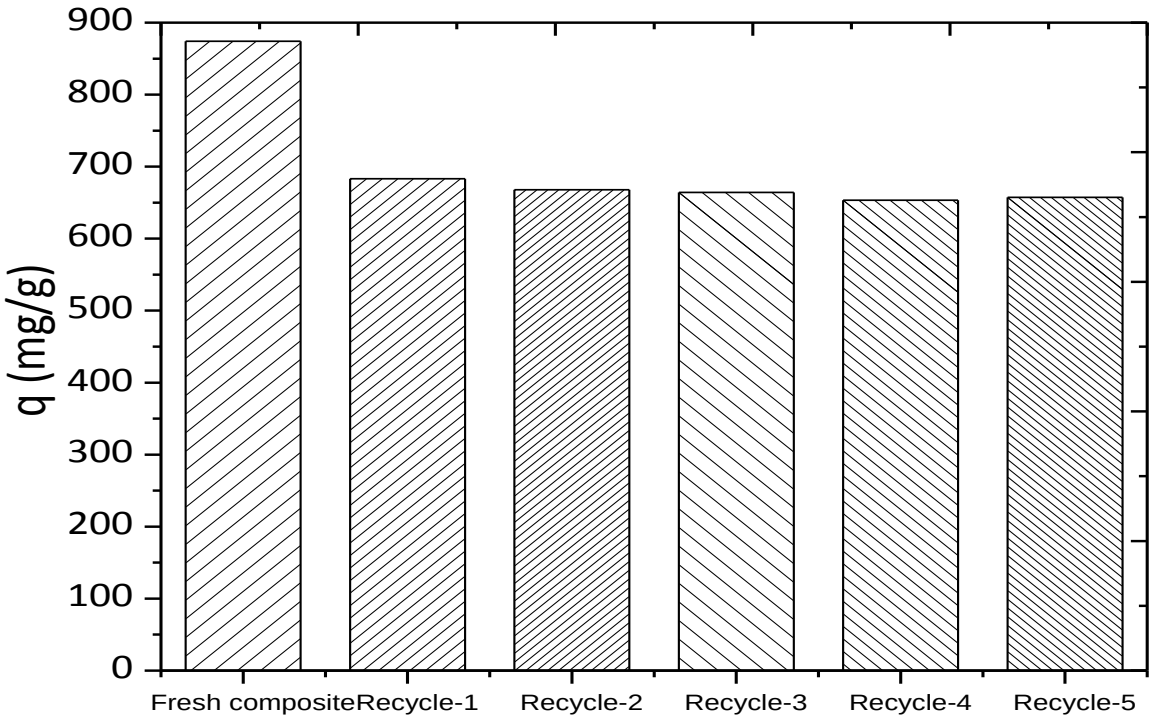

Fig. 99: Reusability of SA-GO composite in the removal of dye MBG

Chapter 5

Conclusions and Scope of Further Study

5.1. **Conclusions**

The following conclusions may be drawn from the present study.

- Graphene oxide (GO) was prepared from graphite powder and applied for the removal of industrially used dyes FD-R H/C, TURQUOISE GN and Maxilon Blue (GRL) from aqueous solutions. For FD-R H/C the adsorption capacity was 151.29 mg/g at pH of 2. For TURQUOISE GN the adsorption capacities were 565.61 mg/g and 294.12 mg/g at pH of 2 and 7, respectively. For Maxilon Blue (GRL) the adsorption capacity was 1253.13 mg/g at pH of 7.
- Reduced graphene oxide (RGO) was prepared by the reduction of GO with hydrazine hydrate and RGO was applied for the removal of dye TURQUOISE GN from aqueous solutions and the adsorption capacity was 588.24 mg/g at pH of 7.
- Composite of sodium-alginate (SA) and GO (SA-GO) was prepared by adding the mixture of sodium-alginate, $CaCO_3$ and GO dropwise into 2% HCl. Sodium alginate and GO ratio was maintained as 10:1. The composite was applied for the removal of dye Maxilon Blue (GRL) from aqueous solutions and the adsorption capacity was found 1111.11 mg/g at pH of 7.
- The used GO, RGO and SA-GO composite were regenerated by using 2 % HCl and used for adsorption study. For dye TGN, fresh GO showed the adsorption capacity of 102.39 mg/g for 200 ppm dye solution while the regenerated GO of 1^{st}, 2^{nd}, 3^{rd} and 4^{th} recycle showed the adsorption capacities of 75.91 mg/g, 65.73 mg/g, 44.32 mg/g and 41.25 mg/g. For dye MBG, fresh GO showed the adsorption capacity of 1421.10 mg/g for 1000 ppm dye solution while the regenerated GO of 1^{st}, 2^{nd} and 3^{rd} recycle showed the adsorption capacities of 1066.06 mg/g, 792.50 mg/g and 713.18 mg/g. For TGN, fresh RGO showed the adsorption capacity of 414.80 mg/g for 700 ppm dye solution while the regenerated RGO of 1^{st}, 2^{nd}, 3^{rd} and 4^{th} recycle showed the adsorption capacities of 143.03 mg/g, 135.23 mg/g, 111.28 mg/g and 82.53 mg/g. For MBG, fresh SA-GO composite showed the adsorption capacity of 874.26 mg/g for 900 ppm dye solution

while the regenerated SA-GO composite of 1st, 2nd , 3rd , 4thand 5th recycle showed the adsorption capacities of 683.27 mg/g, 667.84 mg/g, 664.31 mg/g, 653.43 mg/g and 657.38 mg/g, respectively.

- The Langmuir and Freundlich isotherm models have been applied to explain the distribution of dye molecules on GO, RGO and SA-GO composite surface. For all the dyes and adsorbents the adsorption isotherm followed the Langmuir model preferably.
- Adsorption kinetics is of great significance to evaluate the performance of an adsorbent and gain insight into the underlying mechanisms. In this study, the experimental data were analyzed using pseudo-first-order and pseudo-second-order models. Analyzing the kinetic parameters it was observed that the pseudo-second order kinetic model showed better correlation for all dyes and adsorbents compared to the pseudo-first-order model.
- To observe the effect of temperature on dye adsorption, the experiments were carried out at three different temperatures (303K, 313 and 323 K). The Gibb's free energy (ΔG^o) gives an assumption about the adsorption process. From thermodynamic analyses Gibb's free energy ΔG^o values were found -1.69, -1.17 and -0.86 KJ mol^{-1} for the adsorption of dye FD-R H/C on GO at 303K, 313K and 323K. While for TURQUOISE GN, ΔG^o values were -3.66, -2.92, -2.39 KJ mol^{-1} and for Maxilon Blue (GRL) ΔG^o values were -4.11, -3.80, -2.77 KJ mol^{-1}. For the adsorption of MBG on SA-GO composite, ΔG^o values were found -5.27, -3.75 and -2.55 KJ mol^{-1} at 303K, 313K and 323K, respectively. These results confirm that the adsorption of the dyes on the adsorbents are more spontaneous at lower temperature and were physical adsorption

5.2. Scope of Further Study

The following suggestions can be made for future study

- Composites can be prepared by mixing of GO with some other polymers and adsorption capacities can be studied with some other commercially used dyes and heavy metals.
- The prepared GO, RGO or composite need to apply for the treatment of different types of industrial effluents.
- Prepared composite should use for the preparation of adsorption column and use for the treatment of industrial effluents.

References

[1] C.I. Pearce, J.R. Lioyd, J.T. Guthire, The removal of colour from textile wastewater using whole bacterial cells: a review, *Dye Pigment* 58 (2003) 179–196.

[2] T. Robinson, G. McMullan, R. Marchant, P. Nigam, Remediation of dyes in textile effluent : a critical review on current treatment technologies with a proposal alternative, *Bioresour Technol* 77 (2001) 247–255.

[3] C. O'Neill, F.R. Hawkes, D.L. Hawkes, N.D. Lourenco, H.M. Pinheiro, W. Delee, Colour in textile effluents–sources, measurement, discharge consents and simulation: a review, *J. Chem. Technol. Biotechnol.* 74 (1999) 1009–1018.

[4] P.C. Vandevivere, R. Bianchi, W. Verstraete, Treatment and reuse of wastewater from the textile wet-processing industry: review of emerging technologies, *J. Chem. Technol. Biotechnol*. 72 (1998) 289–302.

[5] S.M. Ghoreishi, R. Haghighi, Chemical catalytic reaction and biological oxidation for treatment of non-biodegradable textile effluent, *Chem. Eng. J.* 95 (2003) 163–169.

[6] A.K. Jain, V.K. Gupta, A. Bhatnagar, Suhas, Utilization of industrial waste products as adsorbents for the removal of dyes, *J. Hazard. Mater.* B101 (2003) 31–42.

[7] A. Dabrowski, Adsorption, from theory to practice, *Adv. colloid Int. Sci.* 93 (2001) 135–224.

[8] K.R. Ramakrishna, T. Viraraghavan, Dye removal using low cost adsorbents, *Water Sci. Technol.* 36 (1997) 189–196.

[9] S. Babel, T.A. Kurniawan, Low-cost adsorbents for heavy metals uptake from contaminated water: a review, *J. Hazard. Mater.* B 97 (2003) 219–243.

[10] R. M. Lattuada, M.C.R. Peralba, D. Santos, J.H.Z, A.G. Fisch, Peat, rice husk and rice husk carbon as low-cost adsorbents for metals from acidic aqueous solutions, *Sep. Sci. Technol.* 49 (2014) 101–111.

[11] Z.R. Liu, X. S. Chen, L.M. Zhou, P. Wei, Development of a first-order kinetics-based model for the adsorption of nickel onto peat, *Min. Sci. Technol.* 19 (2009) 230–234.

[12] M. Valix, W.H. Cheung, G. Mckay, Preparation of activated carbon using low temperature carbonisation and physical activation of high ash raw bagasse for acid dye adsorption, *Chemosphere* 56 (2004) 493–501.

[13] W.T. Tsai, C.Y. Chang, M.C. Lin, S.F. Chien, H.F. Sun, M.F. Hsieh, Adsorption of acid dye onto activated carbon prepared from agricultural waste bagasse by $ZnCl_2$ activation, *Chemosphere* 45 (2001) 51–58.

[14] N. Kannan and M.M. Sundaram, Kinetics and mechanism of removal of methylene blue by adsorption on various carbons-a comparative study, Dyes and Pigments 51 (2001) 25–40.

[15] M.M. Mohamed, Acid dye removal: Comparison of surfactant-modified mesoporous FSM-16 with activated carbon derived from rice husk, *J. Colloid. Interface Sci.* 272 (2004) 28–34.

[16] V.S. Mane, I.D. Mall, V.C. Srivastava, Kinetic and equilibrium isotherm studies for the adsorptive removal of Brilliant Green dye from aqueous solution by rice husk ash, *J. Environ. Manag.* 84 (2007) 390–400.

[17] P.K. Malik, Use of activated carbons prepared from sawdust and rice-husk for adsorption of acid dyes; a case study of acid yellow 36, *Dye Pigment* 56 (2003) 239–249.

[18] S.R. Shukla and R.S. Pai, Adsorption of Cu(II), Ni(II) and Zn(II) on dye loaded groundnut shells and sawdust, *Sep. Purif. Technol.* 43 (2005) 1–8.

[19] M. Visa, C. Bogatu, A. Duta, Simultaneous adsorption of dyes and heavy metals from multicomponent solutions using fly ash, *Appl. Surf. Sci.* 256 (2010) 5486–5491.

[20] M. Visa, L. Andronic, D. Lucaci, A. Duta, Concurrent dyes adsorption and photo-degradation on fly ash based substrates, *Adsorption* 17 (2011) 101–108.

[21] A. Gurses, S. Karaca, C. Dogar, R. Bayrak, M. Acikyildiz, M. Yalcin, Determination of adsorptive properties of clay/water system: methylene blue sorption, *J. Colloid. Int. Sci.* 269 (2004) 310–314.

[22] S. Wang , Y. Boyjoo, A. Choueib, Z. H. Zhu, Removal of dyes from aqueous solution using fly ash and red mud, *Water. Res.* 39 (2005) 129–138.

[23] G. McMullan, C. Meehan, A. Conneely, N. Kirby, T. Robinson, P. Nigam, I.M. Banat, R. Marchant, W.F. Smyth, Microbial decolourisation and degradation of textile dyes, *Appl. Microbiol. Biotechnol.* 56 (2001) 81–87.

[24] I.M. Banat, P. Nigam, D. Singh, R. Marchant, Microbial decolorization of textile-dye-containing effluents: a review, *Bioresour. Technol*. 58 (1996) 217–227.

[25] M.N.V. Ravi Kumar, T.R. Sridhari, K.D. Bhavani, P.K. Dutta, Trends in color removal from textile mill effluents, *Colorage* 40 (1998) 25–34.

[26] W.G. KUO, Decolorizing dye waste water with Fenton reagent, *Water. Res.* 26 (1992) 881–886.

[27] P.W. Wong, T.T. Teng, N. Abdul, R Nik, Efficiency of the Coagulation-Flocculation Method for the Treatment of Dye Mixtures Containing Disperse and Reactive Dye Efficiency of the Coagulation-Flocculation Method for the Treatment of Dye Mixtures Containing Disperse and Reactive Dye, water Qual. Res. J. 42 (2007) 54-62.

[28] W. Zhang, C. Zhou, W. Zhou, A. Lei, Q. Zhang, Q. Wan, B. Zou, Fast and considerable adsorption of methylene blue dye onto graphene oxide, *Bull. Environ. Contam. Toxicol.* 87 (2011) 86–90.

[29] G. Xie, P. Xi, H. Liu, F. Chen, L. Huang, Y. Shi, J. Wang, A facile chemical method to produce superparamagnetic graphene oxide–Fe_3O_4 hybrid composite and its application in the removal of dyes from aqueous solution, *J. Mater. Chem.* 22 (2012) 1033–1039.

[30] G.K. Ramesha, A.V. Kumara, H.B. Muralidhara, S. Sampath, Graphene and graphene oxide as effective adsorbents toward anionic and cationic dyes, *J. colloid interface sci.* 361 (2011) 270–277.

[31] A. Naseri, R. Barati, F. Rasoulzadeh, M. Bahram, Studies on adsorption of some organic dyes from aqueous solution onto graphene nanosheets, *Iran. J. Chem. Chem. Eng.* 34 (2015) 33–42.

[32] M. Iqbal and A. Abdala, Thermally reduced graphene: synthesis, characterization and dye removal applications, *RSC Adv.* 3 (46) (2013) 24455.

[33] J.H. Deng, X.R. Zhang, G.M. Zeng, J.L. Gong, Q.Y. Niu, J. Liang, Simultaneous removal of Cd(II) and ionic dyes from aqueous solution using magnetic graphene oxide nanocomposite as an adsorbent, *Chem. Eng. J.* 226 (2013) 189–200.

[34] R. Tovar-Gómez, D. A. Rivera-Ramírez, V. Hernández-Montoya, A. Bonilla-Petriciolet, C.J. Durán-Valle, M.A. Montes-Morán, Synergic adsorption in the simultaneous removal of acid blue 25 and heavy metals from water using a $Ca(PO_3)_2$-modified carbon, *J. Hazard. Mater.* 199–200 (2012) 290–300.

[35] K. Hunger, Industrial Dyes: Chemistry, properties and applications. Wiley VCH, (2003), doi:10.1021/ja0335418

[36] N.P. Cheremisinoff, Handbook of Water and Wastewater Treatment Technologies. Butterworth-Heinemann, Boston, 2002, doi:10.1016/B978-075067498-0/50014-0.

[37] N. Al-Bastaki, 2004. Removal of methyl orange dye and Na_2SO_4 salt from synthetic waste water using reverse osmosis, *Chem. Eng. Process*, 43 (2004) 1561–1567.

[38] J.W. Lee, S.P.Choi, R. Thiruvenkatachari, W.G. Shim, H. Moon, Evaluation of the performance of adsorption and coagulation processes for the maximum removal of reactive dyes, *Dyes and Pigments* 69 (2006) 196–203.

[39] F.I. Hai, K. Yamamoto, K. Fukushi, Hybrid treatment systems for dye wastewater, *Crit. Rev. Env. Sci. Technol.* 37 (2007) 315–37.

[40] T. Omura, Design of chlorine-fast reactive dyes: Part 4: degradation of amino-containing azo dyes by sodium hypochlorite, *Dyes and Pigments* 26 (1994) 33–50.

[41] S. Wang, A Comparative study of Fenton and Fenton-like reaction kinetics in decolourisation of wastewater, *Dyes and Pigments* 76 (2008) 714–720.

[42] H. Liu, C. Wang, Xiangzhong, X. Xuan, C. Jiang, H. Cui, A Novel Electro-Fenton Process for Water Treatment: Reaction-controlled pH Adjustment and Performance Assessment, *Environ. Sci. Technol* 41 (8) (2007) 2937–2942.

[43] J. Wu, H. Doan, S. Upreti, Decolorization of aqueous textile reactive dye by ozone. *Chem. Eng. J.* 142 (2) (2008) 156–160.

[44] V.K. Gupta, R. Jain, S. Varshney, Electrochemical removal of the hazardous dye Reactofix Red 3 BFN from industrial effluents, *J. Colloid Interface Sci.* 312 (2007) 292–296.

[45] A.M. Faouzi, B. Nasr, G. Abdellatif, Electrochemical degradation of anthraquinone dye Alizarin Red S by anodic oxidation on boron-doped diamond, *Dyes and Pigments* 73 (2007) 86–89.

[46] F.H. Oliveira, M.E. Osugi, F.M.M. Paschoal, D. Profeti, Electrochemical oxidation of an acid dye by active chlorine generated using Ti/Sn(1-x) Ir x O_2 electrodes, *J. Appl. Electrochem.* 37 (2007) 583–592.

[47] C.A. Martínez-Huitle, M.A.Q. Alfaro, Recent environmental applications of diamond electrode: critical review, *J. Environ. Eng. Manage*, 18(3) (2008) 155-172.

[48] Aken, P. Van, Eyck, K. Van and Lambert, N. Effect of (Partial) Advanced Oxidation Processes (AOPs) on the Decolourisation and Biodegradability of an Industrial Wastewater.

[49] M. Verma, A.E. Ghaly, Treatment of Remazol Brilliant Blue Dye Effluent by Advanced Photo Oxidation Process in TiO_2/UV and H_2O_2/UV reactors, *Am. J. of Eng. and Appl. Sci.* 1 (3) (2008) 230-240.

[50] B.E. Barragan, C. Costa, M. C. Marquez, 2007. Biodegradation of azo dyes by bacteria inoculated on solid media, *Dyes and Pigments* 75 (2007) 73–81.

[51] C.T.M.J. Frijters, R.H. Vos, G. Scheffer, R. Mulder, Decolorizing and detoxifying textile wastewater, containing both soluble and insoluble dyes, in a full scale combined anaerobic/aerobic system, *Water Res.* 40 (2006) 1249–1257.

[52] A.Stolz, Basic and applied aspects in the microbial degradation of azo dyes, *Appl. Microbiol. Biotechnol*, 56 (2001) 69–80.

[53] G. Crini, Recent developments in polysaccharide-based materials used as adsorbents in wastewater treatment, *Prog. Polym. Sci.* 30 (2005) 38–70.

[54] J. Wu, H. Doan, S. Upreti, Decolorization of aqueous textile reactive dye byozone. *Chem. Eng. J.* 142 (2008b) 156–160.

[55] F. Delval, G. Crini, J. Vebrel, M. Knorr, G. Sauvin, E. Conte, Starch-modified filters used for the removal of dyes from waste water. *Macromol. Symp.* 203 (2003)165–171.

[56] Lillo-Rodenas, M. Marco-Lozar, J.P.Cazorla-Amoros, D. Linares-Solano, Activated carbons prepared by pyrolysis of mixtures of carbon precursor/alkaline hydroxide. *J. Anal. Appl. Pyrolysis* 80 (2007) 166–174.

[57] P.M. Carrott, M.M.L. Ribeiro Carrott, J.M.V. Nabais, Influence of surface ionization on the adsorption of aqueous mercury chlorocomplexes by activated carbons, *Carbon* 36 (1998)11–17.

[58] N. Kannan and M.M. Sundaram, Kinetics and mechanism of removal of methylene blue by adsorption on various carbons — a comparative study. 51 (2001) 25–40.

[59] I. Ali, V.K. Gupta, Advances in water treatment by adsorption technology, *Nature Protocols* 1 (2007) 2661–2667.

[60] R.L. Tseng, F.C. Wu, R.S Juang, Liquid-phase adsorption of dyes and phenols using pinewood-based activated carbons, *Carbon* 41 (2003) 487–495.

[61] G. McKay, J.F Porter, G.R. Prasad, 1999. The removal of dye colours from aqueous solutions by adsorption on low-cost materials, *Water Air Soil Pollut.* 114 (1999) 423–438.

[62] Y.S. Ho, G. McKay, Sorption of dye from aqueous solution by peat, *Chem. Eng. J.* 70 (1998b) 115–124.

[63] Q. Sun, L. Yang, The adsorption of basic dyes from aqueous solution on modified peat- resin particle. *Water Res.* 37 (2003) 1535–1544.

[64] Y.C. Wong, Y.S. Szeto, W.H. Cheung, G. McKay, Adsorption of acid dyes on chitosan-equilibrium isotherm analyses, *Proc. Biochem.* 39 (2004) 693–702.

[65] I. Bouzaida, M. Rammah, Adsorption of acid dyes on treated cotton in a continuous system. *Mater. Sci. Eng. C* 21 (2002)151–155.

[66] M. Bagane, S. Guiza, Removal of a dye from textile effluents by adsorption, *Ann. Chim. Sci. Mater.* 25 (2000) 615–626.

[67] Y.S. Ho, C.C. Chiang, Y.C. Hsu, Sorption kinetics for dye removal from aqueous solution using activated clay, *Sep. Sci. Technol.* 36 (2001) 2473–2488.

[68] G.M. Walker, L. Hansen, J.A. Hanna, S.J. Allen, Kinetics of a reactive dyeadsorption onto dolomitic sorbents. *Water Res.* 37 (2003) 2081–2089.

[69] A.S Ozcan, B. Erdem, A. Ozcan, Adsorption of acid blue193 from aqueous solutions onto Na-bentonite and DTMA-bentonite, *J. Colloid Int. Sci*. 280 (2004) 44–54.

[70] M.A. Al-Ghouti, M.A.M. Khraisheh, S.J. Allen, M.N. Ahmad, 2003. The removal of dyes from textile wastewater: a study of the physical characteristics and adsorption mechanisms of diatomaceous earth, *J. Environ. Manage*. 69 (2003) 229–238.

[71] Z. Aksu, S.Tezer, Equilibrium and kinetic modeling of biosorption of Remazol Black B by Rhizopus arrhizus in a batch system: effect of temperature, *Proc. Biochem.* 36 (2000) 431–439.

[72] Z. Aksu, S. Tezer, Biosorption of reactive dyes on the green alga Chlorella vulgaris.*Proc. Biochem.* 40 (2005) 1347–1361.

[73] Z. Aksu, G. Donmez, A comparative study on the biosorption characteristics of some yeasts for remazol blue reactive dye, *Chemosphere* 50 (2003) 1075–1083.

[74] V. Dulman & S.M. Cucu-Man, Sorption of some textile dyes by beech wood sawdust, *J. Hazard. Mater.* 162 (2009) 1457–1464.

[75] R.S. Juang, F.C. Wu, R.L. Tseng, Characterization and use of activated carbons prepared from bagasses for liquid-phase adsorption Colloid Surf. A: *Physicochem, Eng. Aspect* 201 (2002a) 191–199.

[76] M. Valix, W.H. Cheung, G. McKay, Preparation of activated carbon using low temperature carbonisation and physical activation of high ash raw bagasse for acid dye adsorption, *Chemosphere* 56 (2004) 493–501.

[77] C.D. Woolard, J. Strong, C. Erasmus, Evaluation of the use of modified coal ash as a potential sorbent for organic waste streams. *Appl. Geochem.* 17 (2002) 1159–1164.

[78] P. Janos, H. Buchtova, M. Ryznarova, Sorption of dyes from aqueous solutions onto fly ash. *Water Res.* 37 (2003) 4938–4944.

[79] Rajeshwarisivaraj, C. Namasivayam, K. Kadirvelu, Orange peel as an adsorbent in the removal of acid violet 17 (acid dye) from aqueous solutions. *Waste Manage.* 21 (2001b) 105–110.

[80] G. Annadurai, R.S. Juang, D.J. Lee, Use of cellulose-based wastes for adsorption of dyes from aqueous solutions. *J. Hazard. Mater.* B92 (2002) 263–274.

[81] C. Namasivayam, R. Radhika, S. Suba, Uptake of dyes by a promising locally available agricultural solid waste: coir pith, *Waste Manage.* 21 (2001b) 381–387.

[82] O. Gulnaz, A. Kaya, F. Matyar, B. Arikan, Sorption of basic dyes from aqueous solution by activated sludge, *J. Hazardous Mater.* B108 (2004) 183–188.

[83] Z. Aksu, Biosorption of reactive dyes by dried activated sludge:equlibrium and kinetic modeling, *Biochem. Eng. J.* 7 (2001) 79–84.

[84] K. Okada, N. Yamamoto, Y. Kameshima, A. Yasumori, Adsorption properties of activated carbon from waste newspaper prepared by chemical and physical activation, *J. Colloid Int. Sci.* 262 (2003) 194–199.

[85] M.J. Martin, A. Artola, M.D. Balaguer, M. Rigola, Activated carbons developed from surplus sewage sludge for the removal of dyes from dilute aqueous solutions, *Chem. Eng. J.* 94 (2003) 231–239.

[86] Y.H. Magdy, A.A.M. Daifullah, Adsorption of a basic dye from aqueous solutions onto sugar-industry mud, *Waste Manage.* 18 (1998) 219–226.

[87] Y.S. Ho, T.H. Chiang, Y.M. Hsueh, Removal of basic dye from aqueous solutions using tree fern as a biosorbent, *Process Biochem.* 40 (2005) 119–124.

[88] K.S. Chou, J.C. Tsai, C.T. Lo, The adsorption of Congo red and vacuum pump oil by rice hull ash, *Bioresour. Technol.* 78 (2001) 217–219.

[89] G.S. Miguel, G.D. Fowler and C.J. Sollars, Adsorption of organic compounds from solution by activated carbons produced from waste tyre rubber. *Sep. Sci. Technol.* 37 (2002) 663–676.

[90] V. Ravi, S.C. Bose, T.M.P. Kumar and Siddaramaiah, Decolorization of distillery effluent using poly(vinyl chloride) and cellulose acetate phthalate as adsorbents, *J. Macromol. Sci.* 43 (2006) 1247–1254.

[91] V.K. Gupta, A. Mittal, V. Gajbe and J. Mittal, Removal and recovery of the hazardous azo dye acid orange 7 through adsorption over waste materials: Bottom ash and de-oiled soya, *Ind. Eng. Chem. Res.* 45 (2006) 1446–1453.

[92] V.K. Gupta, I. Ali, V.K. Saini, T.V Gerven, B.V.D. Bruggen, C. Vandecasteele, Removal of dyes from wastewater using bottom ash, *Ind. Eng. Chem. Res.* 44 (2005) 3655–3664.

[93] A. Gurses, C. Dogar, S. Karaca, M. Acikyildiz, R. Bayrak, Production of granular activated carbon from waste *Rosa canina* sp. seeds and its adsorption characteristics for dye, *J. Hazard. Mater.* 131 (2006) 254–259.

[94] A. Elsagh, O. Moradi, A. Fakhri, F. Najafi, R. Alizadeh, V. Haddadi, Evaluation of the potential cationic dye removal using adsorption by graphene and carbon nanotubes as adsorbents surfaces, *Arab. J. Chem.* 10 (2017) S2862–S2869.

[95] J. Qin, F. Qiu, X. rong, J. Yan, H. Zhao, D. Yang, Adsorption behvior of crystalviolet from aqueous solutions with chitosan-graphite oxide modified polyurethane as an adsorbent, *J. Appl. Polym. Sci.* 132 (2015)1–10.

[96] K. Atrak, A. Ramazani, S.T. Fardood, Green synthesis of $Zn_{0.5}Ni_{0.5}AlFeO_4$ magnetic nanoparticles and investigation of their photocatalytic activity for degradation of reactive blue 21 dye, *Environ. Tech.* (2019), DOI: 10.1080/09593330.2019.1581841

[97] Y. Zhu, S. Murali, W. Cai, X. Li, J.W. Suk, J.R. Potts, R.S. Ruoff, Graphene and graphene oxide: synthesis, properties and applications, *Adv. mater.* 22 (2010) 3906–24.

[98] G. Uslu and M. Tanyol, Equilibrium and Thermodynamic parameters of single and binary mixture biosorption of lead (ii) and copper (ii) ions onto pseudomonas putida: Effect of Temperature, *J. Hazard. Mater.* B 135 (2006) 87–93.

[99] H.M.F. Freundlich, Over the adsorption in solution, *J. Phy. Chem.* 57 (1906) 385.

[100] M. Ionita, M. A. Pandele and H. Iovu, Sodium alginate/graphene oxide composite films with enhanced thermal and mechanical properties, *Carbohydr. Polym.* (2013). doi:10.1016/j.carbpol.2013.01.065

[101] W. Chen, L. Yan and P.R. Bangal, Chemical Reduction of Graphene Oxide to Graphene by Sulfur-Containing Compounds, J. Phys. Chem. C 114 (2010) 19885–19890.

[102] R. Rezaee, S. Nasseri, A.H. Mahi, R. Nabizadeh, S.A. Mousavi, A. Rashidi, A. Jafari and S. Nazmara, Fabrication and characterization of a polysulfone-graphene oxide nanocomposite membrane for arsenate rejection from water, *J. Environ. Heal. Sci. Eng.* 13(1) (2015) 61.

[103] W. Chen, L. Yan, and P. R. Bangal, Preparation of graphene by the rapid and mild thermal reduction of graphene oxide induced by microwaves, *Carbon* 48 (2010) 1146–1152.

[104] L.G.B. Machuno, A.R. Oliveira , R.H. Furlan, A.B. Lima, L.C. Morais, R.V. Gelamo Multilayer Graphene Films Obtained by Dip Coating Technique, Mater. Res. 18 (4) (2015) 775–780.

[105] M. Ghorbani, H. Abdizadeh, M.R. Golobostanfard, Reduction of Graphene Oxide via Modified Hydrothermal Method, *Procedia Mater. Sci.* 11 (2015) 326–330.

[106] N.D. Luong, N. Pahimanolis, U. Hippi, J.T. Korhonen, J. Ruokolainen, L. Johansson, J. Namd and J. Seppala, Graphene/cellulose nanocomposite paper with high electrical and mechanical performances, *J. Mater. Chem.* 21 (2011) 13991–13998.

[107] W. Chen, L. Yan, and P. R. Bangal, Preparation of graphene by the rapid and mild thermal reduction of graphene oxide induced by microwaves, *Carbon* 48 (2010) 1146–1152.

[108] J.I. Paredes, S. Villar-Rodil, P. Solis-Fernandez, A. Martinez-Alonso, and J.M.D. Tascon, Atomic Force and Scanning Tunneling Microscopy Imaging of Graphene Nanosheets Derived from Graphite Oxide, Langmuir 25 (10) (2009) 5957–5968.

[109] G.G. Wallace, R.B. Kaner, M. Muller, S. Gilje, D. Li, Processable aqueous dispersions of graphene nanosheets, 3 (2008) 101–105.

[110] P. Bartezak, M. Norman, L. Klapiszewski, N. Karwanska, M. Kawalec, M. Baczynska, M. Wysokowski, J. Zdarta, F. Ciesielczyk, T. Jesionowski, Removal of nickel(II) and lead(II) ions from aqueous solution using peat as a low-cost adsorbent: A kinetic and equilibrium study, *Arab. J. Chem.* (2015) doi:10.1016/j.arabjc.2015.07.018

[111] P. Nuengmatcha, S. Chanthai, Adsorption Capacity of The As-Synthetic Graphene Oxide for The Removal of Alizarin Red S Dye from Aqueous Solution, *O. J. Chem.* (2016) 1399-1410. doi:10.13005/ojc/320314

[112] A. Shukla, Y.H. Zhang, P. Dubey, J.L. Margrave, S.S. Shukla, The role of sawdust in the removal of unwanted materials from water, *J. Hazard. Mater.* 95 (2002) 137–152.

[113] Tajiki, Alireza, Abdouss, Majid, Synthesis and Characterization of Graphene Oxide Nano-sheets for Effective Removal of Phthalocyanine from Aqueous Media, Iran. J. Chem. Chem. Eng. 36 (4) (2017) 1–9.

[114] C.R. Minitha, M. Lalitha, Y.L. Jeyachandran, L. Senthilkumar, R.T.R. Kumar, Adsorption behaviour of reduced graphene oxide towards cationic and anionic dyes: Co-action of electrostatic and π – π interactions, *Mater. Chem. Phys*. (2017) DOI: 10.1016/j.matchemphys.2017.03.048

[115] G.K. Ramesha, A.V. Kumara , H.B. Muralidhara, and S. Sampath, Graphene and graphene oxide as effective adsorbents toward anionic and cationic dyes, *J. Colloid. Interface Sci.* 361 (1) (2011) 270–277.

[116] L. Nie, C. Liu, J. Wang, Y. Shuai, X. Cui and L. Liu, Effects of surface functionalized graphene oxide on the behavior of sodium alginate, *Carbo. Poly*. 117 (2015) 616-623.

[117] X. Yang, T. Zhou, B. Ren, A. Hursthouse and Y. Zhang, Removal of Mn (II) by Sodium Alginate/Graphene Oxide Composite Double-Network Hydrogel Beads from Aqueous Solutions. *Sci. Rep.* 8 (2018) 1–16.